

**FUNCTIONALIZED NANOPARTICLE CROSSLINKING FOR ENHANCED
AFFINITY PRECIPITATION OF MONOCLONAL ANTIBODIES**

by

Andrew R. Swartz

A dissertation submitted to the Faculty of the University of Delaware
in partial fulfillment of the requirements for the degree of
Doctor of Philosophy in Chemical Engineering

Summer 2018

© 2018 Andrew R. Swartz
All Rights Reserved

**FUNCTIONALIZED NANOPARTICLE CROSSLINKING FOR ENHANCED
AFFINITY PRECIPITATION OF MONOCLONAL ANTIBODIES**

by

Andrew R. Swartz

Approved: _____
Eric Furst, Ph.D.
Chair of the Department of Chemical and Biomolecular Engineering

Approved: _____
Babatunde Ogunnaike, Ph.D.
Dean of the College of Engineering

Approved: _____
Douglas J. Doren, Ph.D.
Interim Vice Provost for Graduate and Professional Education

I certify that I have read this dissertation and that in my opinion it meets the academic and professional standard required by the University as a dissertation for the degree of Doctor of Philosophy.

Signed:

Wilfred Chen, Ph.D.
Professor in charge of dissertation

I certify that I have read this dissertation and that in my opinion it meets the academic and professional standard required by the University as a dissertation for the degree of Doctor of Philosophy.

Signed:

Abraham Lenhoff, Ph.D.
Member of dissertation committee

I certify that I have read this dissertation and that in my opinion it meets the academic and professional standard required by the University as a dissertation for the degree of Doctor of Philosophy.

Signed:

Christopher Roberts, Ph.D.
Member of dissertation committee

I certify that I have read this dissertation and that in my opinion it meets the academic and professional standard required by the University as a dissertation for the degree of Doctor of Philosophy.

Signed:

Steven Traylor, Ph.D.
Member of dissertation committee

ACKNOWLEDGMENTS

I would like to thank my advisor, Prof. Wilfred Chen, my lab group members, my dissertation committee, Prof. Abraham Lenhoff, Prof. Christopher Roberts, and Dr. Steven Traylor, and my collaborators at Bristol-Meyers Squibb (BMS) and Rensselaer Polytechnic Institute for their technical guidance, scientific expertise, and insightful discussions during my PhD research. I would like to acknowledge my funding source supported by grants from NSF (CBET1403724 and DMR1609621) and BMS via the GOALI program collaboration. I would like to thank BMS Biologics Process Development (Devens, MA) and Dr. Xuankuo Xu, Dr. Steven Traylor, and Dr. Zheng Jian Li for providing the mAb samples and for their technical and analytical support. I would also like to thank Prof. Kelvin Lee and Dr. Jongyoun Baik and for access and guidance with the Octet RED96e instrument in the NIIMBL laboratory at the University of Delaware Biotechnology Institute. I would like to acknowledge the Center of Biomedical Research Excellence Microscopy and Mechanical Testing Core (COBRE-MMT) with a grant from the National Institute of General Medical Sciences – NIGMS (1 P30 GM110758-01) at NIH for use of the Malvern Zetasizer dynamic light scattering instrument.

TABLE OF CONTENTS

LIST OF TABLES	x
LIST OF FIGURES	xi
ABSTRACT	xv

Chapter

1	INTRODUCTION	1
1.1	Therapeutic Monoclonal Antibody Production	1
1.2	Protein Purification with Affinity Precipitation	2
1.2.1	Primary Effect Affinity Ligand Crosslinking	2
1.2.2	Secondary Effect Stimuli-responsive Affinity Ligands	3
1.3	Antibody Affinity Precipitation with Z-Elastin-Like Polypeptides	4
1.4	Z-ELP-Nanoparticle Scaffold for Multivalent Crosslinking	5
1.5	E2 Nanocage Functionalization using Sortase A Ligation	6
1.6	Dissertation Objectives	8
	FIGURES	9
	REFERENCES	15
2	ANTIBODY BINDING INDUCED CROSSLINKING OF Z-DOMAIN- ELASTIN-LIKE-POLYPEPTIDE FUNCTIONALIZED E2 NANOPARTICLES	20
2.1	Introduction	21
2.2	Materials and Methods	22
2.2.1	Materials	22
2.2.2	Protein Expression and Purification	23
2.2.3	Sortase A Mediated Ligation	24
2.2.4	Transition Temperature Measurement	25
2.2.5	Dynamic Light Scattering Measurement	25
2.2.6	Antibody Affinity Precipitation	26
2.2.7	Turbidity Measurement	27

2.3	Results and Discussion	27
2.3.1	Z-ELP functionalization of E2 by sortase A ligation	27
2.3.2	Effect of Z-ELP-E2 ligation density on nanoparticle properties..	28
2.3.3	Enhanced precipitation by antibody-inducible crosslinking	29
2.4	Conclusion.....	32
	FIGURES	33
	REFERENCES	39
3	ONE-STEP AFFINITY CAPTURE AND PRECIPITATION FOR IMPROVED PURIFICATION OF AN INDUSTRIAL MONOCLONAL ANTIBODY	42
3.1	Introduction	43
3.2	Materials and Methods	46
3.2.1	Materials	46
3.2.2	Experimental Methods.....	46
3.2.2.1	Protein Expression and Purification	46
3.2.2.2	High-throughput Affinity Precipitation Optimization..	47
3.2.2.3	mAb Cell Culture Affinity Precipitation	48
3.2.3	Analytical Methods	49
3.2.3.1	PLSR Model of Two Component Absorption Spectra.	49
3.2.3.2	Analytical Size Exclusion Chromatography	50
3.2.3.3	Analytical Impurity Content.....	50
3.2.3.4	Dynamic Light Scattering Measurement.....	50
3.3	Results and Discussion	51
3.3.1	High-throughput optimization of mAb binding and precipitation.....	51
3.3.2	High-throughput optimization of mAb elution and nanocage recovery	52
3.3.3	Process stability of the mAb and nanocage	54
3.3.4	Removal of process impurities	55
3.3.5	Optimized affinity precipitation of mAb cell culture harvest.....	56
3.4	Conclusion.....	58
	TABLES	60

FIGURES	63
REFERENCES	75
4 HIGH-EFFICIENCY AFFINITY PRECIPITATION OF INDUSTRIAL MABS AND FC-FUSION PROTEINS FROM CELL CULTURE HARVESTS	78
4.1 Introduction	79
4.2 Materials and Methods	80
4.2.1 Materials	80
4.2.2 Z-ELP-E2 Nanocage Production	81
4.2.3 High-throughput Affinity Precipitation Experiments.....	82
4.2.4 Aggregation Kinetic Measurement.....	83
4.2.5 mAb Culture Affinity Precipitation.....	84
4.2.6 Analytical Size Exclusion Chromatography	85
4.2.7 Analytical Impurity Content.....	85
4.3 Results and Discussion	86
4.3.1 Impact of Z-domain-target binding ratio on precipitation yield..	86
4.3.2 Effect of solution pH on aggregation kinetics	87
4.3.3 Elution buffer pH and mAb stability	90
4.3.4 Affinity precipitation from cell culture harvests	91
4.4 Conclusion.....	93
TABLES	95
FIGURES	99
REFERENCES.....	107
5 SPYTAG/SPYCATCHER FUNCTIONALIZATION OF E2 NANOCAGES WITH Z-ELP AFFINITY DOMAINS FOR TUNABLE ANTIBODY BINDING AND PRECIPITATION PROPERTIES	110
5.1 Introduction	111
5.2 Materials and Methods	113
5.2.1 Materials	113
5.2.2 Genetic Manipulations and Vector Construction	114
5.2.3 Protein Expression and Purification	114
5.2.4 Sortase A Ligation of ELP-LPETG Fusions to GGG-E2.....	116
5.2.5 Z-ELP-SpyCatcher Conjugation to SpyTag-E2	116
5.2.6 Transition Temperature Measurement	116

5.2.7	Absorbance Measurement	117
5.2.8	Z-ELP-E2 Nanocage mAb Binding Capacity	117
5.2.9	mAb-Nanocage Crosslinking and Precipitation Yield	118
5.2.10	Nanocage Regeneration and mAb Affinity Precipitation.....	118
5.3	Results and Discussion	119
5.3.1	Evaluation of Sortase A ELP-fusion protein E2 ligation efficiency	119
5.3.2	Expression and conjugation of Spytag-E2 and Z-ELP- SpyCatcher	120
5.3.3	Effect of ligation density on nanocage aggregation and IgG Binding	122
5.3.4	Effect of ligation density on crosslinking and precipitation yield	123
5.3.5	Nanocage selective precipitation and regeneration after mAb Elution	124
5.4	Conclusion.....	126
	TABLES	128
	FIGURES	131
	REFERENCES	145
6	RAPID DETECTION AND QUANTIFICATION OF MONOCLONAL ANTIBODY CONCENTRATION IN CELL CULTURE HARVESTS THROUGH ANTIBODY-NANOPARTICLE CROSSLINKING TURBIDITY.....	148
6.1	Introduction	149
6.2	Materials and Methods	151
6.2.1	Materials	151
6.2.2	Protein Expression Purification and Conjugation	151
6.2.3	Turbidity Measurement and Analysis	152
6.2.4	mAb-Nanoparticle Crosslinking Turbidity.....	152
6.2.5	Octet Bridging Study	153
6.2.6	mAb Purification after Turbidity Measurement	153
6.3	Results and Discussion	154
6.3.1	Optimization of turbidity measurement.....	154
6.3.2	mAb-Nanoparticle crosslinking kinetics	155

6.3.3	Quantification and validation of mAb-nanoparticle crosslinking turbidity.....	156
6.4	Conclusion.....	158
	TABLES.....	161
	FIGURES.....	162
	REFERENCES.....	173
7	CONCLUSIONS AND FUTURE WORK: PLATFORMED ANTIGEN DETECTION AND PURIFICATION THROUGH NANOBODY FUNCTIONALIZED NANOPARTICLE CROSSLINKING	176
7.1	Motivation for new affinity precipitation ligand design.....	176
7.2	IgG-binding induced crosslinking with Z-ELP-E2 nanoparticles	176
7.3	Development of a platform for industrial mAb purification	177
7.4	Improved nanoparticle functionalization with SpyTag/SpyCatcher	178
7.5	Quantification of mAb-nanoparticle crosslinking turbidity	179
7.6	Generalized protein purification and detection with nanobodies	179
7.7	GFP-nanoparticle crosslinking with orthogonal nanobody-ELP-E2.....	181
7.8	Future research opportunities	183
	FIGURES	184
	REFERENCES	188
Appendix		
A	LIST OF ABBREVIATIONS	191
B	REPRINT PERMISSIONS	194

LIST OF TABLES

Table 3.1	Optimized affinity precipitation process conditions.	60
Table 3.2	Analytical characterization of nanocage affinity precipitation of mAb cell culture over three cycles. Average results compared to protein A chromatography performance.....	61
Table 3.3	Comparison of HCP and DNA impurity clearance between affinity precipitation and protein A chromatography.....	62
Table 4.1	Molecular properties and concentrations for the five molecules used in the study. MW = molecular weight, pI = isoelectric point.....	95
Table 4.2	Buffer composition for use in aggregation kinetics investigation.....	96
Table 4.3	Affinity precipitation conditions used for purification of the molecules from cell culture.	97
Table 4.4	Comparison of average affinity precipitation performance for mAbs A-D with expected protein A chromatography performance. Average affinity precipitation values reported with 95% confidence intervals.....	98
Table 5.1	Primers and oligos used for gene construction.....	128
Table 5.2	Affinity precipitation process steps corresponding to the lane number in Figure 5.14C.....	129
Table 5.3	Comparison of SrtA ligation and SpyTag/SpyCatcher methods for Z-ELP conjugation to E2 nanocages.....	130
Table 6.1	Properties of mAbs used in this study. MW = molecular weight, pI = isoelectric point, HCP = host cell protein.....	161

LIST OF FIGURES

Figure 1.1	Affinity precipitation process for protein purification	9
Figure 1.2	Effect of valency on primary effect affinity precipitation.....	10
Figure 1.3	Secondary effect affinity precipitation with a stimuli-responsive bifunctional affinity ligand.....	11
Figure 1.4	Elastin-like polypeptide aggregation after addition of 0.5 M ammonium sulfate	12
Figure 1.5	mAb purification by Z-ELP secondary effect affinity precipitation.	13
Figure 1.6	Strategy for antibody-nanoparticle crosslinking with multivalent Z-ELP functionalized nanoparticles.....	14
Figure 2.1	Mechanism for affinity precipitation of IgG using Z-ELP-E2 nanoparticles.....	33
Figure 2.2	Production of Z-ELP-E2 Nanocages	34
Figure 2.3	Nanocage Sortase A ligation and aggregation properties	35
Figure 2.4	T_i comparison between free and ligated ELP	36
Figure 2.5	Characterization of antibody binding-induced crosslinking	37
Figure 2.6	IgG-Nanoparticle crosslinking and elution	38
Figure 3.1	Z-ELP affinity precipitation process from mAb purification from cell culture	63
Figure 3.2	SDS-PAGE analysis of protein expression and Z-ELP-E2 ligation.....	64
Figure 3.3	Effect of Z:mAb molar binding ratio and salt concentration on mAb precipitation yield.....	65
Figure 3.4	mAb-nanocage aggregation kinetics	66
Figure 3.5	Effect of buffer pH on the mAb elution yield	67

Figure 3.6	Effect of elution buffer and VCF on resuspension pH.....	68
Figure 3.7	Effects of volume concentration and salt concentration on mAb and nanocage recovery.	69
Figure 3.8	mAb elution stability.....	70
Figure 3.9	Nanocage process stability.....	71
Figure 3.10	Effects of washing step on HCP clearance.....	72
Figure 3.11	SDS-PAGE analysis of mAb affinity precipitation.....	73
Figure 3.12	mAb affinity precipitation with pictures.....	74
Figure 4.1	mAb binding and precipitation yield.....	99
Figure 4.2	Effect of solution pH on aggregation kinetics at 3:1 Z:mAb molar binding ratio.....	100
Figure 4.3	F-W model rate constants k_1 and k_2A_0	101
Figure 4.4	Effect of the time to reach maximum aggregation rate on buffer pH ...	102
Figure 4.5	Effect of 50 mM sodium citrate buffer pH on mAb elution yield.....	103
Figure 4.6	mAb elution stability.....	104
Figure 4.7	Characterization of mAb affinity precipitation from cell culture.....	105
Figure 4.8	Characterization of mAb affinity precipitation.....	106
Figure 5.1	SDS-PAGE gel of SrtA ligation comparison of the conjugation of Z-ELP ₄₀ -LPETG or Z-ELP ₈₀ -LPETG to GGG-E2.....	131
Figure 5.2	Low Z-ELP ₈₀ -LPETG ligation efficiency to GGG-E2.....	132
Figure 5.3	Low Z-ELP ₈₀ -LPETG ligation efficiency to GGG-ELP.....	133
Figure 5.4	SDS-PAGE gel of SrtA ligation comparison with flexible linker (G ₄ S) ₃ and rigid linker (EA ₃ K) ₃	134
Figure 5.5	SpyTag-E2 nanocage expression and partial purification.....	135
Figure 5.6	Confirmation of E2 assembly by DLS.....	136

Figure 5.7	Z-ELP-SpyCatcher expression and SpyTag/SpyCatcher reaction	137
Figure 5.8	SDS-PAGE gel for comparison of SrtA and SpyCatcher-SpyTag conjugation methods with Z-ELP ₄₀ -LPETG and Z-ELP ₈₀ -LPETG conjugation to GGG-E2(158).....	138
Figure 5.9	Ligation efficiency comparison.....	139
Figure 5.10	T _i and mAb binding.....	140
Figure 5.11	mAb-Nanocage crosslinking and precipitation	141
Figure 5.12	Mechanism for mAb-crosslinking with high and low Z-ELP-E2 ligation density	142
Figure 5.13	Optimization of ammonium sulfate concentration in 50 mM sodium citrate pH 3.5 buffer for selective nanocage precipitation	143
Figure 5.14	mAb affinity precipitation from cell culture harvest using ~100% ligation density Z-ELP ₄₀ -Spy-E2 or Z-ELP ₈₀ -Spy-E2.	144
Figure 6.1	Procedure for measuring mAb-nanocage crosslinking turbidity and optional mAb purification.	162
Figure 6.2	Optimization of turbidity measurement	163
Figure 6.3	mAb-nanoparticle aggregation kinetics.....	164
Figure 6.4	Dependence of mixing time on logarithmic regression fit.....	165
Figure 6.5	Crosslinking turbidity assay validation	166
Figure 6.6	Nanoparticle crosslinking turbidity assay variability and prediction error	167
Figure 6.7	mAb titer measurement using ForteBio Octet instrument.....	168
Figure 6.8	Comparison of turbidity assay and Octet assay for validation samples of mAb cell culture harvests.....	169
Figure 6.9	mAb cell culture titration and nanoparticle crosslinking with a human polyclonal IgG.....	170
Figure 6.10	SDS-PAGE of mAb purification after turbidity measurement	171

Figure 6.11	Plate layout for ForteBio Octet experiment	172
Figure 7.1	Mechanism for target protein-nanoparticle crosslinking with multimeric and monomeric proteins.....	184
Figure 7.2	Orthogonal Anti-GFP nanobody (GBP2, GBP7) binding and crosslinking with GFP	185
Figure 7.3	GFP capture in soluble E. coli lysate through crosslinking with GBP2+7-ELP ₈₀ -Spy-E2 nanoparticles without added salt.....	186
Figure 7.4	Concentration dependent detection of GFP-nanoparticle crosslinking turbidity and crosslinking sensitivity at low GFP concentrations.....	187

ABSTRACT

Recent advances in upstream therapeutic monoclonal antibody (mAb) production have posed significant challenges to the downstream purification platform. Protein A affinity chromatography has been identified as a potential process bottleneck due to limitations in throughput, scale-up, and cost. Affinity precipitation is a promising non-chromatographic alternative because it combines the selectivity of an affinity ligand with the operational benefits of conventional precipitation. After binding to a target protein in solution, phase transition is induced through crosslinking with multivalent affinity ligands (primary effect; multimeric protein only) or using stimuli-responsive affinity ligands (secondary effect; monomer or multimer). Primary effect affinity precipitation is not widely used due to low precipitation yields, but there are several examples of mAb purification using protein A ligands conjugated to a responsive domain of synthetic or natural origin.

Our group has demonstrated the feasibility of using a recombinant antibody binding domain (Z-domain) genetically fused to a temperature responsive elastin-like polypeptide (ELP) biopolymer (Z-ELP) for mAb capture and precipitation. However, the high temperature and salt concentrations and the heating/cooling steps required for reversible Z-ELP phase transition impacted antibody stability and operational efficiency. We proposed a two-part solution: Increase the affinity ligand multivalency and dimension by scaffolding Z-ELP to a nanoparticle using site-specific conjugation. We hypothesized that this would enable primary effect mAb-nanoparticle crosslinking, while also improving ELP precipitation by enlarging the scale of aggregate formation.

The first objective was to engineer and characterize the functionalization of Z-ELP to a self-assembled, thermostable E2 nanocage (Z-ELP-E2), derived from *Bacillus stearothermophilus* using Staphylococcal Sortase A bioconjugation. We demonstrated a significant decrease in ELP transition temperature and an increase in aggregate size upon antibody binding at isothermal solution conditions. We concluded this was due to multivalent antibody-Z-ELP-E2 interactions that nucleated into a crosslinked network. The second objective was to develop an affinity precipitation process capable of purifying industrial monoclonal antibodies at ambient temperature with minimal added salt. We discovered that the nanoparticles rapidly aggregated upon mixing with mAb cell culture harvests due to multivalent crosslinking into large, insoluble particles. After optimization of key process steps, the affinity precipitation mAb yield and impurity clearance was found to be comparable to Protein A chromatography performance.

The third objective of the research was to establish a platform that can be applied to any target mAb or F_c-containing protein with minimal optimization of process parameters. Z-ELP-E2 affinity precipitation was evaluated using four industrial mAbs (mAbs A–D) and one F_c fusion protein (F_c A) with different molecular properties. For all molecules, a molar binding ratio of 3:1 Z:mAb was sufficient to precipitate > 95% mAb in solution at ambient temperature and without added salt. After centrifugation, the pelleted mAb-nanoparticle complex remained insoluble, and was capable of being washed at pH ≥ 5 and eluted at pH < 4 with > 90% mAb recovery for all molecules. The target proteins were purified using optimal process conditions and > 94% yield and > 97% monomer content were obtained. mAb A–D purification resulted in a reduction of 99.9% host cell protein (HCP) and > 99.99% DNA from the cell culture harvests.

However, Z-ELP-E2 regeneration yields of < 90 % limited the potential for reuse in subsequent purification cycles.

We suspected the regeneration yield may be improved by increasing the ligation density of Z-ELP on the E2 nanocage. Low conjugation efficiency was observed for the Sortase A functionalized nanoparticles due to the reversible nature of enzymatic Sortase A ligation. A 5-fold molar excess Z-ELP reactant was required to drive the reaction to a maximum conversion of ~50%. In our fourth research objective, we report an improved conjugation system using the split SpyTag/SpyCatcher isopeptide bond formation between SpyTag-E2 and Z-ELP-SpyCatcher fusion proteins. E2 ligation efficiencies exceeding 90% enabled the production of nanocages at any target Z-ELP density for tunable aggregation and mAb binding properties. 100% ligation Z-ELP₈₀-Spy-E2 nanocages were capable of selective precipitation using 0.1 M ammonium sulfate at 23°C and improved the nanocage regeneration recovery to > 90%.

The fifth research objective was to apply mAb-nanoparticle crosslinking to quantify mAb concentration in cell culture harvests. Existing mAb titer assays typically require expensive equipment or are limited by low-throughput or complicated protocols. We developed a rapid and cost-effective alternative assay by measuring crosslinking-dependent turbidity after mixing 100% ligation Z-ELP₈₀-Spy-E2 nanoparticles with a mAb cell culture sample. A simple logarithmic regression was found to fit ($R^2 = 0.99$) the turbidity data for mAb concentrations between 100-1000 $\mu\text{g/mL}$. The optimized assay procedure was validated using two industrial mAb cell culture harvests and a bridging study with Octet RED96e biolayer interferometry confirmed accurate and reproducible results.

Our final objective and aim of future work is to generalize the nanoparticle crosslinking strategy for the turbidity-based detection or purification of any target protein (monomer or multimer) using functionalized nanobody-ELP affinity ligands. Nanobodies are small, single-domain antibody fragments that can be engineered to bind to target proteins with high specificity. In addition, multiple nanobodies with orthogonal binding motifs on the same target can be identified through common screening methods. We hypothesized that the conjugation of two or more orthogonal binding nanobodies may induce crosslinking with monomeric proteins. We established proof of concept monomeric protein-nanoparticle crosslinking and turbidity-based quantification using a model green fluorescent protein (GFP) and two orthogonal GFP nanobody-ELP₈₀-SpyCatcher functionalized SpyTag-E2 nanoparticles.

Chapter 1

INTRODUCTION

1.1 Therapeutic Monoclonal Antibody Production

Monoclonal antibodies (mAbs) are proteins that consist of an antigen binding region (F_{ab}) and a constant region (F_c) with 2 heavy and light chains connected by disulfide bonds¹. mAbs can function through many different mechanisms, including antagonistic binding to a ligand, modulating cellular signaling pathways, and immune system activation². Because of this versatility, mAbs are a rapidly expanding class of biopharmaceutical therapeutics that target a wide range of diseases including rheumatoid arthritis, lymphoma, and multiple sclerosis³. In 2014, the global revenue of the 47 approved antibody drugs totaled almost \$70 billion, and current projections expect that the sales will exceed \$120 billion by 2020⁴. To meet the increasing demand, recent advancements in upstream processes and scale-up have yielded antibody concentrations over 10 g/L within bioreactors as large as 20,000 L⁵.

This improved upstream cell culture productivity has placed an increased burden on downstream processing⁶, especially the primary mAb capture step, Protein A affinity chromatography⁷. The protein A ligand, derived from a gene in *Staphylococcus aureus*, binds to the heavy chains in the F_c region of human immunoglobulin G (IgG) at a 2:1 stoichiometric ratio⁸. For decades, Protein A has been widely recognized as the gold standard in platform mAb purification due to its high selectivity and yield⁹. However,

affinity chromatography has been identified as a potential downstream processing bottleneck due to current limitations on throughput and scale-up¹⁰. In addition, the cost of protein A resin has significantly increased over the last 10 years¹¹ to an estimated \$18,000/L in 2017, and is more than 10-fold more expensive than other chromatography resins¹². These factors have generated increased interest in the investigation of higher throughput and more cost-effective non-chromatographic technologies¹³.

1.2 Protein Purification with Affinity Precipitation

Precipitation is a common bioseparation method used in the purification of proteins. This technique involves the phase transition of target molecules from soluble to insoluble using salts such as ammonium sulfate, polymers such as polyethylene glycol, or organic solvents such as ethanol¹⁴. In some antibody purification processes, precipitation is employed after cell culture harvest to reduce the impurity load on the clarification step and other downstream unit operations¹⁵. However, precipitation lacks target specificity, so it cannot function as a suitable alternative to Protein A chromatography. A similar technique called affinity precipitation is ideal because it can combine the high selectivity of an affinity ligand with the operational benefits of conventional precipitation¹⁶. A typical affinity precipitation process involves the binding of an affinity ligand to a target protein, an environmental trigger to precipitate the complex, a separation of insoluble and soluble solution components, and an elution step to dissociate the complex and recover the purified protein (**Figure 1.1**).

1.2.1 Primary Effect Affinity Ligand Crosslinking

The two design strategies for affinity precipitation phase transition utilize multivalent affinity ligand crosslinking (primary effect) or stimuli-responsive affinity

ligands (secondary effect)¹⁶. Primary effect affinity precipitation involves the binding of polyligands to multimeric target proteins that can crosslink into large aggregates and precipitate out of solution above a critical molecular weight¹⁷. This is beneficial operationally, as the ligand-protein binding event can initiate a phase transition without an external stimulus, but salts, such as ammonium sulfate, are commonly added to increase yields¹⁸. A bis-NAD affinity ligand binding to a dimeric alcohol dehydrogenase has been shown to form linear crosslinks, but poor precipitation yields were obtained due to the formation of smaller oligomers or monomeric binding¹⁹ (**Figure 1.2A**). Higher recovery was obtained through bis-NAD ligand crosslinking with a tetrameric lactate dehydrogenase, because the higher valency facilitated the formation of a larger crosslinked network²⁰ (**Figure 1.2B**). Higher order multivalent affinity ligands (**Figure 1.2C**) can also be used to enhance network formation, but these ligands are restricted by steric constraints and complicated syntheses²¹. Bi- and tri-valent haptens have been demonstrated to crosslink with antibodies into oligomeric aggregates²², but the primary effect strategy remains limited by low precipitation yields, slow dissolution kinetics, and the requirement of an additional separation step after elution to remove the dissociated affinity ligand²³.

1.2.2 Secondary Effect Stimuli-responsive Affinity Ligands

In contrast to primary effect, secondary effect affinity ligands are bifunctional, containing an affinity domain conjugated to a stimuli-responsive domain²⁴. After target protein binding, an environmental stimulus is applied, such as a change in pH, temperature, or salt concentration, to induce phase transition and co-precipitate the complex²⁵ (**Figure 1.3**). mAb purification with secondary effect affinity ligands has been demonstrated using synthetic polymer-protein A conjugates such as a pH

responsive Eudragit S-100²⁶ or temperature responsive poly(N-isopropylacrylamide)²⁷, but these methods may require tedious and expensive chemical synthesis and conjugation steps. Natural biopolymer-protein A or protein G conjugates have also been investigated for mAb purification using temperature responsive elastin-like polypeptides (ELP)²⁸⁻²⁹.

1.3 Antibody Affinity Precipitation with Z-Elastin-Like Polypeptides

Elastin-like polypeptides are biopolymers with unique properties that make them an ideal candidate for use in affinity precipitation. ELPs are composed of a pentameric amino acid repeat sequence of Val-Pro-Gly-X-Gly, where X is a guest residue that can be any amino acid except proline, and can be easily expressed recombinantly in *Escherichia coli*³⁰. ELPs are soluble at room temperature in aqueous buffers, but undergo a reversible phase transition dependent on ELP concentration and the ionic strength and temperature of the solution relative to a critical point called the transition temperature (T_t)³¹. The T_t can be tuned by ELP concentration, ELP chain length, or substitution of a more hydrophilic or hydrophobic guest residue³². Kosmotropic salts such as ammonium sulfate are commonly used for ELP precipitation because they significantly lower the T_t ³³. This salt addition leads to the formation of insoluble aggregates that can be separated from other solution components by centrifugation or filtration (**Figure 1.4**). After pelleting the precipitated ELP, the salt is diluted out and the temperature is lowered to below the T_t , allowing the ELP to resolubilize back into solution in a process termed inverse transition cycling (ITC)³⁴.

A gene encoding a protein of interest can be joined with an ELP sequence, resulting in the expression of an ELP-fusion protein that maintains similar aggregation behavior³⁵. We have previously generated an ELP-fusion with a small (7 kDa) synthetic

domain called the Z-domain derived from the B domain in Protein A³⁶. The smaller molecular weight Z-domain-ELP fusion (Z-ELP) resulted in higher *E. coli* soluble expression than a Protein A-ELP fusion. We demonstrated that Z-ELP can bind to mAbs with high affinity, and that the mAb-Z-ELP complex was precipitated after increasing the salt concentration and temperature of the solution³⁷. Upon resuspending in a low pH buffer at a lower temperature and salt concentration, the mAb was dissociated from the Z-domain and recovered after another Z-ELP phase transition (**Figure 1.5**). However, the requirement of several heating/cooling and liquid handling steps is operationally burdensome, especially at manufacturing scale³⁸. In addition, the use of high temperature and salt concentrations, especially at low pH, may result in an increase in mAb aggregation³⁹⁻⁴⁰ or an increase in the co-precipitation of other cell culture impurities⁴¹. For these reasons, ELP-based affinity precipitation has not been widely adopted as an alternative to chromatography.

1.4 Z-ELP-Nanoparticle Scaffold for Multivalent Crosslinking

To improve upon the existing technology, a Z-ELP affinity ligand that reduces the salt concentration necessary for aggregation at ambient temperature would be ideal for mAb process stability and operational efficiency. The salt concentration required for ELP transition at room temperature can be minimized by increasing ELP chain-length or by substituting a more hydrophobic amino acid guest residue in the ELP sequence⁴². However, these methods are constrained because high soluble expression in *E. coli* is limited to 250 repeats⁴³ and ELPs with highly hydrophobic guest residues are more difficult to re-solubilize, resulting in a yield loss of the target protein⁴⁴. We proposed an alternative two-part strategy: We suspected that Z-ELP-based affinity precipitation may be enhanced by increasing the valency and molecular weight of the affinity scaffold via

nanoparticle functionalization. We hypothesized that multivalent interactions between two Z-domains from different nanoparticles binding to one IgG molecule would form a network of crosslinked aggregates (**Figure 1.6**). In addition, the enlarged dimension and high local concentration of scaffolded ELP may lower the salt concentration required for phase transition compared to equal concentrations of free ELP in solution. This strategy would combine the benefits of primary effect crosslinking with secondary effect stimuli responsive behavior.

1.5 E2 Nanocage Functionalization using Sortase A Ligation

Protein-based, nanometer scale scaffolds such as multi-enzyme complexes or viral capsids are ideal nanoparticles because they self-assemble from small subunits and permit the functionalization of specific regions on their surface⁴⁵. One scaffold of interest is the E2 nanocage of the pyruvate dehydrogenase enzyme complex from *Bacillus stearothermophilus*. Sixty identical E2 monomers self-assemble into a thermostable ($T_m > 80^\circ\text{C}$) 25-nm dodecahedron structure with three exposed N-terminal loops at each of the twenty vertices⁴⁶. Assembly of a modified, E2 core subunit has been demonstrated after recombinant expression in *E. coli*⁴⁷. E2's large surface display and flexible structure provides an ideal scaffold for functionalization. However, genetic fusions or modifications to exterior N-terminus of the E2 monomer resulted in inclusion bodies and required a series of denaturing and refolding steps to retain proper assembly⁴⁸.

In vitro conjugation methods after protein isolation are often performed when genetic fusion is not possible⁴⁹. Chemical conjugation is one common technique used to functionalize proteins, but drawbacks include a loss of activity and a lack of control of specificity and orientation⁵⁰. Furthermore, click-chemistry has been studied for site-

specific functionalization, but this technique involves the incorporation of an unnatural amino acid that may lower soluble expression productivity⁵¹.

Sortase A ligation is an enzymatic bioconjugation method derived from Staphylococcal Sortase A, a bacterial transpeptidase that covalently attaches proteins to the bacterial cell wall by catalyzing the condensation reaction between a C-terminal LPXTG motif and an N-terminal polyglycine tag, resulting in the formation of an amide bond in a site-specific manner⁵². Sortase A is ideal for conjugating biomolecules because the enzyme is active at mild pH (7-9) and temperature (25-37°C) and can be expressed recombinantly in *E. coli*⁵³. We recently demonstrated site-specific conjugation of LPETG-tagged fusion proteins to GGG-E2 nanocages without impacting E2 assembly⁵⁴ and investigated this platform as a modular scaffold for biomolecular sensing⁵⁵.

1.6 Dissertation Objectives

We investigated the engineering, development, and application of an enhanced affinity precipitation process using Z-ELP functionalized E2 nanoparticle crosslinking as an alternative capture step for the purification of mAbs. The specific objectives of this dissertation are:

1. Engineer and characterize the functionalization of Z-ELP affinity ligands to E2 nanoparticles using Sortase A ligation and demonstrate antibody binding-induced crosslinking (**Chapter 2**).
2. Develop a high-yielding affinity precipitation process with an industrial mAb through optimization of process variables and compare purification performance to Protein A chromatography (**Chapter 3**).
3. Apply the optimized affinity precipitation process to the purification of five industrial molecules with different properties and establish a platform that may be applied to any Fc-containing protein with minimal optimization of process parameters (**Chapter 4**).
4. Improve the nanoparticle conjugation efficiency using SpyTag/SpyCatcher isopeptide bond formation for increased Z-ELP multivalency and characterize the effects of ligand density on mAb-nanoparticle binding and crosslinking properties (**Chapter 5**).
5. Apply mAb-nanoparticle crosslinking properties to develop a rapid and convenient method for the quantification of mAb titer in cell culture harvests using a concentration dependent turbidity assay (**Chapter 6**).
6. Generalize the nanoparticle crosslinking strategy for the detection or purification of any target protein (monomer or multimer) using functionalized orthogonal nanobody-ELP affinity ligands (**Chapter 7**).

FIGURES

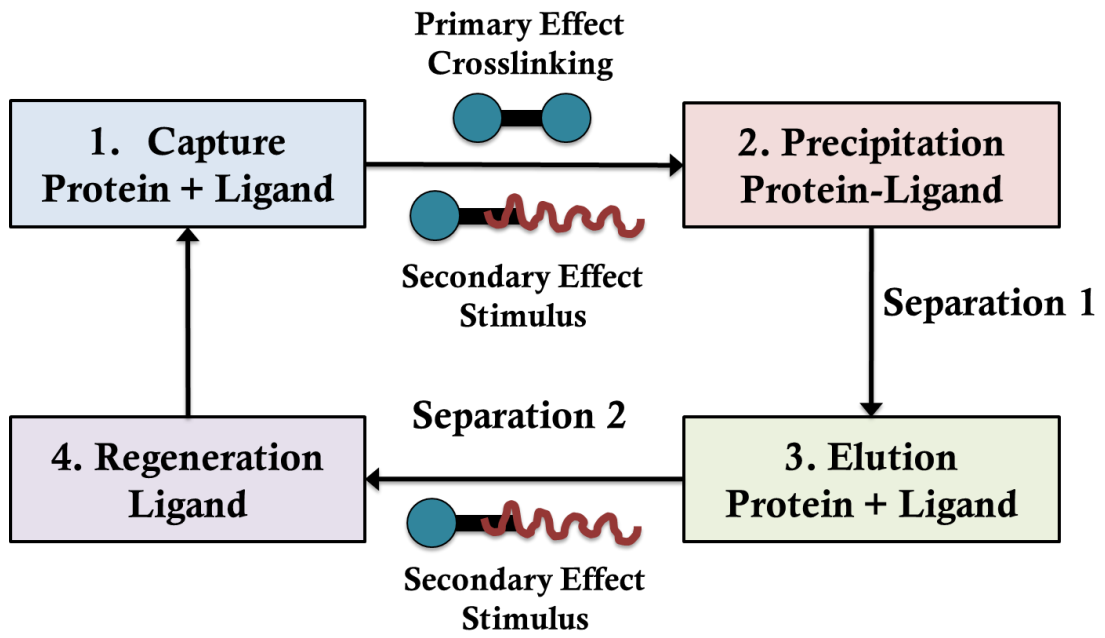


Figure 1.1 Affinity precipitation process for protein purification.

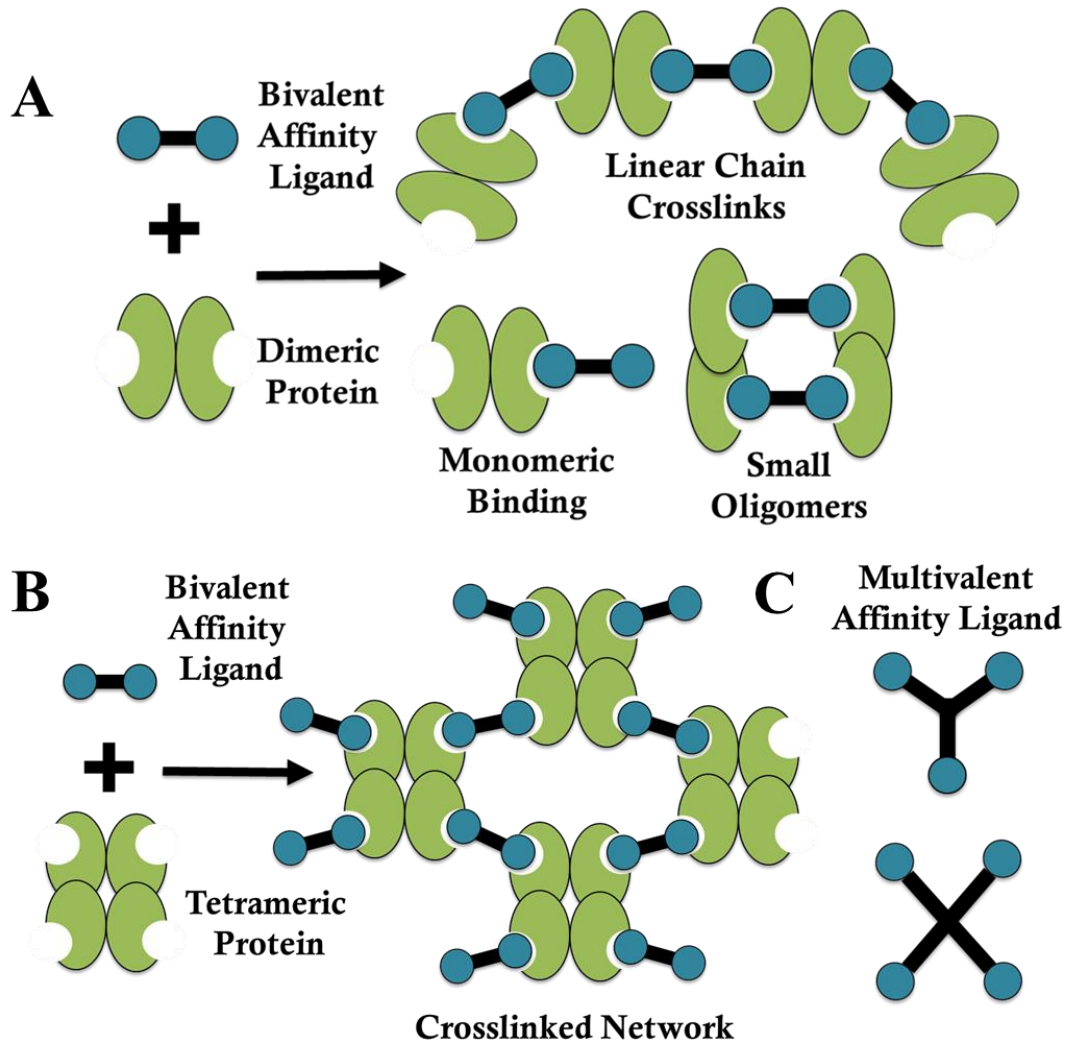


Figure 1.2 Effect of valency on primary effect affinity precipitation. A) Bivalent affinity ligand mixed with dimeric protein. B) Bivalent affinity ligand mixed with tetrameric protein. C) Multivalent affinity ligands.

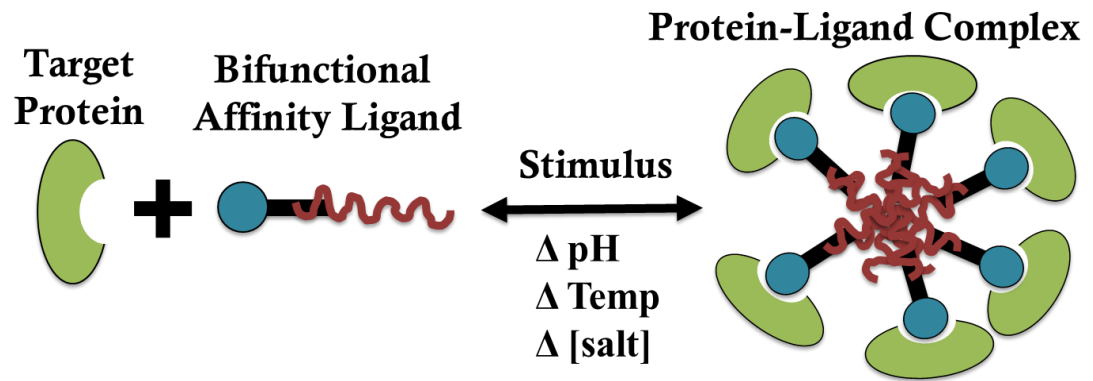


Figure 1.3 Secondary effect affinity precipitation with a stimuli-responsive bifunctional affinity ligand.

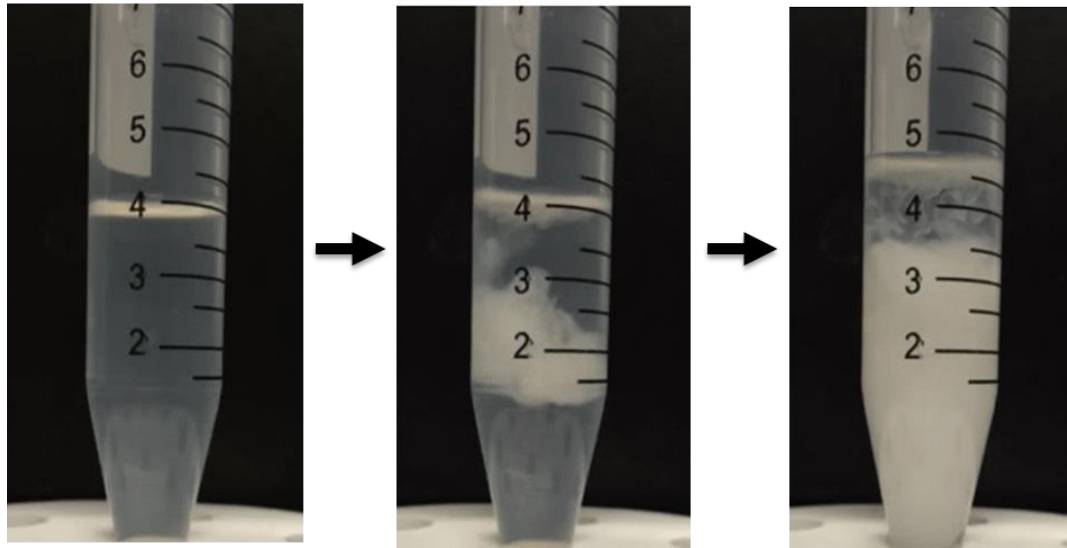


Figure 1.4 Elastin-like polypeptide aggregation after addition of 0.5 M ammonium sulfate.

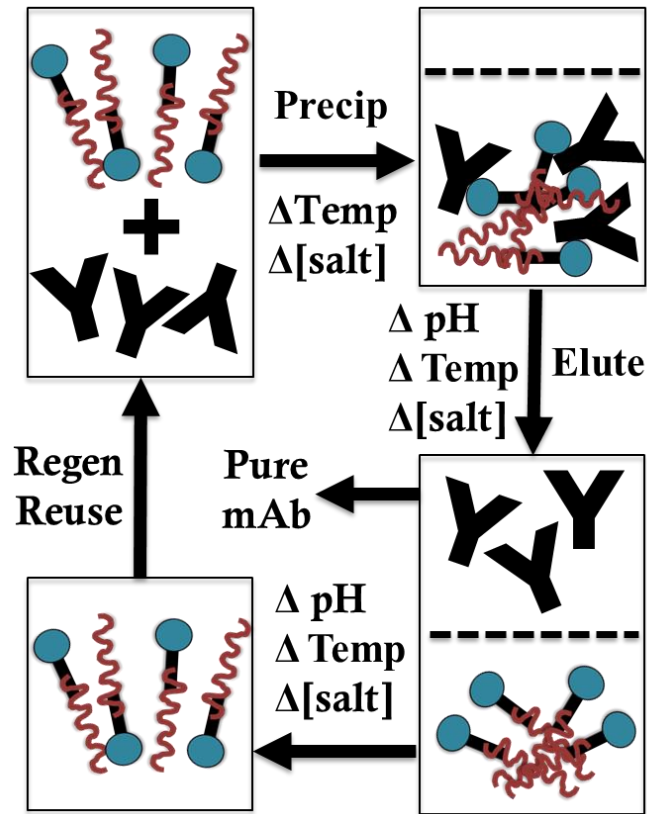


Figure 1.5 mAb purification by Z-ELP secondary effect affinity precipitation.

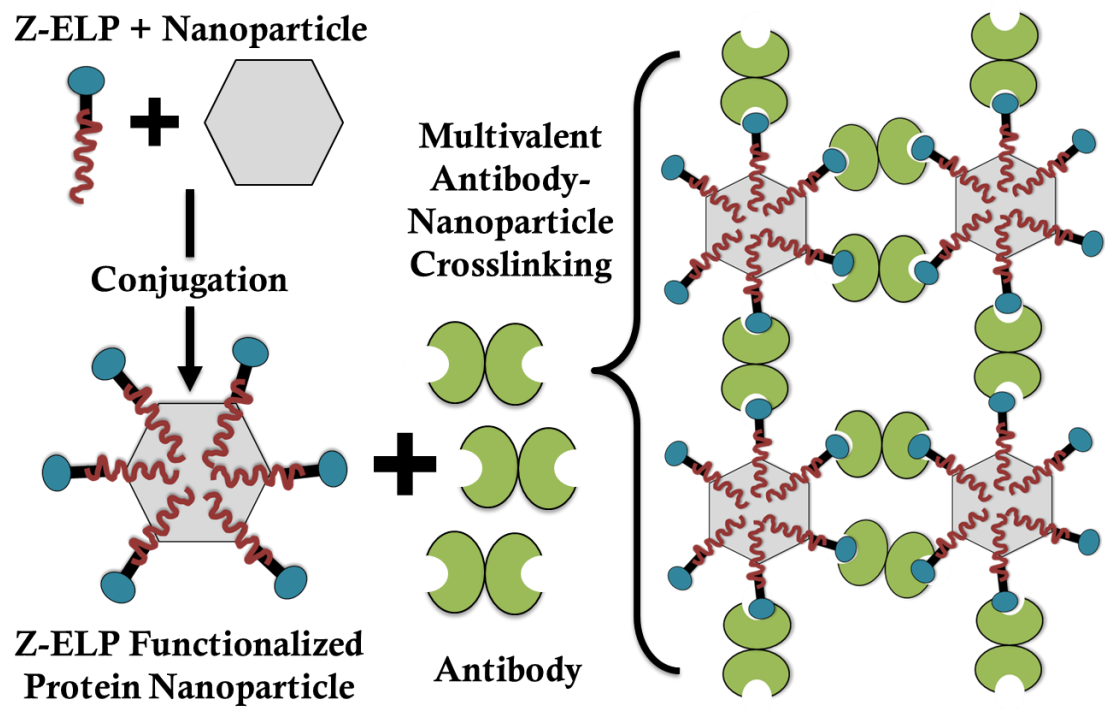


Figure 1.6 Strategy for antibody-nanoparticle crosslinking with multivalent Z-ELP functionalized nanoparticles

REFERENCES

1. L. W. Arbogast, R. G. Brinson and J. P. Marino. Mapping Monoclonal Antibody Structure by 2D ¹³C NMR at Natural Abundance. *Analytical Chemistry* **2015**, 87(7):3556-3561.
2. T. T. Hansel, H. Kropshofer, T. Singer, J. A. Mitchell and A. J. George. The safety and side effects of monoclonal antibodies. *Nat Rev Drug Discov* **2010**, 9(4):325-338.
3. A. Beck, T. Wurch, C. Baily and N. Corvaia. Strategies and challenges for the next generation of therapeutic antibodies. *Nat Rev Immunol* **2010**, 10:345-352.
4. S. D. Ecker, D. Jones and H. Levine. The therapeutic monoclonal antibody market. *mAbs* **2015**, 7(1):9-14.
5. Y.-M. Huang, W. Hu, E. Rustandi, K. Chang, H. Yusif-Makagiansar and T. Ryll. Maximizing productivity of CHO cell-based fed-batch culture using chemically defined media conditions and typical manufacturing equipment. *Biotechnol Prog* **2010**, 26(5):1400-1410.
6. J. H. Chon and G. Zarbis-Papastoitsis. Advances in the production and downstream processing of antibodies. *New Biotechnol* **2011**, 28:458-463.
7. A. A. Shukla and J. Thommes. Recent advances in large-scale production of monoclonal antibodies and related proteins. *Trends Biotechnol* **2010**, 28(5):253-261.
8. S. Lofdahl, B. Guss, M. Uhlen, L. Philipson and M. Linberg. Gene for staphylococcal protein A. *PNAS* **1983**, 80:697-701.
9. S. M. Ghose, M. Allen, B. Hubbard, C. Brooks and S. M. Cramer. Antibody variable region interactions with Protein A: implications for the development of generic purification processes. *Biotechnol Bioeng* **2010**, 96(6):665-677.
10. P. Gronemeyer, R. Ditz and J. Strube. Trends in upstream and downstream process development for antibody manufacturing. *Bioengineering* **2014**, 1:188-212.

11. D. Low, R. O'Leary and N. S. Pujar. Future of antibody purification. *J Chromatogr B* **2007**, 848(1):48-63.
12. N. Hammerschmidt, A. Tscheliessnig, R. Sommer, B. Helk and A. Jungbauer. Economics of recombinant antibody production processes at various scales: Industry-standard compared to continuous precipitation. *Biotechnology Journal* **2014**, 9:766-775.
13. J. Thömmes and M. Etzel. Alternatives to chromatographic separations. *Biotechnology Progress* **2007**, 23(1):42-45.
14. R. R. Burgess. Protein precipitation techniques. *Methods Enzymol* **2009**, 463:331-342.
15. H. F. Liu, J. Ma, C. Winter and R. Mayer. Recovery and purification process development for monoclonal antibody production. *mAbs* **2010**, 2(5):480-499.
16. F. Hillbrig and R. Freitag. Protein purification by affinity precipitation. *Journal of Chromatography B* **2003**, 790(1):79-90.
17. J. E. Morris, A. S. Hoffman and R. R. Fisher. Affinity precipitation of proteins by polyligands. *Biotechnology and Bioengineering* **1993**, 41(10):991-997.
18. K. A. Mirca, M. R. Lockett, P. W. Snyder, N. D. Shapiro, E. T. Mack, S. Nam and G. M. Whitesides. Selective precipitation and purification of monovalent proteins using oligovalent ligands and ammonium sulfate. *Bioconjugate Chemistry* **2012**, 23:293-299.
19. S. Flygare, T. Griffin, P. O. Larsson and K. Mosbach. Affinity precipitation of dehydrogenases. *Anal Biochem* **1993**, 133(2):409-416.
20. J. A. Irwin and K. F. Tipton. Affinity precipitation: a novel approach to protein purification. *Essays Biochem* **1995**, 29:137-156.
21. M. I. Monine, R. G. Posner, P. B. Savage, J. R. Faeder and W. S. Hlavacek. Modeling multivalent ligand-receptor interactions with steric constraints on configurations of cell-surface receptor aggregates. *Biophysical Journal* **2010**, 98(1):48-56.
22. B. Bilgicer, S. W. Thomas III, B. F. Shaw, G. K. Kaufman, V. M. Krishnamurthy, L. A. Estroff, J. Yang and G. M. Whitesides. A non-chromatographic method for the purification of a bivalently active monoclonal IgG antibody from biological fluids. *Journal of American Chemical Society* **2009**, 131(26):9361-9367.

23. J. C. Pearson, Y. D. Clonis and C. R. Lowe. Preparative affinity precipitation of L-lactate dehydrogenase. *Journal of Biotechnology* **1989**, 11(2):267-274.
24. M. N. Gupta, R. Kaul, D. Guogiang, U. Dissing and B. Mattiasson. Affinity precipitation of proteins. *J Mol Recognit* **1996**, 9(5):356-359.
25. B. Mattiasson, A. Kumar and I. Y. Galaev. Affinity precipitation of proteins: design criteria for an efficient polymer. *J Mol Recognit* **1998**, 11(1):211-216.
26. L. Janoschek, M. F. von Roman and S. Berensmeier. Protein A affinity precipitation of human immunoglobulin G. *Journal of Chromatography B* **2014**, 965:72-78.
27. J. P. Chen and A. S. Huffman. Polymer-protein conjugates: II. Affinity precipitation separation of human immunoglobulin by a poly(N-isopropylacrylamide)-protein A conjugate. *Biomaterials* **1990**, 11(9):631-634.
28. J.-Y. Kim, S. O'Malley, A. Mulchandani and W. Chen. Genetically engineered elastin-protein A fusion as a universal platform for homogeneous, phase-separation immunoassay. *Analytical Chemistry* **2005**, 77:2318-2322.
29. J.-Y. Kim, A. Mulchandani and W. Chen. Temperature-triggered purification of antibodies. *Biotechnol Bioeng* **2005**, 90:373-379.
30. A. Chilkoti, T. Christensen and J. A. MacKay. Stimulus responsive elastin biopolymers: applications in medicine and biotechnology. *Cur Op Chem Bio* **2006**, 10(6):652-657.
31. D. L. Nettles, A. Chilkoti and L. A. Setton. Applications of elastin-like polypeptides in tissue engineering. *Adv Drug Deliv Rev* **2010**, 62(15):1479-1485.
32. D. W. Urry. Physical chemistry of biological free energy transduction as demonstrated by elastic protein-based polymers. *J Phys Chem B* **1997**, 101(51):11007-11028.
33. Y. Cho, Y. Zhang, T. Christensen, L. B. Sagle, A. Chilkoti and P. S. Cremer. Effects of Hofmeister anions on the phase transition temperature of elastin-like polypeptides. *J Phys Chem B* **2008**, 112(44):13765-13771.
34. D. E. Meyer and A. Chilkoti. Purification of recombinant proteins by fusion with thermally-responsive polypeptides. *Nat Biotechnol* **1999**, 17(11):1112-1115.
35. T. Christensen, W. Hassouneh, K. Trabbic-Carlson and A. Chilkoti. Predicting transition temperatures of elastin-like polypeptide fusion proteins. *Biomacromolecules* **2013**, 14(5):1514-1519.

36. B. Madan, G. Chaudhary, S. M. Cramer and W. Chen. ELP-z and ELP-zz capturing scaffolds for the purification of immunoglobulins by affinity precipitation. *Journal of Biotechnology* **2013**, 163(1):10-16.
37. R. D. Sheth, M. Jin, B. V. Bhut, Z. Li, W. Chen and S. M. Cramer. Affinity precipitation of a monoclonal antibody from an industrial harvest feedstock using an ELP-Z stimuli responsive biopolymer. *Biotechnology and Bioengineering* **2014**, 111(8):1595-1603.
38. D. Petrides, D. Carmichael, C. Siletti and A. Koulouris. Biopharmaceutical process optimization with simulation and scheduling tools. *Bioengineering* **2014**, 1(4):154-187.
39. R. D. Sheth, B. Madan, W. Chen and S. M. Cramer. High-throughput screening for the development of a monoclonal antibody affinity precipitation step using ELP-Z stimuli responsive biopolymers. *Biotechnology and Bioengineering* **2013**, 110(10):2664-2676.
40. P. Arioso, B. Jaquet, M. Wu and M. Morbidelli. On the role of salt type and concentration on the stability behavior of a monoclonal antibody solution. *Biophysical Chemistry* **2012**, 168:19-27.
41. P. Gagnon. Technology trends in antibody purification. *Journal of Chromatography A* **2012**, 1221:57-70.
42. D. E. Meyer and A. Chilkoti. Quantification of the effects of chain length and concentration on the thermal behavior of elastin-like polypeptides. *Biomacromolecules* **2004**, 5(3):846-851.
43. D. T. McPherson, J. Xu and D. W. Urry. Product purification by reversible phase transition following Escherichia coli expression of genes encoding up to 251 repeats of the elastomeric pentapeptide GVGVP. *Prot Expr Purif* **1996**, 7(1):51-57.
44. D. W. Lim, K. Trabbic-Carlson, A. MacKay and A. Chilkoti. Improved non-chromatographic purification of a recombinant protein by cationic elastin-like polypeptides. *Biomacromolecules* **2008**, 8(5):1417-1424.
45. M. Raeeszadeh-Sarmazdeh, E. Hartzell, J. V. Price and W. Chen. Protein nanoparticles as multifunctional biocatalysts and health assessment sensors. *Current Opinion in Chemical Engineering* **2016**, 13:109-118.
46. H. Z. Zhou, D. B. McCarthy, C. M. O'Connor, L. J. Reed and J. K. Stoops. The remarkable structural and functional organization of the eukaryotic pyruvate dehydrogenase complexes. *PNAS* **2001**, 98(26):14801-14807.

47. M. Dalmau, S. Lim, H. C. Chen, C. Ruiz and S.-W. Wang. Thermostability and molecular encapsulation within an engineered caged protein scaffold. *Biotechnology and Bioengineering* **2008**, 101(4):654-664.
48. G. J. Domingo, S. Orru and R. N. Perham, "Multiple display of peptides and proteins on a macromolecular scaffold derived from a multienzyme complex. *J Mol Biol* **2001**, 305(2):259-267.
49. R. van Vught, R. J. Pieters and E. Breukink. Site-specific functionalization of proteins and their applications to therapeutic antibodies. *Computation and Structural Biotechnology Journal* **2014**, 9(14):e20140.
50. K. Tsuchikama and Z. An. Antibody-drug conjugates: recent advances in conjugation and linker chemistries. *Protein & Cell* **2018**, 9:33-46.
51. K. G. Patel and J. R. Swartz. Surface functionalization of virus-like particles by direct conjugation using azide-alkyne click chemistry. *Bioconjugate Chemistry* **2011**, 22(3):376-387.
52. T. Tanaka, T. Yamamoto, S. Tsukiji and T. Nagamune. Site-specific protein modification on living cells catalyzed by sortase. *ChemBioChem* **2008**, 9:802-807.
53. D. A. Levary, R. Parthasarathy, E. T. Boder and M. E. Ackerman. Protein-protein fusion catalyzed by Sortase A. *PLOS One* **2011**, 6(4):e18342.
54. Q. Chen, Q. Sun, N. M. Molino, S.-W. Wang, E. T. Boder and W. Chen. Sortase A-mediated multi-functionalization of protein nanoparticles. *Chemical Communications* **2015**, 51:12107-12110.
55. Q. Sun, D. Blackstock and W. Chen. Post-translational modification of bionanoparticles as a modular platform for biosensor assembly. *ACS Nano* **2015**, 9(8):8554-8561.

Chapter 2

ANTIBODY BINDING INDUCED CROSSLINKING OF Z-DOMAIN-ELASTIN-LIKE-POLYPEPTIDE FUNCTIONALIZED E2 NANOPARTICLES

Abstract

Affinity precipitation is an ideal alternative to chromatography for antibody purification because it combines the high selectivity of an affinity ligand with the operational benefits of precipitation. However, the widespread use of elastin-like polypeptide (ELP) capture scaffolds for antibody purification has been hindered by the high salt concentrations and temperatures necessary for efficient ELP aggregation. In Chapter 2, we employed a tandem approach to enhance ELP aggregation by enlarging the dimension of the capturing scaffold and by creating IgG-triggered scaffold crosslinking. This was accomplished by covalently conjugating the Z-domain-ELP (Z-ELP) capturing scaffold to a 25-nm diameter E2 protein nanocage using Sortase A ligation. We demonstrated the isothermal recovery of IgG in the virtual absence of salt due to the significantly increased scaffold dimension and crosslinking from multi-valent IgG-E2 interactions. Since IgG crosslinking is reversible at low pH, it may be feasible to achieve a high yielding IgG purification by isothermal phase separation using a simple pH trigger.

Chapter 2 is reproduced with permission from American Chemical Society. Source:

Swartz AR, Sun Q, Chen W. Ligand-induced crosslinking of Z-ELP-functionalized E2 protein nanoparticles for enhanced affinity precipitation of antibodies. *Biomacromolecules* **2017**, 18(5):1654-1659.

2.1 Introduction

Monoclonal antibodies (mAbs) represent a rapidly expanding class of biopharmaceutical therapeutics¹, and the global market is expected to exceed \$120 billion by 2020². This increasing demand has placed a significant burden on the downstream purification platform. The initial capture step, Protein A affinity chromatography, has been especially impacted due to limitations in throughput, scale-up, and cost^{3,4}. This potential production bottleneck has generated increased interest in non-chromatographic capture technologies.

As discussed in Chapter 1, affinity precipitation is an ideal alternative to chromatography because it combines the high selectivity of an affinity ligand with the operational benefits of precipitation⁵. Thermally responsive synthetic polymers have been implemented for antibody affinity precipitation, but the production of these polymers requires tedious and expensive chemical synthesis steps^{6,7}. In contrast, elastin-like polypeptides (ELPs) are environmentally responsive biopolymers that can be easily produced by recombinant hosts^{8,9}, and a wide range of binding partners have been genetically fused to ELP without impacting either the inverse phase transition property or the affinity interaction¹⁰⁻¹³.

We have previously fused a small (7 kDa) immunoglobulin G (IgG)-binding Z-domain derived from Protein A to ELP (Z-ELP) for mAb purification¹⁴. However, this system was limited by the high salt concentrations and temperatures necessary to ensure the formation of large, insoluble aggregates for efficient recovery by centrifugation. In addition, exposure to these harsh solution conditions resulted in increased mAb aggregation and loss of activity¹⁵⁻¹⁷. One way to achieve larger aggregate sizes without requiring an increase in salt or temperature is to enlarge the dimension and valency of the capturing scaffold^{18,19}. Our group has recently demonstrated the feasibility of

attaching multiple proteins onto the E2 core of the pyruvate dehydrogenase complex from *Bacillus stearothermophilus*, a genetically-modifiable, thermostable 25 nm diameter 60-mer protein nanocage, by sortase A (SrtA)-mediated ligation²⁰. SrtA is ideal for conjugating biomolecules because it is active at mild solution conditions, utilizes small N (GGG-) and C (-LPETG) terminal recognition motifs, and is easily expressed in *E. coli*²¹. We hypothesize that ligating Z-ELP onto E2 nanocages will enable the precipitation of bound IgG at much lower salt concentrations and/or temperatures because of the significantly increased dimension and crosslinking from multi-valent IgG-nanocage interactions (**Figure 2.1**).

2.2 Materials and Methods

2.2.1 Materials

Escherichia coli strain BLR(DE3) containing pET24(a) vectors encoding for Z-ELP[KV8F-40]-LPETG and ELP[KV8F-40]-LPETG were constructed and described previously²². *E. coli* strain BL21(DE3) containing a pET11(a) vector encoding for GGG-E2(158) and another BL21(DE3) strain containing a pMR5 vector encoding for SrtA enzyme were constructed and described previously²⁰. Human polyclonal IgG was purchased from Sigma-Aldrich (St. Louis, MO). Bacto tryptone and yeast extract were purchased from BD Biosciences (Franklin Lakes, NJ). Glycerol, kanamycin, ampicillin, isopropyl- β -D-thiogalactoside (IPTG), calcium chloride and sodium chloride were purchased from Fisher Scientific (Pittsburgh, PA). Sodium hydroxide, potassium mono and dibasic phosphate, sodium phosphate dibasic, bovine serum albumin (BSA), L-arginine, tris base, and ammonium sulfate were purchased from Sigma-Aldrich (St.

Louis, MO). 100 kDa Vivaspin 20 columns were purchased from Sartorius Stedim (Gottingen, Germany).

2.2.2 Protein Expression and Purification

Z-ELP[KV8F-40]-LPETG and ELP[KV8F-40]-LPETG were expressed in BLR(DE3) *E. coli* cells grown in Terrific Broth medium (TB) with 50 µg/mL kanamycin at 37°C and 250 rpm for 24 h with leaky expression. SrtA was expressed in BL21(DE3) *E. coli* cells grown in Luria-Bertani Medium (LB) with 50 µg/mL kanamycin at 37°C and 250 rpm until an OD600 of 1.0, where the culture was induced with 1 mM IPTG and subsequently incubated at 37°C for 4 h. GGG-E2 was expressed in BL21(DE3) *E. coli* cells grown in LB with 100 µg/mL ampicillin at 37°C and 250 rpm until an OD600 of 0.5, where the culture was induced with 0.2 mM IPTG and subsequently incubated at 20°C for 20 hours. After protein expression, all cultures were harvested by centrifugation at 4,000g for 15 min at 4°C and resuspended in a tris buffer (50 mM Tris, 150 mM sodium chloride, pH 8.0). Cells were lysed using a Fisher Sonicator (Pittsburgh, PA) using 5 s pulse on and 10 s pulse off for 10 min over ice. Soluble lysate was separated by centrifugation at 15,000 g for 20 min at 4°C. ELPs were purified using 2-3 rounds of inverse transition cycling (ITC) as described previously⁹ using 0.5 M ammonium sulfate for precipitation and were resuspended in the tris buffer. The concentration of purified ELP was determined by measuring absorbance at 280 nm on a Shimadzu UV-1800 spectrophotometer (Kyoto, Japan). The thermostable GGG-E2 cage was purified by incubating at 70°C for 10 min to precipitate contaminant proteins. The soluble E2 was separated by centrifugation at 15,000 xg for 15 min. The protein concentrations of purified GGG-E2 and soluble SrtA lysate were measured by Bradford protein assay purchased from Bio-Rad (Hercules, CA) using BSA as a

standard. Protein expression was confirmed by Coomassie stained, 10% acrylamide SDS-PAGE using a Bio-Rad Mini-PROTEAN electrophoresis system (Hercules, CA). Protein purity was estimated using densitometry analysis of SDS-PAGE gels using Thermo MyImage software (Waltham, MA).

2.2.3 Sortase A Mediated Ligation

Ligation of ELP-LPETG or Z-ELP-LPETG to the E2 cage was catalyzed by the SrtA enzyme. Target molar ratios of ELP-LPETG, GGG-E2 and SrtA were added to a reaction buffer consisting of 50 mM tris, 150 mM sodium chloride, 6 mM calcium chloride, pH 8.0 in a centrifuge tube. The reaction mixture was incubated at 37°C for 4 hr. The ligation product was purified using one round of ITC using 1 M ammonium sulfate and was resuspended in phosphate buffered saline (PBS; 137 mM NaCl, 2.7 mM KCl, 10 mM Na₂HPO₄, 2 mM KH₂PO₄, pH 7.4). The excess, unreacted ELP was removed by 100 kDa diafiltration into PBS using Sartorius Vivaspin 20 spin columns. The purified Z-ELP-E2 or ELP-E2 nanocage was confirmed by Coomassie stained 10% acrylamide SDS-PAGE and ELP ligation density was estimated using densitometry analysis using Thermo MyImage software (Waltham, MA). The ligation products were characterized by the transition temperature (T_t) evaluated using UV spectroscopy on a Shimadzu UV-1800 spectrophotometer (Kyoto, Japan), by dynamic light scattering (DLS) using a Malvern Zetasizer Nano (Malvern, United Kingdom) with a 4 mW He Ne gas laser at 632.8 nm and a 175° scattering angle and by transmission electron microscopy (TEM) with a Zeiss Libra 120 Electron Microscope (Oberkochen, Germany) using 2% uranyl acetate staining on a carbon coated grid from Electron Microscopy Sciences (Hatfield, PA). All statistical analyses were performed using Minitab 17 (State College, PA).

2.2.4 Transition Temperature Measurement

Equal concentrations of free Z-ELP and ligated Z-ELP were prepared at 4°C in PBS with target ammonium sulfate concentrations (0, 0.1, 0.2, 0.3, 0.5 M) or with human polyclonal IgG at a 5:1 Z:IgG molar ratio and were incubated either at 4°C or 20°C for 1-2 hours. After the incubation time, samples were added to an 8-well multicell 100 µL microcuvette (Shimadzu) and the absorbance at 350 nm was measured every 0.5 degrees from either 4-50°C or 20-65°C at a ramp rate of 0.5 degree per min with a 20 second equilibration before each measurement. Three separate measurements were performed for each condition and the T_t was calculated by evaluating the maximum slope of the transition curve. The T_t and absorbance profile analyzed by the provided Tm Analysis Software (Shimadzu) was extracted from each measurement. Two-sample t-tests were employed to determine the statistical significance of the hypothesized difference of T_t s.

2.2.5 Dynamic Light Scattering Measurement

Three replicate DLS measurements were taken using a low volume cuvette (ZEN0040, Malvern) for each sample consisting of 5 runs of 10 s using the settings sample = protein (RI = 1.45, Absorption = 0.001), and dispersant = water (RI = 1.33). The correlation function was analyzed by the Protein Analysis algorithm provided by the Malvern software. The hydrodynamic diameter (Z-ave), polydispersity index, and volume distributions were extracted from each measurement. For the kinetic experiments, equal concentrations of both free Z-ELP and Z-ELP ligated to E2 cages were prepared with a human polyclonal IgG at a 5:1 Z:IgG molar ratio in PBS at 25°C. Samples containing free ELP (with no Z-domain) and ELP ligated to E2 cage were also prepared with IgG at a 5:1 ratio as a control. Immediately after preparing each sample,

the hydrodynamic radius was measured at 25°C and then measured again at approximately 10-20 min intervals over the next 90 min while keeping all samples at 25°C. For all other DLS experiments, samples were prepared in PBS with target ammonium sulfate concentrations or with IgG at a 5:1 Z:IgG molar ratio and incubated at 23°C for 1-2 h before each measurement.

2.2.6 Antibody Affinity Precipitation

IgG affinity precipitation yield was compared between free Z-ELP and Z-ELP ligated to the E2 nanocage at different salt concentrations. First, equal molar concentrations of free Z-ELP and ELP, and ligated Z-ELP-E2 and ELP-E2 cages were mixed with human polyclonal IgG at a 5:1 molar ratio in PBS and incubated at 23°C for two hours in microcentrifuge tubes. ELP and ELP-E2 (no Z-domain) were used as controls. Second, the complex was precipitated using increasing concentrations of ammonium sulfate (0.1, 0.25, and 0.5 M) and incubated at 23°C for 10 minutes. The solution was centrifuged for 10 min at 15,000g at 23°C to pellet the precipitate. Third, the supernatant was removed and the pellet was resuspended in elution buffer (0.5 M arginine, pH 3.7) and incubated for one hour at 4°C. A second precipitation was performed using 1 M ammonium sulfate for all experimental conditions to precipitate the ELP. Upon another centrifugation, the IgG was separated in the supernatant from the ELP in the pellet. Bradford assay was used to quantify IgG recoveries using a standard curve prepared with known IgG concentrations. All experimental samples were run in triplicate.

2.2.7 Turbidity Measurement

Turbidity was measured by absorbance at 350 nm using a Synergy H4 microplate reader purchased from Biotek (Winooski, VT). Samples were prepared with equal concentrations of free and ligated Z-ELP and were mixed with human polyclonal IgG at a 5:1 molar ratio in PBS and incubated at 23°C for two hours in microcentrifuge tubes. After the initial incubation, samples were adjusted to 0.5 M ammonium sulfate and pelleted by centrifugation at 15,000 g. Samples were resuspended back in PBS and incubated for 1 h and 3 days at 4°C with mixing. After incubation, samples were precipitated with 0.5M ammonium sulfate and pelleted by centrifugation at 15,000 g. Samples were resuspended in the elution buffer and incubated at 23°C for 15 min. Turbidity was measured immediately after each sample was taken. All samples were run in triplicate.

2.3 Results and Discussion

2.3.1 Z-ELP functionalization of E2 by sortase A ligation

To enable IgG binding, a new Z-ELP-LPETG fusion protein was created by adding the Z domain to the N-terminus of ELP-LPETG²². A wide range of conditions were tested for expression, and the optimal productivity of >750 mg/L culture was achieved using leaky expression without IPTG addition at 37°C. Highly purified protein was obtained by two rounds of ITC as described previously⁹. GGG-E2 nanocages were expressed and partially purified by heating the cell lysates at 70°C for 10 min as described before²⁰ (**Figure 2.2A**).

Sortase A ligation was performed by incubating the reactants for 4 h in pH 8 buffer with 6 mM CaCl₂ at 37°C. The resulting product was purified using two ITC cycles and filtered using a 100 kDa membrane to remove unreacted ELP, as

characterized by SDS-PAGE (**Figure 2.2B**). TEM and DLS were utilized to confirm the nanocage structure and size using the 60% ligation product as an example. TEM images of a single nanocage and mixture of nanocages (**Figure 2.2C**) depict the expected dodecahedron structure and size consistent with previous characterization²³. From DLS analysis of three ligation products, the samples had a polydispersity <0.3 and an average hydrodynamic diameter of 34.5 ± 2.8 nm. These results indicate that Z-ELP-E2 nanocages can be consistently produced using the indicated procedures.

2.3.2 Effect of Z-ELP-E2 ligation density on nanoparticle properties

We first investigated the impact of ELP-E2 conjugation density on phase transition properties. The initial ligation experiments were performed using ELP:E2 ratios ranging from 1:5 to 5:1 and varying SrtA concentrations. The percentage of Z-ELP ligated onto E2 varied from 25 to 80% as characterized by SDS-PAGE and quantified by densitometry (**Figure 2.3A-B**). The T_t in the absence of any added salt (except for the salt in PBS buffer) was calculated by measuring the absorbance at 350 nm over a temperature gradient from 20-60°C. Consistent with our expectation, higher ELP-E2 ligation densities yielded lower T_t s (**Figure 2.3C**). The T_t was reduced by 20°C by increasing the ELP:E2 ligation density from 25 to 75%. The high ligation density E2 nanocages ($\geq 60\%$) had a T_t over 20°C less than free Z-ELP at the same protein concentration. To further investigate this observation, DLS measurements were performed at the known baseline (0% precipitated), transition (50% precipitated), and peak (100% precipitated) temperatures for a 60% ligation product and free ELP (**Figure 2.3D-E**). Both samples were the expected size at baseline temperature and exhibited a bimodal distribution at the T_t . At its peak temperature of 39°C, the Z-ELP-E2 nanocage was over two orders of magnitude larger than Z-ELP at 39°C and still significantly larger

than Z-ELP at its peak temperature of 61°C. These results support the conclusion that the formation of larger aggregates is a direct result of the larger size of the Z-ELP-E2 nanoparticle scaffold. Moreover, a higher ELP grafting density onto E2 may also increase the local hydrophobicity, resulting in coacervation at reduced temperatures.

It is well known that the T_t of ELP can be significantly lowered by salt addition. Using the 60% ligation Z-ELP-E2 product as an example, the transition property was measured over a wide range of ammonium sulfate concentrations (**Figure 2.4A**). Although the difference in T_t values decreased with increasing salt concentrations, the significant improvement in transition was preserved for the Z-ELP-E2 nanocages. The global nature of the improvement is ideal for affinity precipitation as this allows more flexibility in selecting salt and temperature conditions that maximize recovery. More importantly, the nanocage transition region occurs within a temperature range of < 5°C, as compared to over 15°C for free Z-ELP (**Figure 2.4B**). This observation further suggests the feasibility to achieve complete aggregation of Z-ELP-E2 over a smaller temperature range, a condition essential for IgG recovery.

2.3.3 Enhanced precipitation by antibody-inducible crosslinking

To confirm the IgG-binding capability of Z-ELP-E2 nanocages and to demonstrate the benefit of the lower T_t on IgG recovery, the affinity precipitation process was performed using equal concentrations of either ligated or free Z-ELP and a model polyclonal human IgG at a 5:1 Z:IgG molar ratio. After incubating with IgG for 1 h at 23°C, the complex was precipitated with varying concentrations of ammonium sulfate at ambient temperature followed by elution with a low pH buffer. Control samples consisting of IgG with ELP-E2 and free ELP (no Z-domain) were employed to test for non-specific binding. Independent of salt concentration, the Z-ELP-E2

nanocages significantly improved the antibody yields (**Figure 2.5A**). In comparison, IgG recovery using free Z-ELP decreased precipitously below 0.5 M ammonium sulfate to negligible recovery with 0.1 M salt. SDS-PAGE analysis demonstrated that the initial precipitation step was responsible for the IgG yield loss in the supernatant.

Interestingly, the IgG-nanocage complex with 0.1 M ammonium sulfate was sufficient to precipitate and elute over 80% of the added IgG at 23°C. This result cannot be explained simply by the improved transition property as the nanocage T_t is 30°C in the presence of 0.1 M salt without IgG. It has been shown that ELP domain dimerization can be used to lower the T_t values by increasing the local aggregate size²⁴. Because one IgG molecule can bind two Z domains²⁵, a similar dimerization mechanism likely exists. The addition of IgG can potentially act as a crosslinking agent, resulting in network formation between individual Z-ELP-E2 nanoparticles. This hypothesis was verified by detecting an order of magnitude increase in the particle size of Z-ELP-E2 upon the addition of IgG, while no change in particle size was observed for the control ELP-E2 nanoparticles (**Figure 2.5B**). Only a small increase in particle size was detected for Z-ELP from 8 to 18 nm, consistent with the formation of smaller localized dimers by IgG crosslinking. The addition of salt increased the aggregate size for Z-ELP-E2 by approximately 20-fold, corroborated by the small improvement in IgG recovery. However, the presence of salt significantly increased the aggregate size for Z-ELP, resulting in greater than 100-fold larger particles at 0.5 M ammonium sulfate (**Figure 2.5C**).

Consistent with the spontaneous crosslinking of Z-ELP-E2 nanoparticles by IgG, complete transition was detected for Z-ELP-E2 even at 20°C, while the T_t was lowered by 5-6°C for Z-ELP (**Figure 2.5D**). To investigate whether this dramatic

decrease in T_1 is dependent on the crosslinking density, we evaluated the transition property of a second Z-ELP-E2 conjugate with a significantly lower 35% ligation efficiency. As expected, no visible aggregation was detected upon IgG addition and the T_1 was lowered by a modest 5-6°C with a similar effect observed for Z-ELP (**Figure 2.5D**). This result may be explained by the geometry of the E2 self-assembly. Z-ELP is conjugated to the exterior N-terminus of one of the three E2 subunits existing at each of the 20 vertices of the E2 cage spaced ~5 nm apart²⁰. At each vertex, it has been suggested that the three E2 monomers make hydrophobic contacts with each other at a distance of < 0.5 nm²⁶. A nanocage with 60% ligation density contains an average of two ligated Z-ELP per vertex. Such close proximity may offer an additional crosslinking benefit and may explain why the increase in aggregate size of a low ligation cage (35%) with one Z-ELP per vertex was similar to free Z-ELP after IgG addition (**Figure 2.6A**). These observations highlight the importance of localized network formation on the overall transition property of ELP.

Conventional ELP ITC involves the reversible resolubilization at low salt and temperature after precipitation, a property Z-ELP maintains when bound to IgG, as reflected by the turbidity measurement (**Figure 2.6B**). However, because of the substantial crosslinking, IgG bound Z-ELP-E2 precipitates remained insoluble even after 3 days in PBS at 4°C. This irreversible phase transition enabled the repeated washing in low salt buffers at low temperatures without affecting IgG recovery. Complete resolubilization was only observed after eluting the bound IgG at pH 3.7 (**Figure 2.6B**), indicating the feasibility to achieve IgG purification by isothermal switching of phase separation.

2.4 Conclusion

In conclusion, Chapter 2 presented a new framework to design enhanced IgG-capturing ELP scaffolds by improving aggregation through increased scaffold dimension and IgG-triggered crosslinking. The ability to induce isothermal switching of phase separation by IgG binding significantly minimized the requirement of salt and eliminated the requirement of a heating step. In addition, the multi-valent IgG-nanocage crosslinking yielded stable precipitates allowing for washing and extended storage in low salt buffers until elution at low pH. Because of the flexibility in tuning the transition property of ELP, it may be possible to achieve complete isothermal separation of IgG using this synthetic purification platform.

FIGURES

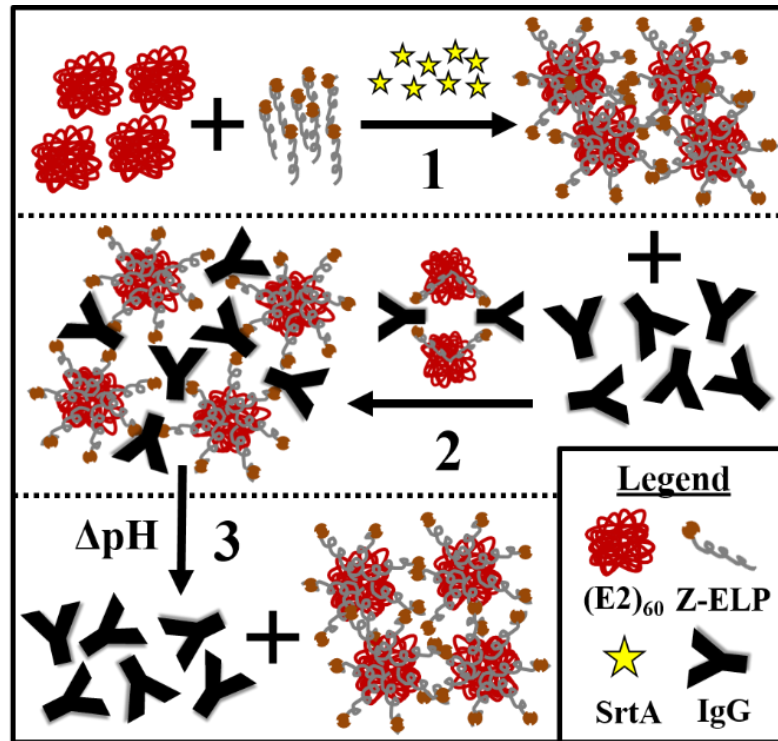


Figure 2.1 Mechanism for affinity precipitation of IgG using Z-ELP-E2 nanoparticles. Step 1: SrtA ligation of Z-ELP onto E2 60-mer nanocage. Step 2: Multi-valent binding between the nanoparticles and IgG result in spontaneous crosslinking into large, insoluble precipitates. Step 3: Reversible dissociation and resolubilization of both IgG and Z-ELP-E2 in a low pH buffer.

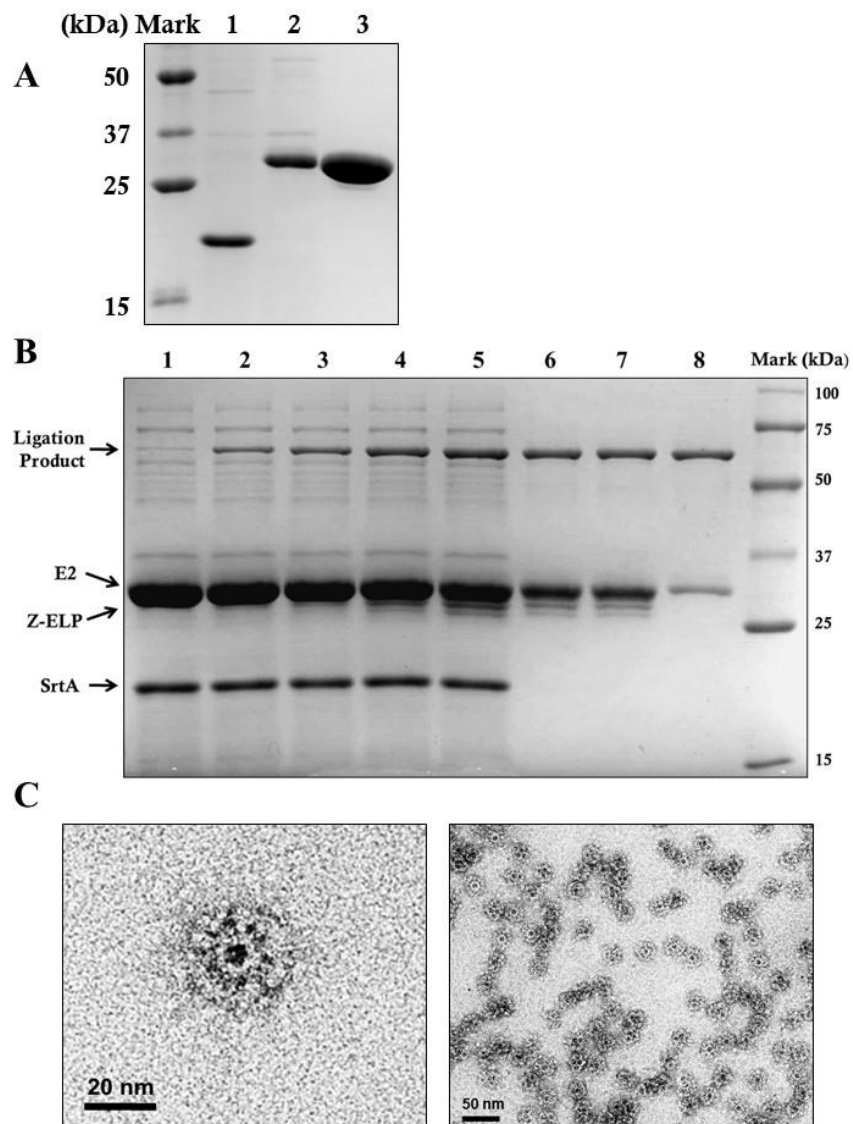


Figure 2.2 Production of Z-ELP-E2 Nanocages. A) SDS-PAGE of the SrtA ligation reactants. Lane 1: 10 μ M SrtA soluble lysate. Lane 2: 10 μ M E2 purified by 70°C heating. Lane 3: 50 μ M Z-ELP purified by two ITC cycles. B) SDS-PAGE of the ligation reaction time-course and nanocage purification. Lane 1: Initial ligation reactants. Lane 2: 30 min reaction. Lane 3: 1 h reaction. Lane 4: 2.5 h reaction. Lane 5: 5 h reaction. Lane 6: ITC cycle 1. Lane 7: ITC cycle 2. Lane 8: 100 kDa filtration retentate. C) TEM images of a single Z-ELP-E2 nanocage particle and a mixture of several Z-ELP-E2 nanoparticles.

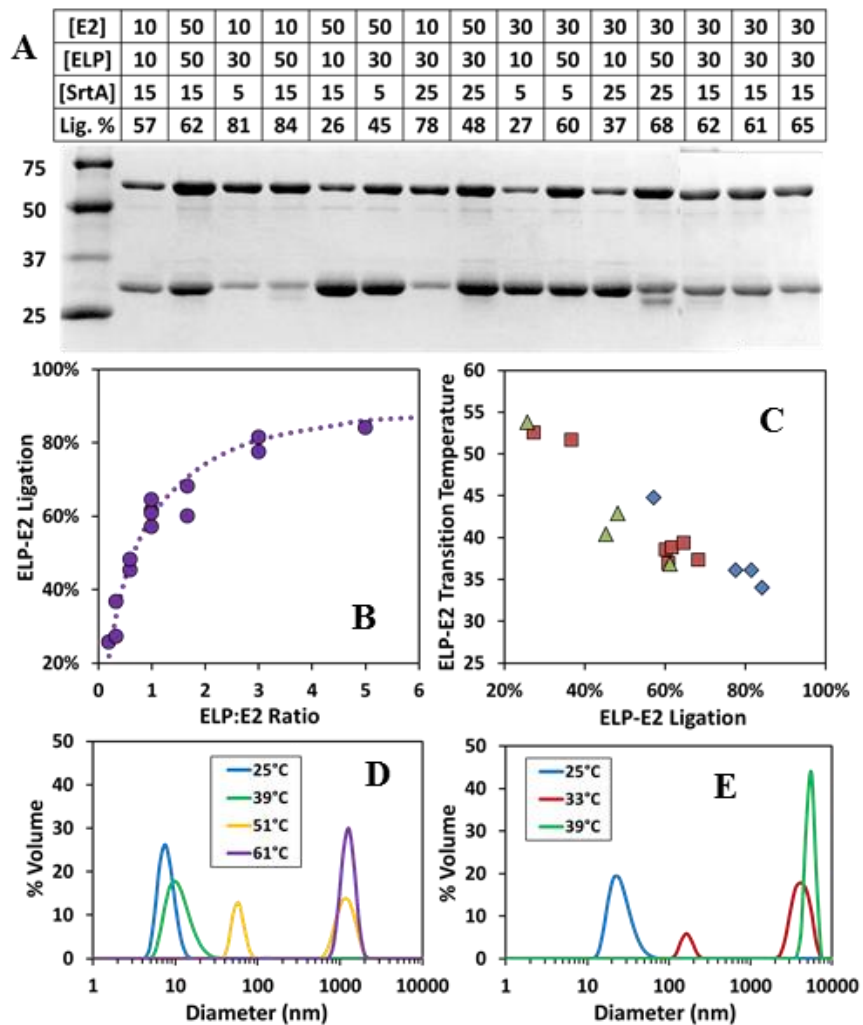


Figure 2.3 Nanocage ligation and aggregation properties. (A) SDS-PAGE of nanocage ligation products using various reactant concentrations. Top band: ELP-E2 subunit. Bottom band: E2 subunit. (B) Dependency of ELP-E2 ligation density on ELP:E2 ratios. (C) Dependency of T_t on ELP-E2 ligation density normalized by E2 concentration (Green triangle: 25 μ M; Red square: 15 μ M; Blue diamond: 5 μ M). DLS % volume distribution of (D) 25 μ M free ELP or (E) 25 μ M ELP ligated on E2 cages at 60% ligation density in PBS at selected temperatures.

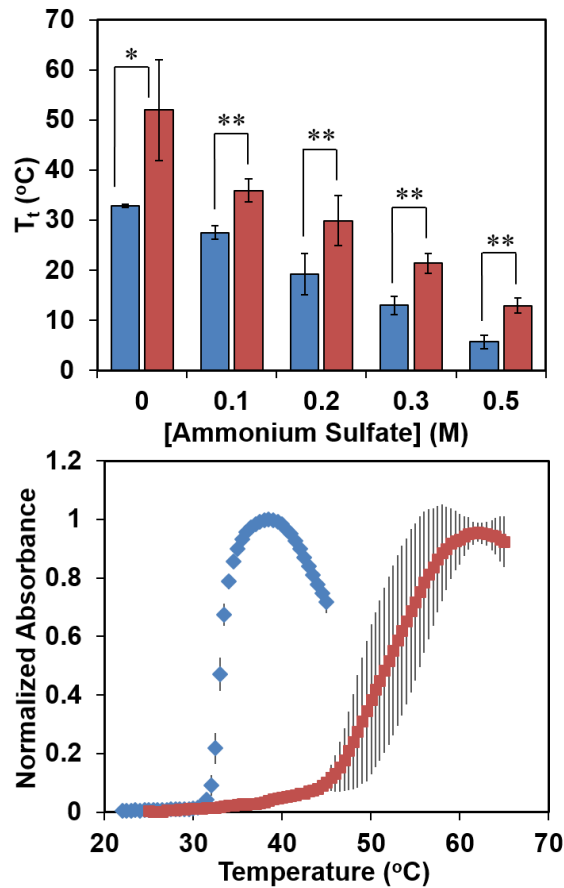


Figure 2.4 T_t comparison between free and ligated ELP. A) T_t of the nanocage (blue) and free Z-ELP (red) in PBS with added ammonium sulfate. Error bars represent 95% confidence intervals of three experiments (* = p-value < 0.01 difference in T_t > 10°C, ** = p-value < 0.01 difference in T_t > 5°C). B) Normalized absorbance curve for nanocage (blue diamonds) and free Z-ELP (red squares) in PBS without ammonium sulfate. Error bars represent one standard deviation of three experiments.

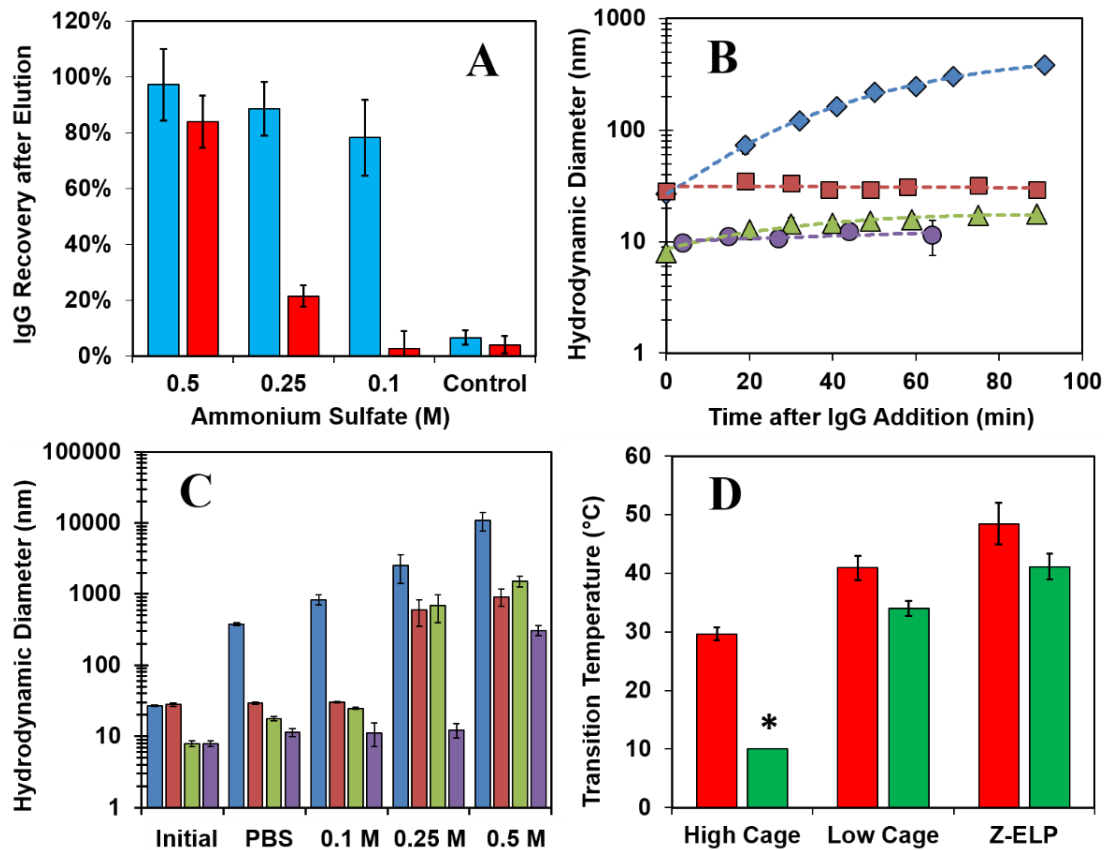


Figure 2.5 Characterization of antibody binding-induced crosslinking. Error bars represent 95% confidence intervals of three experiments. (A) Comparison of antibody recovery after elution from nanocage (blue) or Z-ELP (red). Control bars represent ELP-E2 cages or ELPs with no Z-domain using 0.5 M ammonium sulfate for precipitation. (B) DLS size measurements of IgG-nanocage aggregation kinetics at 25°C in PBS (Z-ELP-E2: blue diamond; ELP-E2: red square; Z-ELP: green triangle; ELP: purple circle) (C) DLS size measurements in PBS at 25°C of the initial mixture with IgG, after a 1 h incubation with IgG and with increasing amounts of ammonium sulfate in PBS (Z-ELP-E2: blue; ELP-E2: red; Z-ELP: green; ELP: purple). (D) Comparison of T_t between 25 μ M high ligation Z-ELP-E2 (65%), low ligation Z-ELP-E2 (35%), and free Z-ELP before (red) and 2 h after (green) addition of IgG in PBS at 20°C. * indicates $T_t \ll 20$ °C.

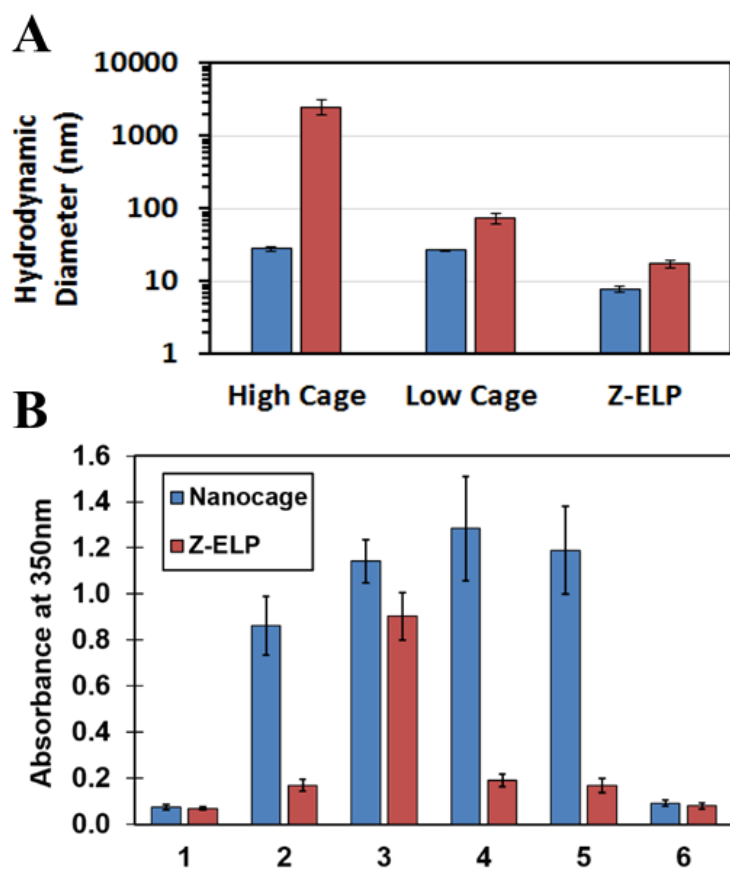


Figure 2.6 IgG-Nanoparticle crosslinking and elution. A) Comparison of aggregate size by DLS for high ligation Z-ELP-E2 (65%), low ligation Z-ELP-E2 (35%), and free Z-ELP before (blue) and 2 h after (red) addition of IgG in PBS at 23°C. B) Solution turbidity for affinity precipitation of IgG using ligated or free Z-ELP. Error bars represent 95% confidence intervals of three experiments. (1) Initial sample before IgG addition. (2) 2 h incubation at 23°C. (3) Adjusted to 0.5 M ammonium sulfate. (4) Centrifuged and resuspended back into PBS and incubated at 4°C for 1 h. (5) Incubated at 4°C for 3 days. (6) Precipitated again and resuspended in elution buffer.

REFERENCES

1. Beck A, Wurch, T, Baily C, Corvaia, N. Strategies and challenges for the next generation of therapeutic antibodies. *Nat. Rev. Immunol* **2010**, 10:345-352.
2. Ecker DM, Jones S, Levine HL. The therapeutic antibody market. *mAbs* **2015**, 7(1):9-14.
3. Shukla AA, Thömmes J. Recent advances in large-scale production of monoclonal antibodies and related proteins. *Trends Biotechnol* **2010**, 28(5):253-261.
4. Ghose, SM, Allen, M, Hubbard B, Brooks C, Cramer SM. Antibody variable region interactions with Protein A: implications for the development of generic purification processes. *Biotechnol Bioeng* **2005**, 92(6):665–667.
5. Hillbrig, F, Freitag R. Protein purification by affinity precipitation. *J. Chromatogr. B* **2003**, 848(1):40-47.
6. Taipa MA, Kaul RH, Mattiasson B, Cabral JMS. Recovery of a monoclonal antibody from hybridoma culture supernatant by affinity precipitation with Eudragit S-100. *Bioseparation* **2001**, 9(5):291–298.
7. Takei YG, Aoki T, Sanui K, Ogata N, Sakurai Y, Okano T, Matsukata M, Kikuchi A. Temperature-responsive bioconjugates. 3. Antibody-Poly(N-isopropylacrylamide) conjugates for temperature-modulated precipitations and affinity bioseparations. *Bioconjugate Chem* **1994**, 5(6):577–582.
8. Kowalczyk T, Hnatuszko-Konka K, Gerszberg A, Kononowicz AK. Elastin-like polypeptides as a promising family of genetically-engineered protein based polymers. *World J Microbiol Biotechnol* **2014**, 30(8):2141–2152.
9. Chilkoti A, Christensen T, MacKay JA. Stimulus responsive elastin biopolymers: applications in medicine and biotechnology. *Cur Op Chem Bio* **2006**, 10(6):652-657.
10. Kim JY, Mulchandani A, Chen W. Temperature-triggered purification of antibodies. *Biotechnol Bioeng* **2005**, 90:373-379.

11. Lao UL, Mulchandani A, Chen W. Simple conjugation and purification of quantum dot-antibody complexes using a thermally responsive elastin-protein L scaffold as immunofluorescent agents. *JACS* **2006**, 128:14756-14757.
12. Liu, F.; Chen, W. Engineering a recyclable ELP capturing scaffold for non-chromatographic protein purification. *Biotechnol Prog* **2013**, 29:968-971.
13. Kim H, Chen W. A non-chromatographic protein purification strategy using src 3 homology domains as generalized capture domains. *J Biotechnol* **2016**, 234:27–34.
14. Madan B, Chaudhary G, Cramer SM, Chen W. ELP-z and ELP-zz capturing scaffolds for the purification of immunoglobulins by affinity precipitation. *J Biotechnol* **2013**, 163(1):10-16.
15. Sheth RD, Madan B, Chen W, Cramer SM. *Biotechnol Bioeng* **2013**, 110:2664-2676.
16. Sheth, RD, Jin M, Bhut BV, Liu J, Lee J, Siegfried R, Li Z, Chen, W, Cramer SM. High throughput screening for the development of a monoclonal antibody affinity precipitation step using ELP-Z stimuli responsive biopolymers. *Biotechnol Bioeng* **2014**, 111:1595-1603.
17. Arosio P, Jaquet B, Wu H, Morbidelli M. On the role of salt type and concentration on the stability behavior of a monoclonal antibody solution. *Biophys Chem* **2012**, 168:19–27.
18. Mirica KA, Lockett MR, Snyder PW, Shapiro ND, Mack ET, Nam S, Whitesides GM. Selective precipitation and purification of monovalent proteins using oligovalent ligands and ammonium sulfate. *Bioconjug Chem* **2012**, 23(2):293–299.
19. Handlogten MW, Stefanick JF, Alves NJ, Bilgicer B. Nonchromatographic Affinity Precipitation Method for the Purification of Bivalently Active Pharmaceutical Antibodies from Biological Fluids. *Anal Chem* **2013**, 85(10):5271–5278.
20. Chen Q, Sun Q, Molino NM, Wang S-W, Boder ET, Chen W. Sortase A-mediated multi-functionalization of protein nanoparticles. *Chem Commun* **2015**, 51:12107-12110.
21. Levary DA, Parthasarathy R, Boder ET, Ackerman, ME. Protein-Protein Fusion Catalyzed by Sortase A. *Bioconjugate Chem* **2011**, 18:469-476.
22. Sun Q, Chen Q, Blackstock D, Chen W. Post-translational modification of bio-nanoparticles as a modular platform for biosensor assembly. *ACS Nano* **2015**, 9(8):8554–8561.

23. Zhou HZ, Liao W, Cheng RH, Lawson JE, McCarthy DB, Reed LJ, Stoops JK. Direct Evidence for the Size and Conformational Variability of the Pyruvate Dehydrogenase Complex Revealed by Three-dimensional Electron Microscopy. *J Biol Chem* **2001**, 276(15):21704-21713.
24. Dhandhukia J, Weitzhandler I, Wang W, MacKay JA. Switchable elastin-like polypeptides that respond to chemical inducers of dimerization. *Biomacromolecules* **2013**, 14(4):976–985.
25. Jendeberg L, Persson B, Andersson R, Karlsson R, Uhlen M, Nilsson B. Kinetic analysis of the interaction between protein a domain variants and human Fc using plasmon resonance detection. *J Mol Recognit* **1995**, 8(4):270-278.
26. Hezaveh S, Zeng A-P, Jandt U. Human Pyruvate Dehydrogenase Complex E2 and E3BP Core Subunits: New Models and Insights from Molecular Dynamics Simulations. *J Phys Chem B* **2016**, 120(19):4399–4409.

Chapter 3

ONE-STEP AFFINITY CAPTURE AND PRECIPITATION FOR IMPROVED PURIFICATION OF AN INDUSTRIAL MONOCLONAL ANTIBODY

Abstract

Affinity precipitation using environmentally responsive, Z-domain-elastin-like polypeptide (Z-ELP) fusion proteins has been shown to be a promising antibody capture technique. Chapter 2 described an enhanced affinity precipitation of antibodies by conjugating Z-ELP to a 25-nm diameter, self-assembled E2 protein nanocage (Z-ELP-E2). The enlarged scale of aggregate formation and IgG-triggered crosslinking through multi-valent binding significantly outperformed traditional Z-ELP-based methods. In Chapter 3, we sought to develop an affinity precipitation process capable of purifying industrial monoclonal antibodies (mAbs) at ambient temperature with minimal added salt. We discovered the mAb-nanocage complex spontaneously aggregated upon mixing due to the enhanced multi-valent cross-linking. Through optimization of key process parameters, 95% mAb elution yield was obtained with >99.9% HCP and DNA impurity clearance. Because of the operational flexibility afforded by this one-step affinity capture and precipitation process, the Z-ELP-E2 based approach has the potential to be a viable alternative to platform mAb purification.

Chapter 3 is reproduced with permission from John Wiley and Sons. Source:

Swartz AR, Xu X, Traylor S, Li ZJ, Chen W. One-step affinity capture and precipitation for improved purification of an industrial monoclonal antibody using Z-ELP functionalized nanocages. *Biotechnol Bioeng* **2018**, 115(2):423-432.

3.1 Introduction

Monoclonal antibodies (mAbs) represent a rapidly expanding class of biopharmaceutical therapeutics that target a wide range of diseases¹. In 2014, the global revenue of the 47 approved antibody drugs totaled almost \$70 billion, and current projections expect that sales will exceed \$120 billion by 2020². To meet the increasing demand, recent advancements in upstream culture productivity and scale-up have yielded antibody titers over 10 g/L within 20,000 L bioreactors³. This has placed a significant burden on the downstream purification platform, especially the primary capture step, protein A affinity chromatography⁴. The protein A ligand, derived from a gene in *Staphylococcus aureus*, binds to the F_c region of human immunoglobulin G (IgG) and can be recombinantly expressed in *Escherichia coli*⁵. Protein A chromatography has been widely recognized as the gold standard in platform mAb purification due to its high selectivity and yield⁶. However, current limitations on throughput, scale-up, and cost have generated increased interest in alternative non-chromatographic antibody capture methods⁷.

As discussed in Chapter 1, affinity precipitation is one promising alternative, because it combines the high selectivity of an affinity ligand, such as Protein A, with the operational benefits of precipitation⁸. A typical affinity precipitation process requires an initial binding step to a ligand, an environmental trigger to precipitate the complex, a separation step to recover the precipitated complex, and an elution step to remove the target from the ligand. Elastin-like polypeptides (ELPs) are stimuli responsive biopolymers that undergo a reversible phase transition dependent on the ionic strength and/or temperature of the solution relative to a critical point called the transition temperature (T_t)⁹⁻¹⁰. Above the T_t , a conformational change occurs, leading to the formation of large, insoluble aggregates that can be separated from other solution

components by centrifugation or filtration. After isolating the precipitated ELP, salt can be diluted out and/or the temperature can be lowered below T_i , allowing the resolubilization of ELP in a process termed inverse transition cycling (ITC)¹¹.

Our group has demonstrated the feasibility of employing a wide range of ELP-fusion proteins for various affinity capture applications¹²⁻¹⁵. We have previously generated an ELP fusion protein with a small (7 kDa) synthetic antibody-binding Z-domain (Z-ELP) derived from the B domain in Protein A, and demonstrated efficient antibody binding and precipitation¹⁶. Using this Z-ELP construct, antibody purification was optimized using high-throughput methods and was evaluated with industrial mAbs¹⁷⁻¹⁸. However, one major drawback of this approach was the requirement of elevated salt and temperature for ELP precipitation, as mAbs are more sensitive to aggregation or degradation under these solution conditions¹⁹⁻²⁰. Moreover, the requirement of a heating step presents an additional operational burden, and excess heat or salt may cause non-specific precipitation of unwanted impurities, decreasing purification capacity. For these reasons, affinity precipitation using conventional ELP-based purification has not been widely adopted as a viable antibody purification alternative to chromatography.

We sought to improve upon the limitations of conventional ELP precipitation by designing a new ELP scaffold that can efficiently capture antibodies at ambient temperature (19-25°C) while minimizing the salt required for aggregation. To accomplish this, we described a tandem approach in Chapter 2 to significantly enhance ELP aggregation by increasing the scaffold dimension and valency²¹. Z-ELP was covalently conjugated to a self-assembled 25 nm, 60-mer E2 protein nanocage (Z-ELP-E2) from *Bacillus stearothermophilus* using post-translational Sortase A (SrtA)

ligation²²⁻²³. We demonstrated how the enlarged dimension significantly decreased the ELP transition temperature and increased aggregate size, and how the multi-valent interactions between Z-ELP-E2 nanocages and a polyclonal human IgG resulted in spontaneous crosslinking into insoluble aggregates. The aggregated complex remained precipitated even at low salt and temperatures until both components were resolubilized after the antibody was eluted from the Z-ELP-E2 nanocage at low pH. We believe that these enhanced features are ideal for the purification of industrial mAbs directly from cell culture harvests at ambient temperature with a minimal amount of added salt. In addition, the stable precipitates enable additional wash steps in various buffers to remove host cell protein and nucleic acid contaminants.

To evaluate the nanocage's utility as an alternative antibody capture method, Chapter 3 describes the development and optimization of an affinity precipitation process using an industrial therapeutic mAb from Chinese hamster ovary (CHO) cell culture. The proposed baseline affinity precipitation process (**Figure 3.1**) was established using high-throughput methods with purified mAb and nanocage stocks. Binding, precipitation, and elution operational conditions were optimized to maximize mAb yield and monomer content while performing all steps at 23 °C. The nanocage-based affinity precipitation method was applied to clarified cell culture harvest, and the mAb yield, monomer content, and impurity clearance (host cell protein and DNA) were compared to typical Protein A performance attributes over multiple purification cycles.

3.2 Materials and Methods

3.2.1 Materials

Escherichia coli strain BLR(DE3) containing pET24(a) vectors encoding for Z-ELP[KV₈F-40]-LPETG and ELP[KV₈F-40]-LPETG, *E. coli* strain BL21(DE3) containing a pET11(a) vector encoding for GGG-E2(158), and another BL21(DE3) strain containing a pMR5 vector encoding for SrtA were constructed and described previously²¹. A purified and clarified cell culture mAb was provided by Bristol-Myers Squibb (BMS) (New York City, NY). Bacto tryptone and yeast extract were purchased from BD Biosciences (Franklin Lakes, NJ). Kanamycin, ampicillin, bovine serum albumin (BSA), isopropyl- β -D-thiogalactoside (IPTG), and 96-well 200 μ L conical PCR plates were purchased from Fisher Scientific (Pittsburgh, PA). Sodium hydroxide, sodium phosphate, citric acid, acetic acid, tris base, ammonium sulfate, sodium chloride, sodium sulfate, L-arginine, and polysorbate-80 (PS-80) were purchased from Sigma-Aldrich (St. Louis, MO). 100 kDa Vivaspin 20 columns were purchased from Sartorius Stedim (Gottingen, Germany). 0.8/0.2 μ m Supor Acrodisc syringe filters were purchased from Pall (Port Washington, NY). 96-well half area UV-transparent plates were purchased from Corning (Corning, NY). An Acquity UPLC BEH SEC Column (200 \AA , 1.7 μ m, 4.6 x 300 mm) was purchased from Waters (Milford, MA). All statistical analyses were performed in Minitab 17 software.

3.2.2 Experimental Methods

3.2.2.1 Protein Expression and Purification

Z-ELP[KV₈F-40]-LPETG, GGG-E2, and SrtA were expressed and purified from 250 mL *E. coli* cultures in 1 L Erlenmeyer flasks following previously indicated

procedures²¹. Z-ELP purified by ITC, E2 partially purified by 70°C heating, and SrtA soluble lysate were added at a 3:1:1 reactant ratio (Z-ELP:E2:SrtA) in 100 mL of reaction buffer (50 mM tris, 150 mM sodium chloride, 6 mM calcium chloride, pH 8.0). After 8 hours at 23°C, the Z-ELP-E2 nanocage ligation reaction was purified by ITC into phosphate buffered saline (PBS; 20 mM sodium phosphate, 150 mM sodium chloride, pH 7.2). 100 kDa Sartorius Vivaspin 20 spin columns were used to remove excess Z-ELP. Two more ITC cycles were used to further concentrate the purified Z-ELP-E2 stock. The ligation reaction was characterized by Coomassie stained 10% acrylamide SDS-PAGE and Z-ELP ligation density was estimated using densitometry analysis using Thermo MyImage software (Waltham, MA).

3.2.2.2 High-throughput Affinity Precipitation Optimization

High-throughput affinity precipitation experiments were performed using 200 µL 96-well conical PCR plates. All experiments were performed at ambient temperature (23°C) using solutions consisting of purified mAb and Z-ELP-E2 nanocages or Z-ELP stocks mixed at target concentrations in PBS pH 7.2. For initial precipitation experiments, samples were pelleted by centrifugation at 1,500 g for 30 min. For a comparison of mAb precipitation using equal molar concentrations of ligated Z-ELP or free Z-ELP, samples were adjusted to a target ammonium sulfate concentration prior to centrifugation. After pelleting insoluble components, supernatants were removed using a multi-channel pipette and transferred to a UV-transparent half-area 96-well plate. The concentration of mAb and nanocage in the supernatant was analyzed by measuring the UV absorption spectrum and applying a partial least squares regression (PLSR) model (see analytical methods). For mAb elution experiments, the pellet was resuspended in a target volume of low pH elution buffer using a multi-channel pipette and mixed on a

shake plate for 30-60 min. The resuspension pH was measured using a Thermo Orion pH meter with a micro pH electrode purchased from Thermo Fisher Scientific (Waltham, MA). Samples were adjusted to a target ammonium sulfate concentration and centrifuged at 1,500 g for 30 min. Elution supernatants were transferred to a UV-transparent half-area 96-well plate and the mAb concentration was estimated either by the PLSR model for samples containing mixtures of mAb and nanocage or by absorbance at 280 nm using the theoretical mAb extinction coefficient for samples containing only mAb. Samples were analyzed by SDS-PAGE using a BioRad 4-20% Tris-glycine TGX stain-free gel and imaged by a BioRad ChemiDoc XRS+. The monomer content of eluted mAb was determined by SEC. All experimental conditions were performed in triplicate.

3.2.2.3 mAb Cell Culture Affinity Precipitation

Clarified mAb culture harvest was purified using the optimized nanocage affinity precipitation procedure with all steps performed at 23°C. Purified nanocage stock was added to mAb culture at a 3:1 molar ratio of Z-ELP:mAb in centrifuge tubes and mixed for 5 min. Samples were centrifuged at 15,000 g for 5 min and the supernatant was removed. The pellet was washed by series of 3 wash buffers consisting of PBS, pH 7.2, followed by a buffer containing salt, an excipient, and 0.05% (w/v) PS-80 at pH 9.0, and finally 25 mM sodium citrate pH 5.0. The pellet of each wash step was suspended in solution by pipetting up and down and then centrifuged at 15,000 g for 5 min. The supernatant was removed before washing the pellet again with the subsequent buffer. mAbs were eluted from the nanocage by resuspending in 3-fold less volume 50 mM sodium citrate, pH 3.5, and mixed for 15 min. The sample was adjusted to 0.25 M ammonium sulfate and centrifuged at 15,000 g for 5 min. Elution supernatants were

titrated to pH 5.5 using 2 M tris, pH 11, and assayed for mAb concentration, monomer content, and impurity content. The pelleted nanocage was regenerated in 50 mM sodium citrate, pH 3.0, and recycled back into PBS using ITC. The nanocage was filtered through a 0.8/0.2 μm Supor syringe filter and assayed for concentration. The same regenerated nanocage was used to repeat the affinity precipitation of a new mAb culture sample for three consecutive cycles. The affinity precipitation steps were characterized by SDS-PAGE analysis with normalized sample loading. Protein A chromatography purification of mAb culture was performed by BMS.

3.2.3 Analytical Methods

3.2.3.1 PLSR Model of Two Component Absorption Spectra

The concentration of pure mAb or nanocage was measured by determining the absorbance at 280 nm in 96-well half area UV-transparent plates using a Tecan Infinite M1000 plate reader (Männedorf, Switzerland) and calculated using the respective theoretical extinction coefficients. For samples consisting of a mixture of the two components, a partial least squares regression (PLSR) model was developed²⁴ to estimate mAb and nanocage concentrations from the combined absorption spectra using the SIMPLS algorithm in the MATLAB 9.1 software package²⁵. The PLSR coefficients were determined using a training data set in the appropriate buffer and pH and the model was optimized by tuning the absorption wavelength range and PLSR parameters using a validation data set at the same solution conditions. A PLSR model was developed for mixtures of pure mAb and nanocage and pure mAb and Z-ELP in target buffers.

3.2.3.2 Analytical Size Exclusion Chromatography

mAb monomer content was measured using size exclusion chromatography (SEC). Samples were diluted to 1 mg/mL mAb, added to a low volume UPLC vial (Waters), and placed in a temperature controlled auto injector set at 4 °C in a Waters Acquity UPLC system. A mobile phase of 200 mM potassium phosphate, 150 mM sodium chloride, pH 6.8, was used at a flow rate of 0.4 mL/min. Three injections of 10 µL were performed and the column effluent was monitored at 280 nm. Peak areas were analyzed by Empower Software (Waters).

3.2.3.3 Analytical Impurity Content

The CHO cell host cell protein (HCP) concentration was determined using an ELISA kit from Cygnus Technologies. The CHO cell DNA concentration was determined by an in-house quantitative PCR (qPCR) assay developed at BMS. Details of these assays have been discussed previously¹⁸. Log reduction value (LRV) was calculated by $LRV = (-\log([final]/[initial]))$

3.2.3.4 Dynamic Light Scattering Measurement

The particle size was measured using dynamic light scattering (DLS) using a Malvern Zetasizer Nano (Malvern, United Kingdom) with a 4 mW He Ne gas laser at 632.8 nm and a 175° scattering angle. Samples were prepared in a low volume cuvette (ZEN0040, Malvern). The scattering intensity was measured at 30 s intervals at 25°C using a sample refractive index = 1.45, sample absorption = 0.001, and dispersant refractive index = 1.33 and the correlation function was analyzed by the Protein Analysis algorithm provided by the Malvern software. For nanocage assembly with PS-80, 1 mg/mL nanocage samples were prepared in PBS in triplicate with PS-80

concentrations ranging from 0.01 – 2.00 % (w/v), mixed for 1 hour at 23 °C, and run on DLS.

3.3 Results and Discussion

3.3.1 High-throughput optimization of mAb binding and precipitation

Chapter 2 describes how IgG binding can induce crosslinking of the Z-ELP-E2 scaffold into large aggregated particles due to multi-valent IgG-nanocage interactions²¹. We suspected that the Z-ELP-E2 nanocage may be able to achieve close to 100% mAb recovery in the absence of added salt. High-throughput, small scale (50-200 μ L) affinity precipitation experiments using 96-well plates were performed to evaluate this possibility. A wide range of salt concentrations and Z-domain to mAb binding ratios were tested using a purified industrial mAb produced from CHO cell culture. The Z-ELP-E2 nanocage was generated by conjugating Z-ELP to E2 nanoparticles using SrtA ligation, resulting in a self-assembled 60-mer scaffold with approximately 30 Z-ELP molecules displayed on the surface (**Figure 3.2**).

Nanocage-mAb mixtures were prepared using equal concentrations of ligated (Z-ELP conjugated to E2) and free Z-ELP at a Z-domain to mAb molar ratio ranging from 1:1 to 4:1. After binding, precipitation was performed using 0 to 0.6 M ammonium sulfate at 23°C. Using the Z-ELP-E2 nanocages, salt concentration had a minimal effect on the mAb precipitation yield (**Figure 3.3A**). Samples with no added salt exhibited equivalent mAb precipitation yields as those with high salt concentrations. In contrast, the molar binding ratio of Z-ELP-E2:mAb was far more significant on mAb recovery (**Figure 3.3A**). A 3:1 Z-domain:mAb ratio was sufficient to precipitate >95% mAb without the addition of salt and was selected as the optimal binding condition. In

comparison, a 4:1 binding ratio of free Z-ELP and 0.4 M ammonium sulfate was required for similar mAb yields (**Figure 3.3B**). These observations suggest that mAb-nanocage crosslinking confers the ability for efficient mAb recovery and eliminates the requirement of salt for ELP aggregation.

The importance of crosslinking was further demonstrated by observing the instantaneous formation of large visible aggregates, which settled out of solution shortly after mixing the nanocage with clarified mAb cell culture harvest (**Figure 3.4A-B**). The kinetics of mAb capture was measured over various time intervals (**Figure 3.4C**) and more than 95% of mAb was pelleted by centrifugation after mixing for 10 min. Dynamic light scattering was used to monitor the increase in aggregate size of the nanocage or free Z-ELP mixed with mAbs at a 3:1 molar ratio over time (**Figure 3.4D**). A 10-fold lower protein concentration was used in this case to avoid the formation of aggregates larger than 5 μm as demonstrated previously²¹. The bound mAb-nanocage aggregate diameter exceeded 500 nm within 1 min of mixing and continued to grow over 10 min to more than 2.5 μm , while the free Z-ELP did not significantly increase in size. These findings offer unprecedented operational advantages for this E2-based affinity precipitation process, allowing for a one-step capture and aggregation through mAb-induced crosslinking without the need of an environmental trigger (**Figure 3.4B**).

3.3.2 High-throughput optimization of mAb elution and nanocage recovery

After binding and precipitation, mAbs are dissociated from the Z-domain at low pH by the same mechanism mAbs are eluted from protein A chromatography columns⁶. To study the effect of elution buffer pH on mAb yield, the mAb-nanocage complex was pelleted and resuspended in an equal volume of acetate or citrate buffer ranging from pH 3.5 to 4.5. mAb elution yields of greater than 95% were achieved at both pH 3.5 and

3.75 (**Figure 3.5A-B**), while recovery dropped below 60% at pH values 4 or higher, signifying that mAb was not fully dissociated from the Z-domain and remained crosslinked within the nanocage precipitates.

It has been reported that the Protein A chromatography elution pool typically exhibits a basic pH shift due to buffer mixing and protein-buffer interactions²⁶. Because the protein A ligand is fixed within the chromatography resin, this pH change of the eluate pool has little impact on the dissociation of mAbs from the column. For affinity precipitation, the pellet is dissolved directly in the elution buffer. Therefore, controlling the elution pH upon resuspension is crucial to ensure high mAb yield. Furthermore, it is desirable to concentrate the mAbs during elution. This can be easily accomplished with affinity precipitation by eluting the mAb using a smaller volume of elution buffer (defined as the volume concentration factor; VCF). However, at higher VCFs, the pH drift may be more significant due to increased buffer and protein interactions.

This tradeoff between protein concentration and pH drift was investigated for acetate and citrate elution buffers. The resuspension solution pH using acetate was found to be more susceptible to a pH drift than citrate at pH values less than 4 (**Figure 3.6A**). This is consistent with the weaker buffering capacity of 50 mM acetate ($pK_a = 4.76$) compared to 50 mM citrate ($pK_{a1} = 3.13$, $pK_{a2} = 4.76$) within the pH range tested. The pH drift was even more prominent for more concentrated mAb-nanocage samples in the acetate buffer (**Figure 3.6B**). For samples with 3 and 5-fold VCF, the final pH values drifted above the critical value (~ 3.8) required to dissociate the mAb from the Z-domain and resulted in a significant yield loss (**Figure 3.6B**). For these reasons, citrate buffer at pH 3.5 was selected as the optimal elution condition.

To separate the dissociated mAb, ammonium sulfate was used to selectively precipitate the nanocage, leaving the mAb in the supernatant. To investigate how this can impact mAb yield and nanocage recovery, the effect of VCF and salt concentration was investigated. The mAb yields were mostly unaffected at low salt concentrations, but with high VCF and salt, lower yields were observed (**Figure 3.7A**). Extensive nanocage aggregation from excess salt may have caused some mAb to non-specifically precipitate out of solution. As expected, nanocage yield was highly dependent on both protein and salt concentrations (**Figure 3.7B**) and the yield loss was a direct result of incomplete precipitation. Since the presence of the mAb had a minimal effect on nanocage precipitation (**Figure 3.7C**), the required salt concentration for 100% nanocage precipitation could be easily mapped given the known ELP concentration. For example, a cell culture with a 20 μM mAb titer ($\sim 3 \text{ g/L}$) would require 60 μM Z-ELP-E2 for precipitation. After eluting with 3x volume concentration, the 180 μM nanocage would require 0.1 M ammonium sulfate for precipitation.

3.3.3 Process stability of the mAb and nanocage

mAbs are known to become increasingly unstable at a solution pH less than 4.0 and may form high molecular weight aggregates and/or insoluble precipitates under these conditions²⁷. After Protein A elution, mAbs are typically titrated down to a pH value less than 3.8 for a viral inactivation hold before neutralization back up to a pH value greater 5 for improved stability. Therefore, to simulate platform purification, mAb stability was evaluated after 1 h in pH 3.5 elution buffer before titrating up to pH 5.5 using 2 M tris base (**Figure 3.8A**). The mAb in the current study was stable at low pH even with up to 0.3 M ammonium sulfate. The stability profile of a mAb affinity elution

was compared to protein A elution and both samples had an equivalent monomer content (**Figure 3.8B**).

After isolating the eluted mAb in the supernatant, the nanocage must be regenerated to remove trace levels of mAb and recycled for future use. It was found that the nanocage became insoluble at $\text{pH} < 3$ and was not capable of being recycled (**Figure 3.9A**). This is likely due to E2 subunit degradation, because ELP is known to be relatively stable at pH extremes¹⁸. Fortunately, the nanocage remained soluble in pH 3 citrate buffer and this was selected as the regeneration condition. After incubation at pH 3 for 1 h, the nanocage was re-suspended back in PBS using one ITC cycle and sterile filtered using a 0.2 μm membrane. Successful regeneration was confirmed by detecting no leftover mAb in the regenerated sample (**Figure 3.11A**, Lane 11).

3.3.4 Removal of process impurities

The initial mAb purification experiments from CHO cell culture were performed without any wash step, and the level of host cell protein (HCP) clearance was comparable to a platform protein A chromatography process (**Figure 3.10A**). Since the protein A column was usually washed with a series of three buffers optimized for impurity clearance, we investigated whether a similar procedure can be adapted. Repeated washing is particularly easy to execute because the precipitated mAb-nanocage complex remains insoluble until elution²¹. The second protein A wash contains PS-80, a detergent shown to improve impurity clearance by dissociating non-specific interactions²⁸. The only minor issue is that this detergent can potentially disrupt the E2 nanocage assembly²⁹. DLS was used to monitor nanocage size in solutions containing PS-80, and the highest concentration that can be used, 0.05% (w/v), without

inducing nanocage dissociation was adopted for subsequent experiments (**Figure 3.9B-C**), and was shown to increase HCP clearance by over 100-fold (**Figure 3.10A**).

3.3.5 Optimized affinity precipitation of mAb cell culture harvest

The optimized mAb affinity precipitation conditions (**Table 3.1**) were applied to the purification of mAb from clarified cell culture. A purified nanocage stock was mixed with the culture media at the optimal 3:1 binding ratio and resulted in the single-step capture and precipitation, as noted by a significant increase in turbidity (**Figure 3.12A-B**). After centrifugation, the mAb-nanocage complex was pelleted and the supernatant was removed before washing with the three protein A wash buffers (**Figure 3.12C-E**). The final wash pellet was resuspended in 3x less volume of citrate buffer pH 3.5 (**Figure 3.12F**) to elute the bound mAbs. Finally, the released E2 nanocages were removed by inducing aggregation by adjusting the ammonium sulfate concentration to 0.25 M. After centrifugation, the purified mAb was collected in the supernatant and the aggregated nanocage was removed for regeneration. At laboratory scale, mAbs can be purified from cell culture in less than 1 h following these procedures. From SDS-PAGE analysis, cell culture impurities were removed in the initial supernatant (**Figure 3.11A**, Lane 5), no mAb or nanocage was detected in the three washes (**Figure 3.11A**, Lanes 6-8), and the mAb was eluted with high purity (**Figure 3.11A**, Lane 9).

mAb purification from harvested culture was compared between the optimized affinity precipitation process and a platform protein A chromatography process. Three affinity precipitation cycles were performed using the same regenerated nanocage (**Figure 3.11B-C**) and the average elution mAb yield of $94.7 \pm 6.2\%$ and monomer content of $97.1 \pm 6.2\%$ were equivalent to protein A chromatography purification (**Table 3.2**). The overall HCP and DNA clearance using affinity precipitation was

comparable to or exceeded that of protein A chromatography, resulting in a 3-fold lower HCP content and an undetectable level of DNA. The three washes adapted from protein A were effective in reducing the final HCP concentration (**Figure 3.10B**). In addition, DNA clearance was improved with over 5.5 logs of clearance from cell culture compared to 4.4 log reduction for protein A chromatography (**Table 3.3**). This enhanced impurity reduction may be a result of less non-specific binding of impurities to the mAb-nanocage scaffold when compared to protein A resin. Lastly, SDS-PAGE confirmed minimal leaching of nanocage in the mAb elution sample (**Figure 3.11B**, Lanes 2-4), but a more sensitive assay may be necessary to further quantify any trace amount of nanocage remaining in the elution. However, because of its large size (50 nm, ~ 2 MDa), any residual nanocage should be easily removed in subsequent downstream processing steps.

Furthermore, the nanocage affinity precipitation HCP and DNA reduction was about one log higher than previously reported studies using Z-ELP¹⁸. This result is likely attributed to the ability to wash the mAb-nanocage complex with different buffers optimized for impurity clearance due to the crosslinking nature of the aggregates. This is in sharp contrast to the mAb-Z-ELP complex, which was resolubilized without sufficient salt, making it difficult to execute the proper washing steps. More importantly, the regenerated nanocages can be reused for additional cycles while maintaining similar mAb recovery efficiencies and HCP and DNA clearance.

After mAb elution, the nanocage was regenerated with citrate pH 3 buffer and then concentrated 10-fold into PBS by ITC for use in the next purification cycle. The average nanocage regeneration yield of $84.1 \pm 8.9\%$ over three cycles is not economically viable compared to protein A resin capable of >100 regeneration cycles.

One source of yield loss is likely the final concentration step after regeneration. Operationally, it is very difficult to resuspend highly concentrated Z-ELP-E2 in a small volume and protein losses to the container surfaces are more likely. A larger scale operation would minimize the container surface area to volume ratio and allow for more efficient resuspension. Moreover, longer ELP can be used to further enhance overall recovery³⁰. We expect that a nanocage recovery of 95% is feasible with further optimization of the regeneration and recycling steps. However, nanocage regeneration is not likely to achieve the 100-cycle lifetime commonly used for protein A chromatography resin mAb³¹.

3.4 Conclusion

Chapter 3 describes the development and optimization of a one-step affinity capture and precipitation procedure for an industrial mAb using Z-ELP-E2 nanocages. High-throughput screening was exploited to optimize a high yielding purification process with superior impurity clearance compared to protein A chromatography. A 3:1 Z-ELP:mAb molar binding ratio resulted in a >95% precipitation yield without the addition of any salt at ambient temperature. The multivalent nanocage-mAb binding initiated the rapid formation of a crosslinked network of large, insoluble particles. The pelleted complex was suspended in protein A wash buffers already optimized for impurity clearance and remained insoluble until resuspension in a sodium citrate pH 3.5 elution buffer. Citrate buffer minimized pH drift even with 5-fold concentrated samples and maintained high mAb elution yields. The mAb was highly stable at low pH even with added ammonium sulfate and was unaffected by the selective nanocage precipitation after elution. The regenerated nanocages were used for three purification

cycles, while maintaining the same mAb yield of 95% with 3.7 logs of HCP clearance and more than 5 logs of DNA clearance.

The results of this study highlight the significant improvements over conventional ELP-based precipitation methods for mAb purification. The one-step binding and precipitation allows for an immediate, selective capture of mAbs directly from a complex mixture of impurities and media components without the need for salt or temperature control. Over time, a visible phase separation occurs such that a settle decant separation may be possible instead of centrifugation. Once precipitated, the mAb-nanocage complex can be suspended with many different wash buffers or may be stored as pellets for extended periods of time. After elution, a selective precipitation step with a salt concentration as low as 0.1 M can be used to separate the nanocage from the mAb. However, this precipitation step may be replaced by other separation techniques such as filtration by exploiting the large size (50 nm, ~ 2 MDa) of the E2 nanocage.

Moreover, affinity precipitation using Z-ELP-E2 nanocages is ideally suited for use in continuous processing. Hammerschmidt and coworkers³² recently demonstrated the economic and operational benefits of a continuous precipitation process consisting of caprylic acid, polyethylene glycol, calcium chloride, and ethanol precipitation steps compared to platform mAb purification. Because of its efficient impurity clearance and high yield, Z-ELP-E2 nanocages have the potential to replace several or all steps proposed in the continuous precipitation process. To further demonstrate the general utility of the nanocage affinity precipitation system, we are in the process of evaluating the purification of other industrial mAbs and Fc fusion proteins that are known to be less stable in high salt or low pH.

TABLES

#	Purpose	Sample	Target Molecule	Buffer	pH	[Am Sulf] (M)	Step Time (min)
1	<u>Initial Mix</u>	Mix	3:1 [Cage]:[mAb]	Culture Media	~7	0.0	10
2	<u>Precipitation</u>	Sup	Impurity	Culture Media	~7	0.0	5
3		Pellet	Cage + mAb	PBS	7.2	0.0	
4	<u>Washes 1-3</u>	Sup	Impurity	Wash Buffers	5-9	0.0	3 x 5
5		Pellet	Cage + mAb	Wash Buffers	5-9	0.0	
6	<u>Elution</u>	Sup	Purified mAb	Citrate	3.5	0.25	15
7		Pellet	Cage	Citrate	3	0.0	
8	<u>Regeneration</u>	Sup	Trace impurity	Citrate	3	0.5	5
9		Pellet	Cage	PBS	7.2	0.0	
10	<u>Solubility</u>	Sup	Soluble Cage	PBS	7.2	0.0	5
11		Pellet	Insoluble	PBS	7.2	0.0	

Table 3.1 Optimized affinity precipitation process conditions.

Elution Cycle #	Culture mAb (mg/ml)	Elution VCF (x)	Elution mAb (mg/mL)	mAb Yield (%)	SEC Mon (%)	HCP (ppm)	DNA (ppb)	Cage Regen Yield (%)
Cycle 1	1.6	2.7	4.18	96.9	97.1	617	<10	88.2
Cycle 2	1.5	2.7	3.73	92.0	97.3	600	<10	82.5
Cycle 3	1.4	2.7	3.61	95.2	96.9	601	<10	81.6
Affinity Precipitation Elution Average				94.7	97.1	606	<10	84.1
Protein A Chromatography Elution				95.0	96.7	1730	172	n/a

Table 3.2 Analytical characterization of nanocage affinity precipitation of mAb cell culture over three cycles. Average results compared to protein A chromatography performance.

Host Cell Impurity	Clarified Bulk Cell Culture	Affinity Precipitation		Protein A Chromatography	
		Elution	LRV	Elution	LRV
HCP (ppm)	3150000 ± 710000	606 ± 3	3.72 ± 0.10	1730 ± 300	3.26 ± 0.12
DNA (ppb)	3990000 ± 1040000	< 10	> 5.60	172 ± 63	4.37 ± 0.20

Table 3.3 Comparison of HCP and DNA impurity clearance between affinity precipitation and protein A chromatography.

FIGURES

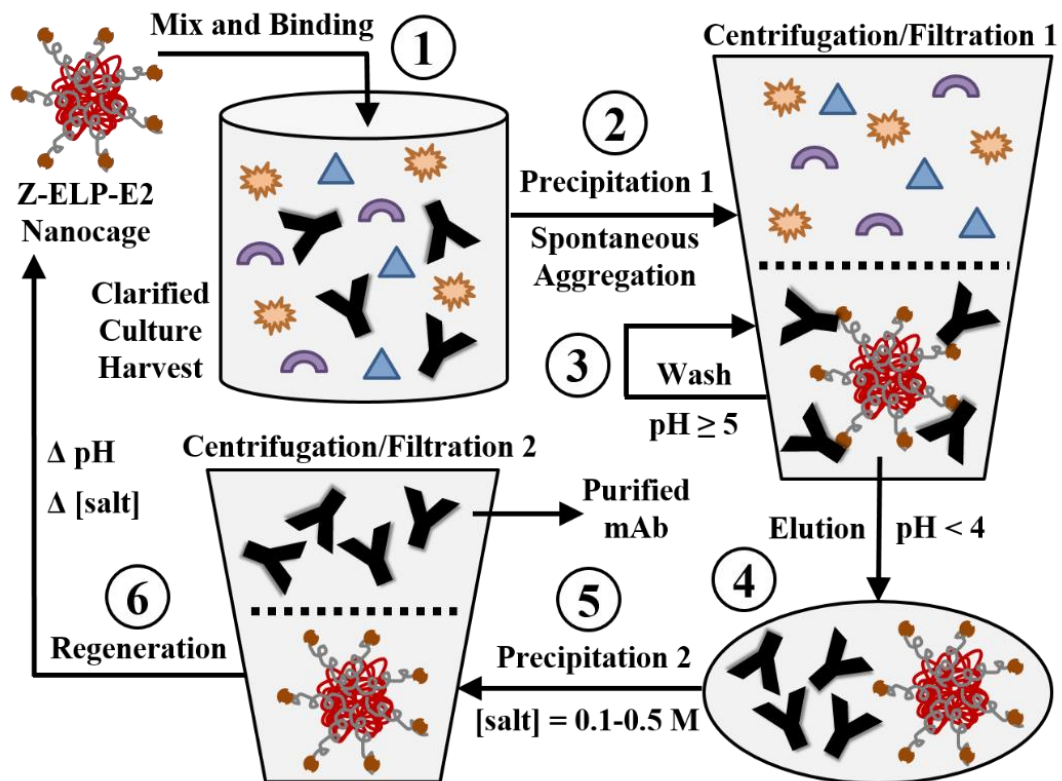


Figure 3.1 Z-ELP affinity precipitation of mAbs from cell culture. 1) Mix nanocage stock with clarified culture. 2) Spontaneous aggregation through multivalent crosslinking 3) Wash pellet by suspending in target wash buffer $\text{pH} > 5$. 4) Elute by suspending pellet in buffer $\text{pH} < 4$. 5) Add salt for selective precipitation of nanocage. Collect purified mAb in supernatant. 6) Regenerate nanocage to recycle for future use.

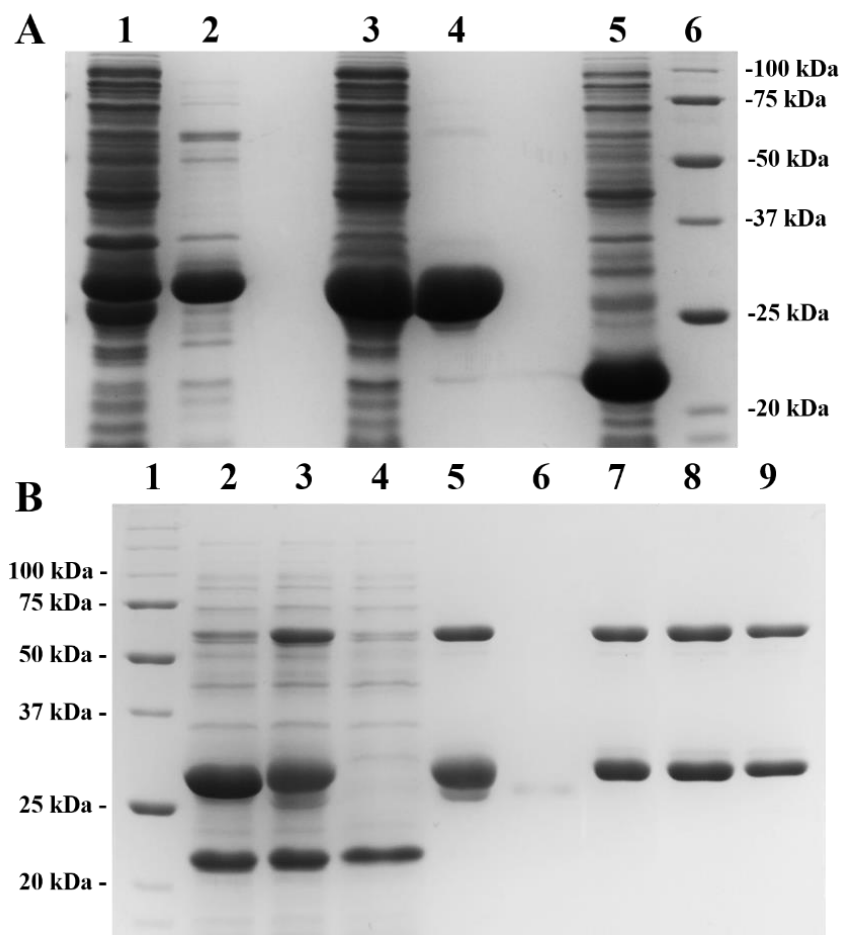


Figure 3.2 SDS-PAGE analysis of protein expression and Z-ELP-E2 ligation.
 A) Protein expression. Lane 1-2: E2 soluble lysate and 70°C pure. Lane 3-4: Z-ELP soluble lysate and ITC pure. Lane 5: Sortase A soluble lysate. Lane 6: MW marker B) Ligation. Lane 1: MW marker. Lane 2: Initial reaction. Lane 3: Final reaction. Lane 4: ITC hot spin supernatant. Lane 5: ITC 1 pure. Lane 6: 100 kDa filtrate. Lane 7: 100 kDa final retentate. Lane 8: ITC 2 pure. Lane 9: ITC 3 pure.

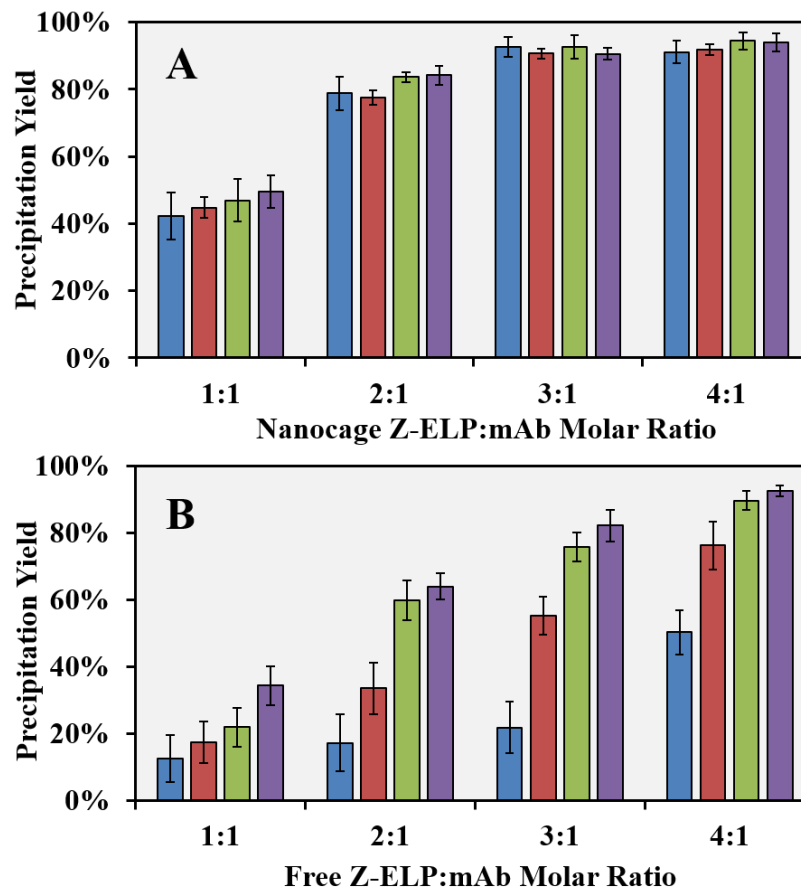


Figure 3.3 Effect of Z:mAb molar binding ratio and salt concentration on mAb precipitation yield. Either Z-ELP-E2 (A) or free Z-ELP (B) was mixed with 10 μ M mAb at target molar ratios in PBS at 23°C and adjusted to 0 M (blue), 0.2 M (red), 0.4 M (green), or 0.6 M (purple) ammonium sulfate.

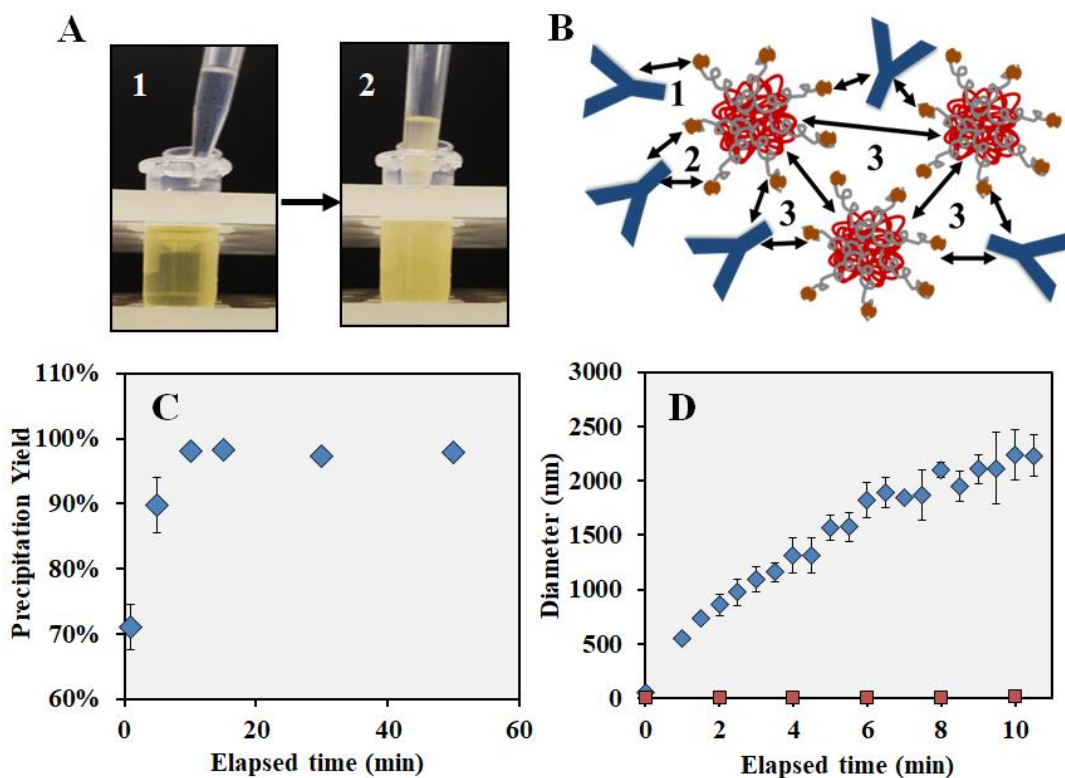


Figure 3.4 mAb-nanocage aggregation kinetics. A) Rapid formation of large aggregates. 1: Mixing soluble nanocages with mAb cell culture. Time = 0 sec. 2: Solution turbid immediately after pipetting up and down. Time = 10 sec. B) mAb-nanocage crosslinking mechanism. mAb binding to either 1: a single Z-domain on a nanocage, 2: two Z-domains from the same nanocage; or 3: two Z-domains from two different nanocages for crosslinking. C) The mAb precipitation yield vs mixing time in 96-well plate format. D) DLS analysis of mAb-nanocage (blue) and mAb-Z-ELP (red) aggregation after mixing.

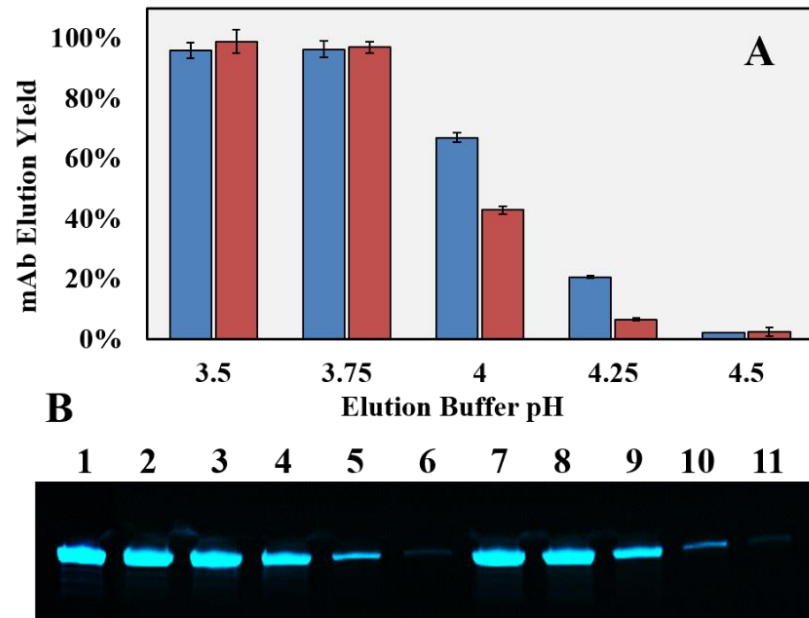


Figure 3.5 Effect of buffer pH on the mAb elution yield. A) The mAb elution yield in 50 mM sodium acetate (blue) or sodium citrate (red) buffers. B) SDS-PAGE analysis of eluted mAb. Lane 1: Initial mAb. Lane 2-6: sodium acetate pH 3.5-4.5. Lane 7-11: sodium citrate pH 3.5-4.5.

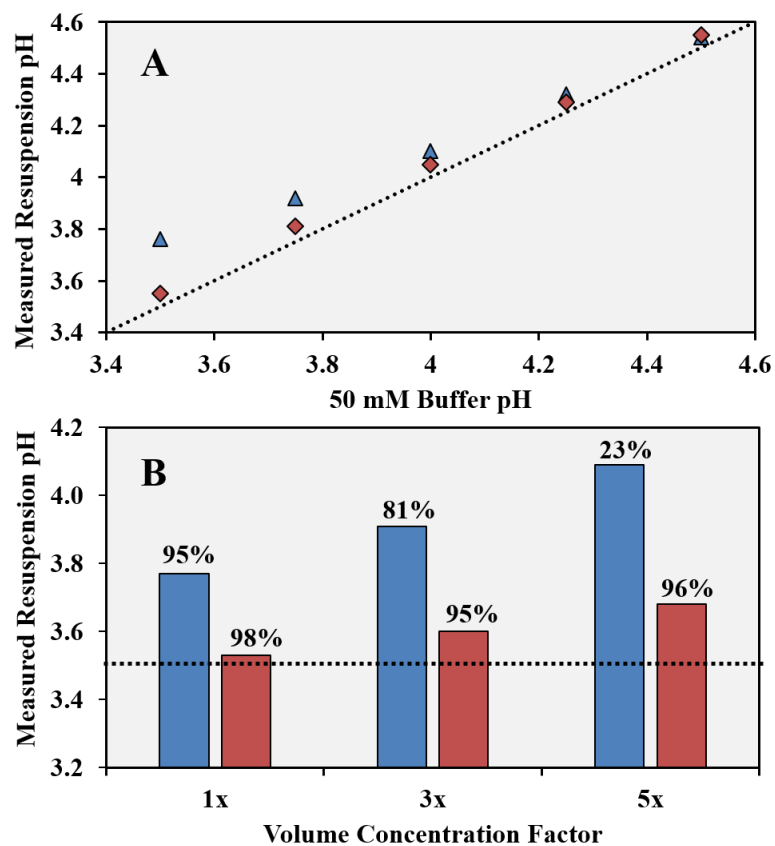


Figure 3.6 Effect of elution buffer and VCF on resuspension pH. A) Measured resuspension pH for 50 mM sodium acetate (blue triangles) buffer or 50 mM sodium citrate (red diamonds). Black line represents expected pH with no pH drift. B) Measured resuspension pH for 50 mM sodium acetate (blue) or 50 mM sodium citrate (red) at 1, 3, and 5x VCF. Numbers above bars represent the average mAb elution yield. Black line represents expected pH with no pH drift.

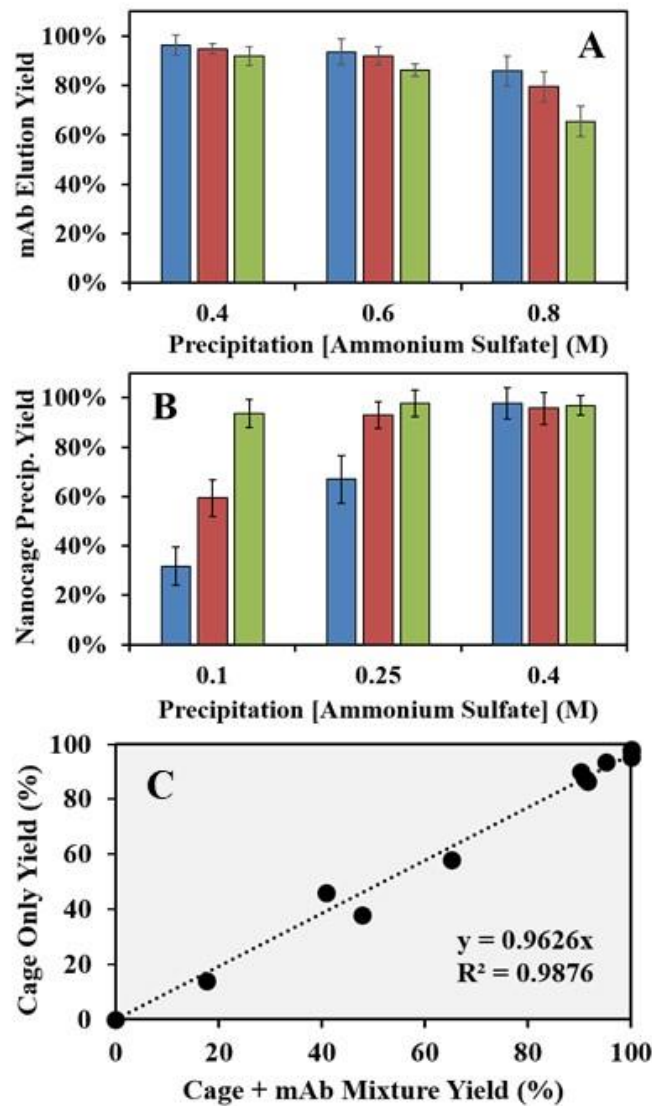


Figure 3.7 Effects of volume concentration and salt concentration on mAb and nanocage recovery. A) The mAb elution yield for 1x (blue), 3x (red), and 5x (green) volume concentration at various ammonium sulfate concentrations. B) The nanocage recovery yield for 1x (blue), 3x (red), and 5x (green) volume concentration at various ammonium sulfate concentrations. C) Relationship between nanocage precipitation yield with and without the presence of mAb.

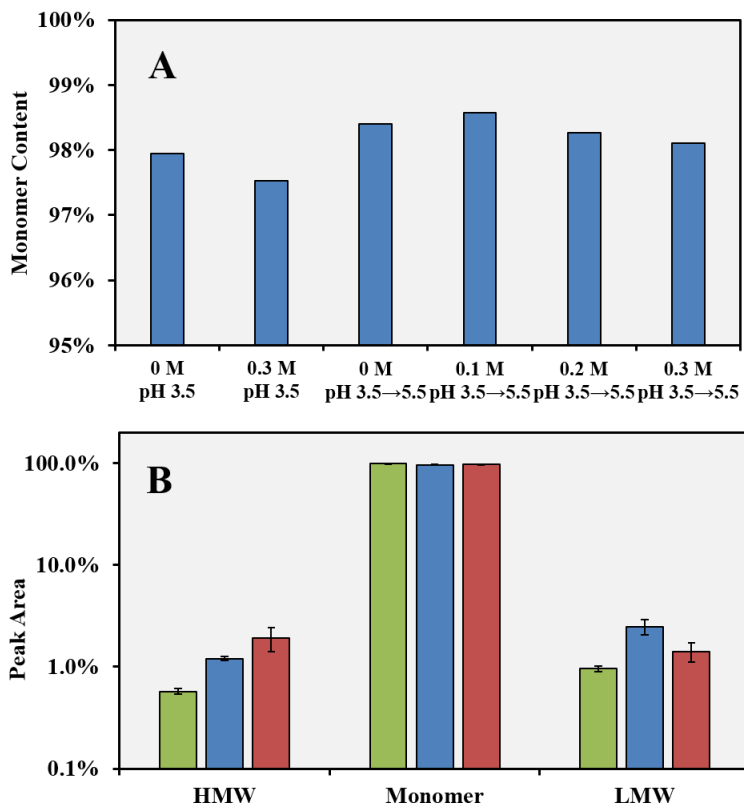


Figure 3.8 mAb elution stability. A) Monomer content for mAb in 50 mM sodium citrate with salt and with titration to pH 5.5 with 2 M tris pH 11. B) Stability profiles for pure mAb in PBS (green), mAb eluted from nanocage at pH 3.5 with 5-fold volume concentration and 0.3 M ammonium sulfate (blue), and mAb elution pool sample from protein A chromatography (red). The levels of high molecular weight (HMW) and low molecular weight (LMW) aggregates are included.

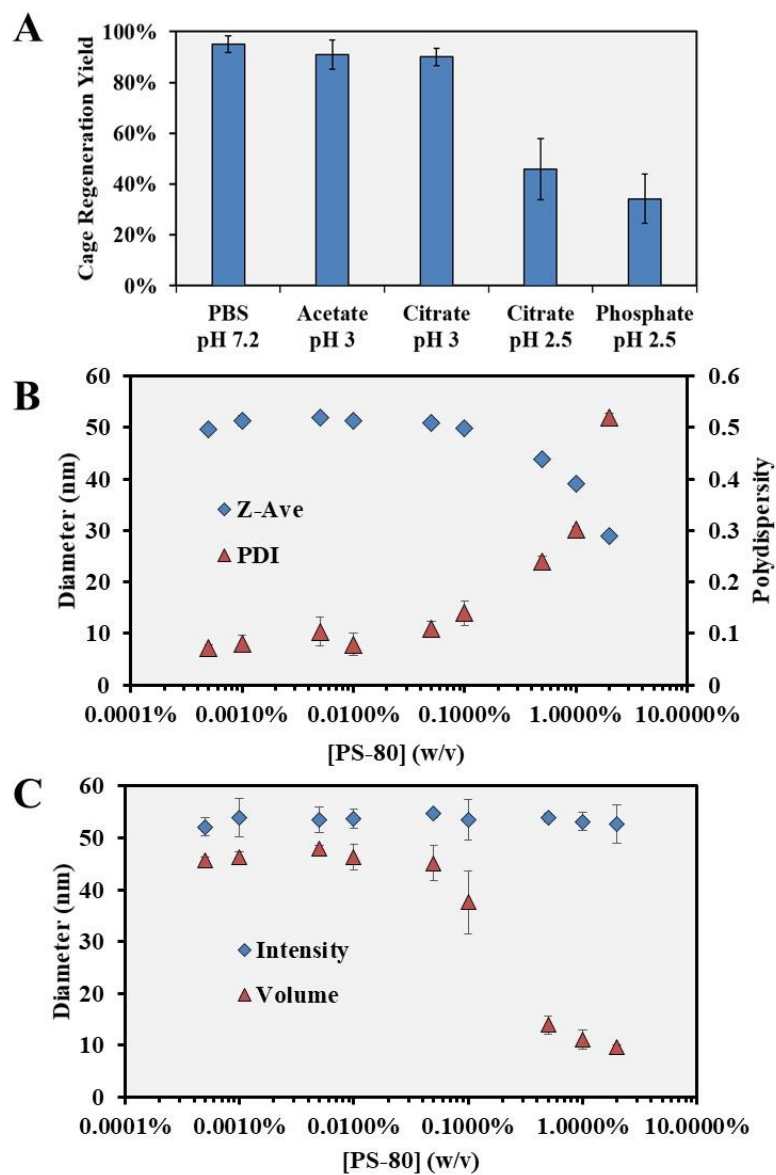


Figure 3.9 Nanocage process stability. A) Nanocage regeneration yield in low pH buffers. B) Effect of PS-80 on hydrodynamic diameter and polydispersity index. C) Effect of PS-80 on intensity and volume distribution means.

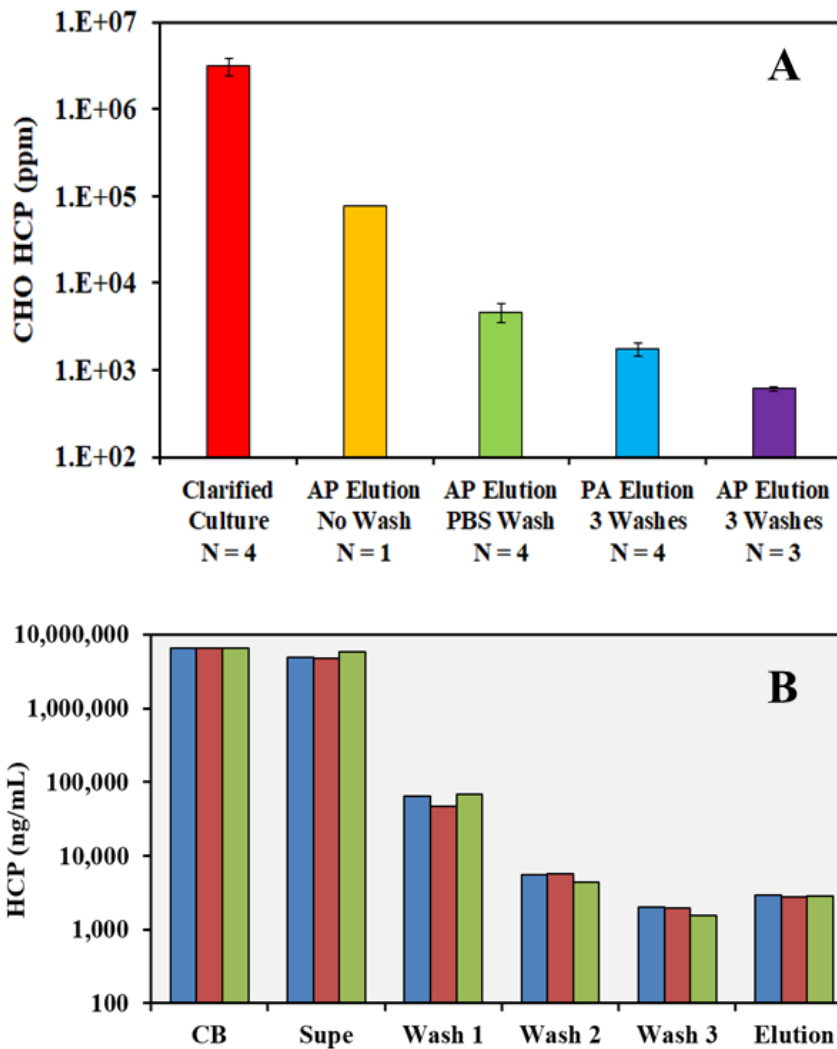


Figure 3.10 Effects of washing step on HCP clearance. A) HCP content for initial mAb cell culture (red) and affinity precipitation (AP) HCP content in elution using no wash (yellow), one PBS wash (green), or using same three wash buffers (purple) that were optimized for protein A chromatography (PA) (blue) HCP clearance. N = number of replicate purification runs. Error bars represent 95% confidence intervals. B) Affinity precipitation HCP clearance over intermediate steps for cycle 1 (blue), cycle 2 (red), and cycle 3 (green).

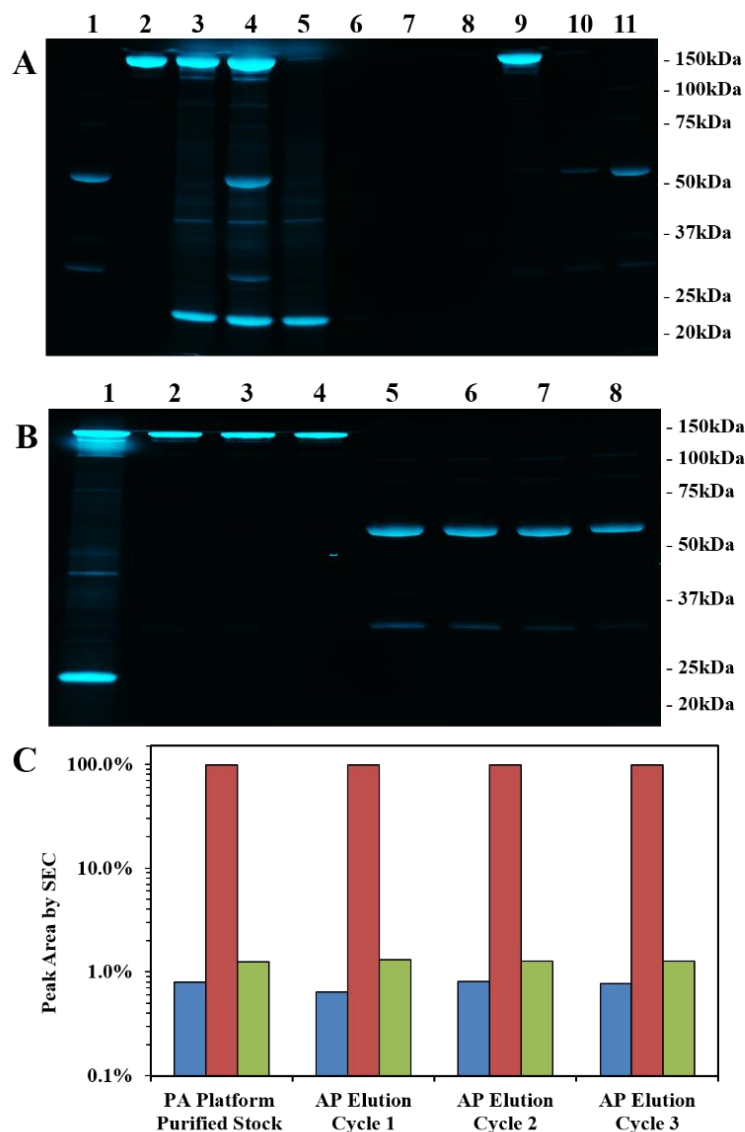


Figure 3.11 SDS-PAGE analysis of mAb affinity precipitation. A) Steps of the purification process. Lane 1: Pure nanocage. Lane 2: Pure mAb. Lane 3: mAb cell culture. Lane 4: Mixture of nanocage with mAb cell culture. Lane 5: Precipitation supernatant. Lane 6-8: Wash 1-3 supernatant. Lane 9: mAb elution supernatant. Lane 10: Regeneration supernatant. Lane 11: Regenerated nanocage. B) Three consecutive cycles of mAb affinity precipitation. Lane 1: mAb cell culture. Lane 2-4: Cycles 1-3 mAb Elution. Lane 5: Initial nanocage. Lanes 6-8: Regenerated nanocages from cycles 1-3. C) Comparison of mAb quality of the protein A (PA) purified mAb stock and affinity precipitation (AP) elution from the three purification cycles. (Blue) HMW aggregates, (Red) Monomers, (Green) LWM aggregates.

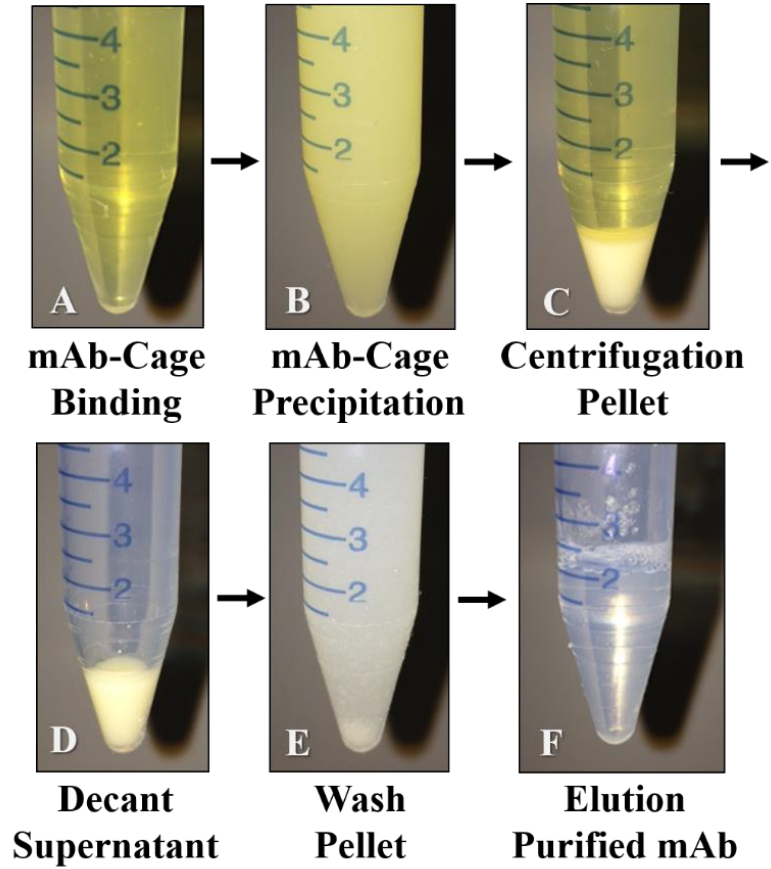


Figure 3.12 mAb affinity precipitation with pictures. A) mAb culture. B) After adding nanocage at 3:1 Z-ELP:mAb ratio. C) Pellet after centrifugation. D) Remove supernatant. E) Suspend pellet in was buffer. F) Resolubilize pellet in elution buffer with volume concentration.

REFERENCES

1. Beck A, Wurch T, Baily C, Corvaia N. Strategies and challenges for the next generation of therapeutic antibodies. *Nat Rev Immunol* **2010**, 10:345-352.
2. Ecker DM, Jones S, Levine HL. The therapeutic antibody market. *mAbs* **2015**, 7(1):9-14.
3. Huang Y-M, Hu W, Rustandi E, Chang K, Yusif-Makagiansar H, Ryll T. Maximizing productivity of CHO cell-based fed-batch culture using chemically defined media conditions and typical manufacturing equipment. *Biotechnol Prog* **2010**, 26(5):1400-1410.
4. Shukla AA and Thömmes J. Recent advances in large-scale production of monoclonal antibodies and related proteins. *Trends Biotechnol.* **2010**, 28(5):253-261.
5. Löfdahl S, Guss B, Uhlén M, Philipson L, Lindberg M. Gene for staphylococcal protein A. *Proc Natl Acad Sci* **1983**, 80:697-701.
6. Ghose SM, Allen M, Hubbard B, Brooks C, Cramer SM. Antibody variable region interactions with Protein A: implications for the development of generic purification processes. *Biotechnol Bioeng* **2005**, 92(6):665–667.
7. Thömmes J, Etzel M. Alternatives to chromatographic separations. *Biotechnol Prog* **2007**, 23(1):42-45).
8. Hillbrig F, Freitag R. Protein Purification by affinity precipitation. *J Chromatogr B* **2003**, 848(1):40-47.
9. Chilkoti A, Christensen T, MacKay JA. Stimulus responsive elastin biopolymers: applications in medicine and biotechnology. *Cur Op Chem Bio* **2006**, 10(6):652-657.
10. Urry DW. Physical chemistry of biological free energy transduction as demonstrated by elastic protein-based polymers. *J Phys Chem B* **1997**, 101(51):11007-11028.
11. Meyer DE, Chilkoti A. Purification of recombinant proteins by fusion with thermally-responsive polypeptides. *Nat Biotechnol* **1999**, 17(11):4.

12. Kim JY, Mulchandani A, Chen W. Temperature-triggered purification of antibodies. *Biotechnol Bioeng* **2005**, 90:373-379.
13. Lao UL, Mulchandani A, Chen W. Simple conjugation and purification of quantum dot-antibody complexes using a thermally responsive elastin-protein L scaffold as immunofluorescent agents. *J Am Chem Soc* **2006**, 128:14756-14757.
14. Liu F, Chen W. Engineering a recyclable ELP capturing scaffold for non-chromatographic protein purification. *Biotechnol Prog* **2006**, 29:968-971.
15. Kim H, Chen W. A non-chromatographic protein purification strategy using src 3 homology domains as generalized capture domains. *J Biotechnol* **2016**, 234:27-34.
16. Madan B, Chaudhary G, Cramer SM, Chen W. ELP-z and ELP-zz capturing scaffolds for the purification of immunoglobulins by affinity precipitation. *J Biotechnol* **2013**, 163(1):10-16.
17. Sheth RD, Madan B, Chen W, Cramer SM. High throughput screening for the development of a monoclonal antibody affinity precipitation step using ELP-Z stimuli responsive biopolymers. *Biotechnol Bioeng* **2013**, 110:2664-2676.
18. Sheth RD, Jin M, Bhut BV, Liu J, Lee J, Siegfried R, Li Z, Chen W, Cramer SM. Affinity precipitation of monoclonal antibody from industrial harvest feedstock using ELP-Z stimuli responsive biopolymers. *Biotechnol Bioeng* **2013**, 111:1595-1603.
19. Boulet-Audet M, Byrne B, Kazarian SG. High-throughput thermal stability analysis of a monoclonal antibody by attenuated total reflection FT-IT spectroscopic imaging. *Anal Chem* **2014**, 86(19): 9786–9793
20. Arosio P, Jaquet B, Wu H, Morbidelli A. On the role of salt type and concentration on the stability behavior of a monoclonal antibody solution. *Biophys Chem* **2012** 168:19-27.
21. Swartz AR, Sun Q, Chen W. Ligand-induced crosslinking of Z-ELP-functionalized E2 protein nanoparticles for enhanced affinity precipitation of antibodies. *Biomacromolecules* **2017**, 18(5):1654-1659.
22. Sun, Q, Chen Q, Blackstock D, Chen W. Post-translational modification of bio-nanoparticles as a modular platform for biosensor assembly. *ACS Nano* **2015**, 9(8):8554–8561.

23. Chen, Q, Sun, Q, Molino NM, Wang S-W, Boder ET, Chen W. Sortase A-mediated multi-functionalization of protein nanoparticles. *Chem Commun* **2015**, 51:12107-12110.
24. Hansen SK, Jamali B, Hubbuch J. Selective high throughput protein quantification based on UV absorption spectra. *Biotechnol Bioeng* **2013**, 110(2):448-460.
25. Swartz AR, Xu X, Traylor SJ, Li ZJ, Chen W. One-step affinity capture and precipitation for improved purification of an industrial monoclonal antibody using Z-ELP functionalized nanocages. *Biotechnology and Bioengineering* **2018**, 115(2):423-432.
26. Shukla AA, Hinckley PJ, Gupta P, Yigzaw Y, Hubbard B. Strategies to address aggregation during Protein A chromatography. *Bioproc Int* **2005**, 3(5):36-44.
27. Shukla AA, Hubbard B, Tressel T, Guhan S, Low D. Downstream processing of monoclonal antibodies – Application of platform approaches. *J Chrom B* **2007**, 848(1):28-39.
28. Shukla AA and Hinckley P. Host cell protein clearance during protein a chromatography: Development of an improved column wash step. *Biot Prog* **2008**, 24(5):1115-1121.
29. Domingo GJ, Orru S, Perham RN. Multiple display of peptides and proteins on a macromolecular scaffold derived from a multienzyme complex. *J Mol Biol* **2001**, 305(2):259-267.
30. Kostal, J, Mulchandani, A, Chen, W. Tunable Biopolymers for Heavy Metal Removal. *Macromolecules* **2002**, 34:2257-2261.
31. Jiang C, Liu J, Rubacha M, Shukla AA. A mechanistic study of Protein A chromatography resin lifetime. *J Chromatogr A* **2009**, 1216:5849-5855.
32. Hammerschmidt N, Tscheliessnig A, Sommer R, Helk B, Jungbauer A. Economics of recombinant antibody production processes at various scales: Industry standard compared to continuous precipitation. *Biotechnol J.* **2017**, 9:766-775.

Chapter 4

HIGH-EFFICIENCY AFFINITY PRECIPITATION OF INDUSTRIAL MABS AND FC-FUSION PROTEINS FROM CELL CULTURE HARVESTS

Abstract

Chapter 3 described a high-yielding, affinity precipitation process capable of rapidly capturing mAbs from cell culture through spontaneous, multi-valent crosslinking into large aggregates. To challenge the capabilities of this technology, nanocage affinity precipitation was investigated using four industrial mAbs (mAbs A–D) and one Fc fusion protein (Fc A) with diverse molecular properties. A molar binding ratio of 3:1 Z:mAb was sufficient to precipitate > 95% mAb in solution for all molecules evaluated at ambient temperature without added salt. The four mAbs and one Fc fusion were purified from cell culture using optimal process conditions and > 94% yield and > 97% monomer content were obtained. Affinity precipitation impurity clearance was equivalent to expected Protein A chromatography performance. Chapter 4 highlights the benefits of nanoparticle crosslinking for enhanced affinity capture and presents a robust platform that may be applied to any target mAb or Fc-containing proteins with minimal optimization of process parameters.

Chapter 4 is reproduced with permission from John Wiley and Sons. Source:

Swartz AR, Xu X, Traylor S, Li ZJ, Chen W. High-efficiency affinity precipitation of multiple industrial mAbs and Fc-fusion proteins from cell culture harvests using Z-ELP-E2 nanocages. *Biotechnol Bioeng* **2018**, 1-9. (in press)

4.1 Introduction

Advances in upstream production of therapeutic monoclonal antibodies (mAbs) have challenged current platform downstream purification technologies¹. Protein A affinity chromatography is commonly used as the primary antibody capture step because of the high selectivity of the Protein A ligand to the Fc region present on human immunoglobulin G (IgG)². However, economic, throughput, and scale-up limitations make Protein A affinity chromatography a potential bottleneck in the overall mAb production process³. Affinity precipitation has been investigated as a more cost-effective and scalable alternative⁴⁻⁵, but the technique has not been widely implemented in industry because of low mAb yields, co-precipitation of contaminants, and use of harsh chemicals or solution conditions⁶.

Affinity precipitation using a stimuli-responsive, recombinant elastin-like polypeptide (ELP) genetically fused to an IgG binding domain called the Z-domain (Z-ELP) has been shown to be a promising scaffold for selective IgG capture⁷⁻⁹. However, the elevated salt and temperature required for ELP precipitation resulted in increased mAb aggregation and decreased operational efficiency. Chapter 2 described the production of an enhanced antibody capture scaffold by covalently conjugating Z-ELP to a 25 nm self-assembled, 60-mer E2 protein nanocage (Z-ELP-E2) using Sortase A ligation¹⁰. Multi-valent IgG binding triggered spontaneous crosslinking into large IgG-Z-ELP-E2 aggregates that allowed for easy precipitation and separation, and the recovered IgG-Z-ELP-E2 complex remained insoluble until dissociation with a low pH elution.

In Chapter 3, we performed high-throughput process optimization using a model industrial mAb, and developed a simple, one-step antibody affinity capture and precipitation platform for mAb purification from CHO cell culture fluids with

equivalent yields and impurity clearance compared to Protein A chromatography¹¹. Upon mixing at a 3:1 Z-domain:mAb molar ratio, > 95% mAb was precipitated within minutes at ambient temperature without added salt due to extensive nanocage crosslinking. High mAb recovery was obtained after washing at $\text{pH} \geq 5$ followed by elution at $\text{pH} < 4$, and the purification process was repeated over several cycles using the same regenerated nanocage with a similar process efficiency.

For a more robust examination of this technology as an alternative to Protein A chromatography, the general utility of the approach was further evaluated in Chapter 4 using four industrial mAbs and one Fc fusion protein with diverse attributes such as IgG subclass, isoelectric point (pI), and culture harvest titers (**Table 4.1**). Key process conditions such as the molar binding ratio, aggregation time, and elution pH were tested using purified mAb and nanocage stocks. A two-step kinetic model was applied to examine the dependence of the solution pH on aggregation rates. Operational conditions were identified to maximize mAb yield and monomer content for each target molecule, while minimizing operation time (**Table 4.3**). Finally, the mAb yield, monomer content, and host cell protein (HCP) and DNA clearance from clarified Chinese hamster ovary (CHO) cell cultures were compared to typical Protein A chromatography¹².

4.2 Materials and Methods

4.2.1 Materials

Escherichia coli strain BLR(DE3) containing pET24(a) vectors encoding for Z-ELP[KV₈F-40]-LPETG, *E. coli* strain BL21(DE3) containing a pET11(a) vector encoding for GGG-E2(158), and another BL21(DE3) strain containing a pMR5 vector encoding for SrtA were constructed and described previously¹⁰. Purified and clarified

cell culture mAb and Fc-fusion samples were provided by Bristol-Myers Squibb (BMS) (New York City, NY). Bacto tryptone and yeast extract were purchased from BD Biosciences (Franklin Lakes, NJ). Kanamycin, ampicillin, bovine serum albumen (BSA), isopropyl- β -D-thiogalactoside (IPTG), and 96-well 200 μ L conical PCR plates were purchased from Fisher Scientific (Pittsburgh, PA). A human polyclonal IgG, sodium hydroxide, sodium phosphate, citric acid, tris base, ammonium sulfate, sodium chloride, L-arginine, and polysorbate-80 (PS-80) were purchased from Sigma-Aldrich (St. Louis, MO). 0.8/0.2 μ m Supor Acrodisc syringe filters were purchased from Pall (Port Washington, NY). 100 kDa Sartorius Vivaspin 20 spin columns were purchased from Sartorius (Göttingen, Germany). 96-well half area UV-transparent plates were purchased from Corning (Corning, NY). An Acquity UPLC BEH SEC Column (200Å, 1.7 μ m, 4.6 x 300 mm) was purchased from Waters (Milford, MA).

4.2.2 Z-ELP-E2 Nanocage Production

Z-ELP[KV₈F-40]-LPETG, a modified GGG-E2 from *Bacillus stearothermophilus*, and Sortase A from *Staphylococcus aureus* were expressed in *Escherichia coli* and Z-ELP was conjugated to E2 using previously indicated procedures¹¹. Briefly, Z-ELP purified by inverse transition cycling (ITC)¹³, E2 partially purified by 70°C heating, and Sortase A soluble lysate were mixed in a reaction buffer for 8 h at 23°C and the ligation product was purified by ITC into phosphate buffered saline (PBS; 20 mM sodium phosphate, 150 mM sodium chloride, pH 7.2). 100 kDa Sartorius Vivaspin 20 spin columns were used to remove excess Z-ELP and two more ITC cycles were used to further concentrate the purified Z-ELP-E2 stock. Z-ELP ligation density on E2 was determined by densitometry analysis of an SDS-PAGE gel

and Z-ELP concentration was measured using absorbance at 280 nm and an experimentally determined extinction coefficient.

4.2.3 High-throughput Affinity Precipitation Experiments

Previous work utilized a mAb designated “mAb C” in the current investigation¹¹. All experiments using mAb C were repeated using the indicated procedures below. High-throughput affinity precipitation experiments were performed using 200 μ L 96-well conical PCR plates at 23°C with previously purified mAbs and Z-ELP-E2 nanocage stocks. For all centrifugation steps, the plate was spun at 1,500 g for 30 min at 23°C. Supernatant samples were collected using a multi-channel pipette and transferred into a UV-transparent 96-well plate for measurement of absorbance at 280 nm on a Tecan Infinite M1000 plate reader (Männedorf, Switzerland). mAb concentrations were determined using the theoretical extinction coefficient for each molecule. The supernatants were assumed to contain only mAb based on previous results¹¹. For binding ratio experiments, 20 μ M mAb samples were mixed with 20-100 μ M Z-ELP-E2 (1:1 to 5:1 Z-domain:mAb molar ratio) in PBS for 1 h before centrifugation for mAbs A-D. Fc A was mixed for 3 h before centrifugation. The supernatant was collected and the mAb precipitation yield was calculated ($\text{Yield} = 1 - [\text{mAb}_{\text{supe}}]/[\text{mAb}_{\text{initial}}]$). For precipitation kinetics experiments, 10 μ M mAb was mixed with 30 μ M Z-ELP-E2 in PBS for various incubation times ranging from 2 min to 3 h before centrifugation. The supernatant was collected and mAb precipitation yield was calculated. For mAb elution experiments, 10 μ M mAb was mixed with 30 μ M Z-ELP-E2 in PBS for 1-3 h before centrifugation. The precipitation supernatant was removed and the pellet was suspended in a 25 mM sodium citrate, pH 5.0, wash buffer by aspirating and dispensing using a pipette. After another spin, the wash supernatant was

removed and the pellet was suspended in 50 mM sodium citrate buffers with a pH ranging from 3.50-4.50 and mixed for 30 min. Samples were adjusted to 0.4 M ammonium sulfate using a 3 M stock before centrifuging again. The supernatant was collected and mAb elution yield was calculated ($\text{Yield} = 1 - [\text{mAb}_{\text{elution}}]/[\text{mAb}_{\text{initial}}]$). All experimental conditions were performed in triplicate and 95% confidence intervals of the mean value were reported.

4.2.4 Aggregation Kinetic Measurement

Solutions were prepared ranging from pH 5-9 using the indicated buffers and were adjusted to 150 mM total ionic strength by addition of sodium chloride (**Table 4.2**). Samples were prepared with 1 μM mAb and 3 μM Z-ELP-E2 in a target buffer in a 96-well UV transparent plate and immediately placed in a Synergy plate reader from BioTek (Winooski, VT) for kinetic measurement of absorbance at 350 nm for various times ranging from 5-300 min. A human polyclonal antibody used in previous work was included in this investigation¹⁰. Data were collected until peak absorbance, as some samples settled out of solution over time causing a decrease in signal. The Finke-Watzky two-step model of pseudoelementary nucleation (equation 1) and autocatalytic growth (equation 2) was applied¹⁴:



where A represents the monomeric nanocage with bound mAbs, B represents the polymeric mAb-nanocage aggregate and k_1 and k_2 represent average rate constants for nucleation and autocatalytic growth. Rate constants were assumed to be independent of aggregate size or morphology. The overall reaction rate for A is expressed as:

$$\frac{d[A]}{dt} = -k_1[A] - k_2[A][B] \quad (3)$$

where $[A]$ and $[B]$ represent concentrations of A and B at time t . It was assumed that there are no aggregates initially, $[B]_0 = 0$, such that $[B] = [A]_0 - [A]$ at all times. Upon integration of the rate law and further simplification, the expression for the increase in B over time was obtained:

$$[B] = [A]_0 - \frac{\frac{k_1}{k_2} + [A]_0}{1 + \frac{k_1}{k_2[A]_0} e^{(k_1 + k_2[A]_0)t}} \quad (4)$$

The values of k_1 and k_2 were fit by non-linear regression in Minitab 17 using normalized absorbance curves representing aggregate (B) formation over time and the 95% confidence interval of the fit was reported. The time at inflection (t_{max}) of the aggregation curve (maximum aggregation rate) was calculated by setting the second derivative of $[B]$ to zero¹⁵:

$$t_{max} = \frac{\ln\left(\frac{k_2 A_0}{k_1}\right)}{k_1 + k_2 A_0} \quad (5)$$

4.2.5 mAb Culture Affinity Precipitation

All purification steps were performed at 23°C using optimized process conditions reported in **Table 4.3**. For Fc A and mAb B, the culture was titrated to pH 5.0 using 1 M citric acid before adding the nanocage. For the other molecules, no titration was performed and precipitation was performed directly in cell culture (pH 7.0-7.5). Purified nanocage stock was mixed with mAb culture at a 3:1 Z:mAb molar ratio for 10 min and the mAb-nanocage complex was pelleted by centrifugation. The pellet was washed with a series of 3 wash buffers before elution by resuspending in 3-fold less volume 50 mM sodium citrate pH, 3.50, for mAb C, mAb D, and Fc A or pH 3.75 for

mAb A and mAb B for 60 min. The nanocage was precipitated with 0.2-0.3 M ammonium sulfate and the elution supernatants were titrated to pH 5.5 using 2 M tris, pH 11, and assayed for mAb concentration, monomer content, and impurity content. The pelleted nanocage was regenerated in 50 mM sodium citrate, pH 3.0, and recycled back into PBS pH 7.2 using ITC. The nanocage was filtered through a 0.8/0.2 μm Supor syringe filter before use in a subsequent purification cycle. The affinity precipitation process was repeated for three cycles for mAb C, D, and Fc A and one cycle for mAb A and B.

4.2.6 Analytical Size Exclusion Chromatography

mAb stability was monitored by size exclusion chromatography (SEC). Samples were diluted to 1 mg/mL mAb, added to a low-volume UPLC vial (Waters), and placed in a temperature controlled auto injector set at 4 °C in a Waters Acquity UPLC system. A mobile phase of 200 mM potassium phosphate, 150 mM sodium chloride, pH 6.8, was used at a flow rate of 0.4 mL/min. Three injections of 10 μL were performed and the column effluent was monitored at 280 nm. Peak areas were analyzed by Empower Software (Waters).

4.2.7 Analytical Impurity Content

The CHO cell host cell protein (HCP) concentration was determined using an ELISA kit from Cygnus Technologies. The CHO cell DNA concentration was determined by an in-house quantitative PCR (qPCR) assay developed at BMS. Details of these assays have been discussed previously⁹.

4.3 Results and Discussion

4.3.1 Impact of Z-domain-target binding ratio on precipitation yield

The objective of Chapter 4 was to demonstrate the utility of the Z-ELP-E2 nanocage for the affinity precipitation of multiple mAbs and Fc-fusion proteins with different molecular properties (**Table 4.1**). Results in Chapter 3 using a mAb designated “mAb C” from BMS demonstrated that a 3:1 Z-domain:mAb molar ratio was optimal for precipitation at ambient temperature without any addition of salt¹¹. To investigate whether this was true for other mAbs or Fc-fusion proteins, Z-ELP-E2 nanocages were mixed with the purified target proteins at molar binding ratios ranging from 1:1 to 5:1 in PBS at 23°C (**Figure 4.1A**). Again, a 3:1 binding ratio was sufficient to precipitate ~95% mAb in the mixture for all targets tested, suggesting that this was likely the optimal ratio to trigger both efficient nanocage crosslinking and ELP aggregation for purification.

The ratio was slightly higher than the expected Z:IgG stoichiometry¹⁶ of 2:1, likely due to steric limitations on Z-domain flexibility or accessibility of IgG binding sites. These results confirmed the suitability of using Z-ELP-E2 nanocages to capture different Fc-containing proteins with similar efficiencies. Although a 4:1 binding ratio exhibited a similarly high precipitation yield, increasing the binding ratio further to 5:1 decreased the yield to less than 80%. These observations are consistent with the molar binding ratio used in other affinity precipitation systems. For the purification of multimeric dehydrogenase enzymes using a bivalent affinity ligand, the optimal precipitation yield occurred at a ligand:protein ratio near the expected interaction stoichiometry. In addition, too much excess ligand resulted in lower yields due to the saturation of binding sites on the target protein and reduced crosslinking efficiency¹⁷.

4.3.2 Effect of solution pH on aggregation kinetics

The rapid capture and precipitation of mAb C was previously demonstrated to occur within a few min upon mixing with the nanocages¹¹. However, the binding and crosslinking kinetics appeared to differ significantly among the five target proteins in the current study. Samples containing either purified mAb A, C, or D turned cloudy within seconds upon mixing with nanocages at a 3:1 Z:mAb molar ratio. In contrast, mAb B and Fc A gradually increased in turbidity over several minutes to hours. To evaluate how the crosslinking kinetics can impact target precipitation and recovery, samples were mixed with nanocages at the same 3:1 Z:mAb binding ratio from 2 min to 3 h before pelleting the complex (**Figure 4.1B**). The nanocage precipitated greater than 90% of mAb A, C, and D from the mixture within 10 min, but required 30 min for mAb B and 3 h for Fc A to obtain similar yields. IgG subclass appeared to have no impact on aggregation kinetics because mAbs from both IgG1 (mAb A) and IgG4 (mAb C–D) groups precipitated rapidly. The variable kinetics may be due to differences in the mAb or Fc protein net charge at neutral pH. In PBS at pH 7.2, Fc A (pI = 5.8) and mAb B (pI = 6.8) are both anionic with a pI value less than the buffer pH, while the other mAbs with fast kinetics have pI values greater than 8 (**Table 4.1**).

To quantify the dependence of aggregation kinetics on solution pH, the Finke-Watzky (F-W) model of nucleation (equation 1) and growth (equation 2) was selected to fit aggregation curves over time. This model has been applied to numerous systems to characterize aggregation events^{14,18} and allows for simple quantification of average rate constants by fitting experimental data to the integrated rate law (equation 4). The F-W model was chosen because it appropriately depicts the previously hypothesized aggregation mechanism of an initial multi-valent binding step between two Z-domain

from different nanocages and one mAb, followed by autocatalytic crosslinking into large, insoluble particles¹⁰.

The aggregation curves for mAb B, Fc A, and a human polyclonal IgG displayed a strong dependence on solution pH (**Figure 4.2B, 4.2E, 4.2F**), whereas mAbs A, C, and D demonstrated fast kinetics with minimal pH dependence in the tested range of pH 5-9 (**Figure 4.2A, 4.2C, 4.2D**). The absorbance data was fit to the F-W model and the k_1 and k_2 rate constants were evaluated for each solution condition and molecule (**Figure 4.3**). mAb B exhibited fast aggregation at pH 5-7, but a shift occurred between pH 7 and 8 such that both rate constants decreased by an order of magnitude (**Figure 4.3B**). In addition, the ratio of the rate constants also differed significantly between the two kinetic regimes. At low pH, the nucleation (k_1) and crosslinking ($k_2 \cdot A_0$) rate constants were similar, but at pH 8-9, nucleation was the rate limiting step ($k_1 \ll k_2 \cdot A_0$). Fc A had very slow kinetics at $\text{pH} \geq 7$, requiring > 60 min to reach maximum aggregation rate (t_{max}) (**Figure 4.4**). However, at pH 5, the maximum aggregation rate occurred within 10 min and the rate constants increased ten-fold compared to pH 6 (**Figure 4.3E**). This result is significant as we can dramatically reduce the time required for Fc A precipitation from 3 h to 10 min simply by titrating the cell culture to pH 5. Similarly, the aggregation kinetics of the human polyclonal IgG also increased at lower pH. Using isoelectric focusing, the distribution of pI values for the human polyclonal antibody has been estimated¹⁹ to range between pH 5-7. The rate constants gradually increased at lower buffer pH likely due to a larger majority of cationic antibodies within the polyclonal antibody population. This result validates our previous observations of lower polyclonal antibody precipitation yields and slower aggregation kinetics compared with mAb¹¹. This analysis suggests that the time required for precipitation of

any target mAb with a pI value less than 7 may be minimized to < 10 min by simply titrating the cell culture to a lower pH.

Overall, lowering the buffer pH to 5 resulted in higher kinetic rates for all molecules. These results suggest that molecules with a net positive charge under more acidic solution conditions have a higher propensity for nanocage crosslinking. The higher degree of crosslinking is unlikely the result of improved mAb binding as the binding affinity of Z-domain decreases at more acidic pH (pH 5.0) compared to neutral pH²⁰. Therefore, the increase in kinetics at lower pH is more likely due to other biophysical changes. Electrostatic interactions between the ELP and mAb may play a role in crosslinking. The Z-ELP fusion protein contains a small linker between the tri-helical Z-domain and cationic ELP (pI = 10.6, intrinsically disordered)¹⁰. A negative net charge on the mAb may attract the positively charged ELP (at all solution pH 5–9) and sterically disrupt interaction with the Z-domain. In contrast, higher crosslinking efficiency may be obtained if the net ELP-mAb interaction is repulsive at solution pH less than the mAb pI value as detected here.

The effect of solution pH on aggregation rates has been postulated for other protein systems. For the amyloid protein, α -synuclein, the aggregation rate increases as the solution pH is decreased from 8 to below the isoelectric point (pH ~4) due to conformational changes that increased protein-protein interactions²¹. The aggregation kinetics of amyloid proteins were characterized by the F-W model and a similar result was obtained as in the current work: nucleation rates (k_1) were significantly higher at a solution pH < protein pI²². This provides an easily tunable parameter for minimizing the time required for aggregation using a simple pH shift.

4.3.3 Elution buffer pH and mAb stability

After polymerizing into large aggregates, the mAb-nanocage complex remained insoluble until dissolution with a low pH elution. To separate dissociated mAbs after elution in a low pH buffer, the nanocage was selectively precipitated by adding 0.4 M ammonium sulfate, and the eluted mAbs were collected in the supernatant after centrifugation. Previously in Chapter 3, we demonstrated that citrate elution buffer was ideal for minimizing pH drift when resuspending at higher concentrations¹¹. Consistent with previous results, the critical solution pH to dissociate mAbs from the Z-domain was at pH < 4.0; a mAb recovery yield > 90% was obtained at pH 3.50 and 3.75 for all molecules (**Figure 4.5**). Above pH 4.0, mAbs did not fully dissociate from the Z-domain, resulting in the co-precipitation of mAbs still bound within the crosslinked network. At pH 5, minimal mAb (< 1.5%) was detected in the supernatant, indicating that a solution pH of ≥ 5 was compatible for washing or precipitation. This result corroborates the aggregation kinetics investigation, where all molecules rapidly aggregated into insoluble precipitates at pH 5.

Since some mAbs have been shown to aggregate at pH < 4 in the presence of salt²³, the effect of elution pH and salt concentration on monomer content was further investigated in a 50 mM sodium citrate, pH 3.5, buffer with 0.0–0.3 M ammonium sulfate concentration (**Figure 4.6A**). Samples were combined in a target buffer and mixed for 120 min at 23°C before titrating back to pH 5.5 for measurements by SEC. The titration to pH 5.5 was performed to mimic the procedure used with conventional protein A chromatography where the elution pool is titrated to pH > 5 after a viral inactivation to mitigate any potential detrimental impacts of low pH on mAb stability²⁴. While mAb C, mAb D, and Fc A were all stable at pH 3.5 and ammonium sulfate up to

0.3 M, mAb A and B were only stable in 50 mM sodium citrate, pH 3.5, without added salt, and exhibited significant aggregation in the presence of 0.1 M ammonium sulfate.

To determine the optimal elution pH while providing maximum product recovery, mAb A and B monomer content was measured after an incubation of 120 min in citrate buffers pH 3.5-5.0 with 0.2 M ammonium sulfate followed by a titration to pH 5.5 (**Figure 4.6B**). The monomer content greatly improved at pH 3.75 and was > 98% at pH 4 and 5. Because pH 3.75 was sufficient for high elution yields (**Figure 4.5**), 50 mM citrate pH 3.75 and 0.2 M ammonium sulfate was selected for the precipitation and purification of mAb A and B from cell culture.

4.3.4 Affinity precipitation from cell culture harvests

After optimization of process conditions for each target protein, affinity precipitation was performed from clarified cell culture harvests according to the indicated procedures (**Table 4.3**). mAb A, C, and D were mixed with nanocages at a 3:1 Z:mAb molar ratio directly in cell culture (pH 7.0-7.5). Because of the slower aggregation kinetics, mAb B and Fc A were titrated to pH 5.0 using 1 M citric acid before precipitation with the nanocage. The pelleted mAb-nanocage complex was washed with a series of three buffers. For mAbs A-D, the second wash buffer contained 0.05% (w/v) PS-80 to remove trace contaminants¹¹, while PS-80 was excluded for Fc A because of protein stability concerns. mAb A and B were eluted with a 50 mM citrate buffer (pH 3.75), while other molecules were eluted with a 50 mM citrate buffer (pH 3.50) in 3-fold less volume to concentrate the target proteins. The nanocage was precipitated with 0.2-0.3 M ammonium sulfate and the mAbs were collected in the supernatant and titrated to pH 5.5. After recycling back into PBS, the nanocage was

sterile filtered through a 0.2 μm membrane before reuse in additional purification cycles.

The mAb elution samples were characterized by the overall yield, % monomer, and HCP and DNA impurity content (**Figure 4.7**). The final product yields ranged from 94–97% and the monomer content exceeded 97% for all targets. The HCP and DNA clearance was consistent for mAbs A–D with < 1000 ppm HCP (~3 log reduction) and < 50 ppm DNA (4-5 log reduction) (**Figure 4.8B**). However, Fc A did not have as efficient HCP impurity clearance with only 2 logs of reduction. One reason for this poor clearance could be because the second wash buffer did not contain PS-80, which has been shown to be beneficial for HCP clearance by reducing non-specific interactions²⁵. A further optimization of the wash buffer conditions could potentially improve upon this result. Compared to protein A chromatography, the average affinity precipitation performance of mAbs A–D meet or exceed all expectations for yield, monomer, and impurity content (**Table 4.4**). The average nanocage recovery for an affinity precipitation purification cycle was about 87% (**Figure 4.8A**). As discussed previously¹¹, this low nanocage yield was likely due to losses to the container or sterile filter from operational constraints during the regeneration steps. Furthermore, the nanocage recovery may be improved by more efficient ELP precipitation with longer ELPs and higher ELP grafting density on the E2 nanocage. These results indicate the proposed affinity precipitation process can consistently achieve high yield and impurity clearance for any target mAb with only minor optimization of the binding pH and elution stability profile.

4.4 Conclusion

Affinity precipitation of mAbs using Z-ELP-E2 nanocages has been shown to be a promising alternative to protein A chromatography because of three key features: 1) Spontaneous crosslinking allows for rapid affinity capture and precipitation at ambient temperature without added salt. 2) Irreversible insoluble precipitate formation allows for washing in most target buffer with $\text{pH} \geq 5$ or extended storage of the mAb-nanocage complex. 3) Enlarged nanocage dimension minimizes salt concentration required for precipitation after elution.

In Chapter 4, we challenged the nanocage affinity precipitation process using four industrial mAbs and one Fc fusion protein. For all target proteins, a 3:1 Z:mAb binding ratio was sufficient to precipitate > 95% mAb in the solution mixture. mAb A, C, and D aggregated very quickly (< 10 min), but mAb B (30 min) and more notably Fc A (3 h) displayed slower kinetics in PBS buffer pH 7.2. Because of differences in the pI values for different targets, we hypothesized that the rate of crosslinking may depend on solution pH. A F-W kinetic model was applied to quantify aggregation rate constants representing initial multi-valent binding (nucleation) and network formation into large precipitates (autocatalytic growth). We found that slow aggregation kinetics occurred at a solution pH near or greater than the protein pI, and suspected that this may be due to attractive interactions between the cationic ELP and mAb that sterically decrease multi-valent crosslinking efficiency. For mAb B and Fc A, fast aggregation ($t_{\text{max}} < 10$ min) was obtained at pH 5 and this finding was verified using cell culture titrated to pH 5. All molecules were eluted with > 90% yield at $\text{pH} < 4$ and were stable in 50 mM citrate buffer pH 3.5 without added salt. mAb C, mAb D, and Fc A were stable in up to 0.3 M ammonium sulfate for 120 min followed by titration to pH 5.5. mAb A and B

demonstrated significant aggregation at pH 3.5 with salt, but were more stable at pH 3.75 after titration to pH 5.5.

The five molecules were purified from clarified cell culture using the indicated procedures and high mAb yield (95%) and monomer (> 97%) were obtained. Nanocage affinity precipitation resulted in a clearance of 99.9% HCP and >99.99% DNA impurities from mAb A–D cultures. Fc A impurity clearance was not as efficient as the other mAbs which may be due to the lack of PS-80 in the second wash buffer or due to stronger impurity-Fc A interactions compared to the other molecules. Affinity precipitation of mAbs A–D met or exceeded expectations of Protein A chromatography performance. Future work will focus on a more rigorous examination of nanocage regeneration and number of purification cycles, the use of filtration as more scalable alternative to centrifugation, and the implementation of affinity precipitation in continuous processing.

TABLES

#	Molecule Name	IgG Subclass	MW (kDa)	pI	Culture Titer (mg/mL)	Purified Stock (mg/mL)
1	mAb A	IgG4	147	8.2	6.1	66.8
2	mAb B	IgG4	155	6.8	3.1	63.0
3	mAb C	IgG1	150	8.3	1.8	61.2
4	mAb D	IgG1	152	9.1	5.1	45.6
5	Fc A	Fc-IgG1	79	5.8	2.8	40.8

Table 4.1 Molecular properties and concentrations for the five molecules used in the study. MW = molecular weight, pI = isoelectric point.

#	50 mM Buffer	NaCl (mM)	pH	Total Ionic Strength (mM)	Conductivity (mS/cm)
1	Citrate	19	5.0	150	14.8
2	Phosphate	81	6.0	150	13.4
3	Phosphate	40	7.0	150	13.7
4	Tris	120	8.0	150	14.0
5	Tris	144	9.0	150	13.8

Table 4.2 Buffer composition for use in aggregation kinetics investigation.

Molecule Name	[Z]:[mAb] Binding Ratio	Binding pH	Wash 1 Buffer	Wash 2 Buffer	Wash 3 Buffer	Elution Buffer	Elution Precip [AS]
mAb A	3:1	7.2	PBS, pH 7.2	Salt, Excipient, PS-80, pH 9.0	Citrate pH 5.0	Citrate pH 3.75	0.2 M
mAb B	3:1	5.0	Citrate, pH 5.0	Salt, Excipient, PS-80, pH 9.0	Citrate pH 5.0	Citrate pH 3.75	0.2 M
mAb C	3:1	7.2	PBS, pH 7.2	Salt, Excipient, PS-80, pH 9.0	Citrate pH 5.0	Citrate pH 3.50	0.3 M
mAb D	3:1	7.2	PBS, pH 7.2	Salt, Excipient, PS-80, pH 9.0	Citrate pH 5.0	Citrate pH 3.50	0.2 M
Fc A	3:1	5.0	Citrate, pH 5.0	Citrate, Excipient pH 7.0	Citrate pH 5.0	Citrate pH 3.50	0.3 M

Table 4.3 Affinity precipitation conditions used for purification of the molecules from cell culture.

Unit Operation	mAb Yield (%)	Monomer (%)	HCP (ppm)	DNA (ppb)	Nanocage Yield (%)
Affinity Precipitation	95.2 ± 1.4	98.3 ± 1.6	701 ± 218	< 15.8 ± 11.1 *	86.8 ± 4.6
Protein A Chromatography **	> 95	> 95	200-3000	100-1000	n/a

Table 4.4 Comparison of average affinity precipitation performance for mAbs A-D with expected protein A chromatography performance. Average affinity precipitation values reported with 95% confidence intervals (* < 10 ppb for mAb C and D included calculation; ** from Fahrner et al.¹²).

FIGURES

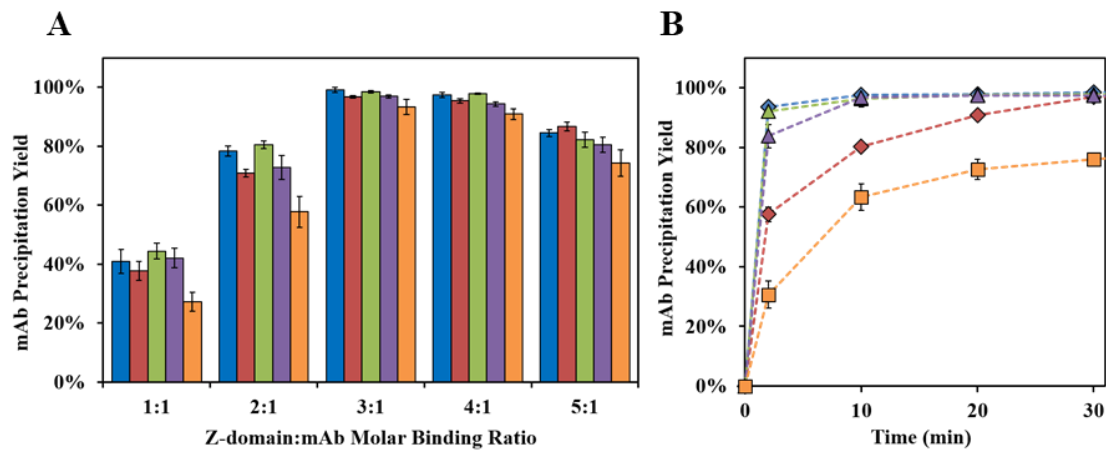


Figure 4.1 mAb binding and precipitation yield. A) Effect of Z:mAb binding ratio on mAb precipitation yield in PBS at 23°C for mAb A (blue), mAb B (red), mAb C (green), mAb D (purple), and Fc A (orange). B) Effect of mixing time on mAb precipitation yield with 3:1 Z:mAb in PBS at 23°C for mAb A (blue diamond), mAb B (red diamond), mAb C (green triangle), mAb D (purple triangle), and Fc A (orange square).

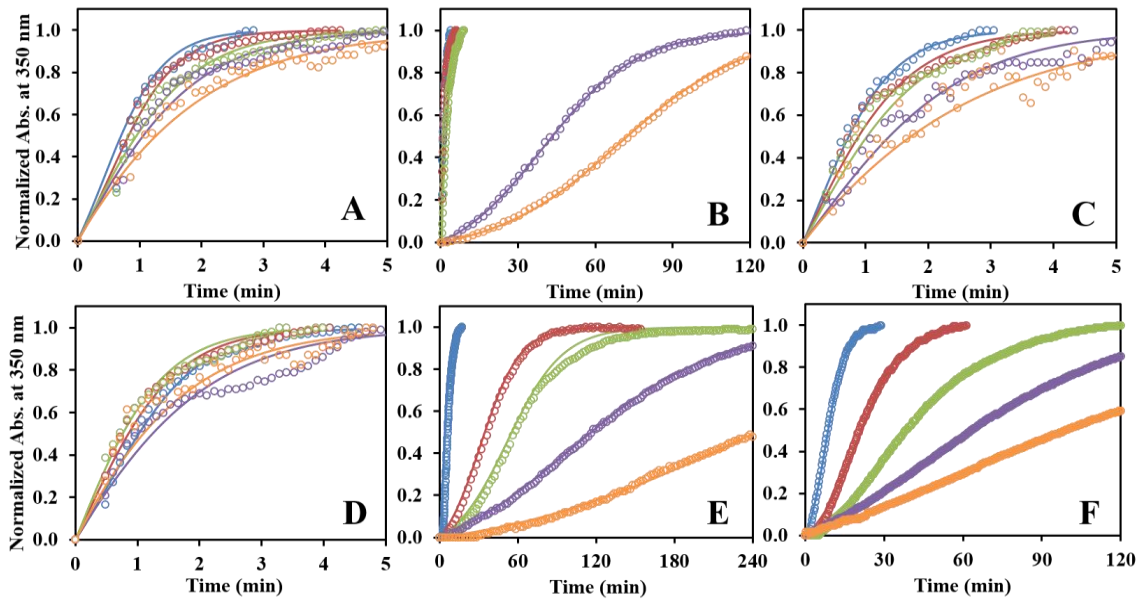


Figure 4.2 Effect of solution pH on aggregation kinetics at 3:1 Z:mAb molar binding ratio for mAb A (A), mAb B (B), mAb C (C), mAb D (D), Fc A (E), and polyclonal antibody (F). Normalized absorbance data (open circle) and F-W model fit (solid line) shown at solution pH 5 (blue), pH 6 (red), pH 7 (green), pH 8 (purple), and pH 9 (orange).

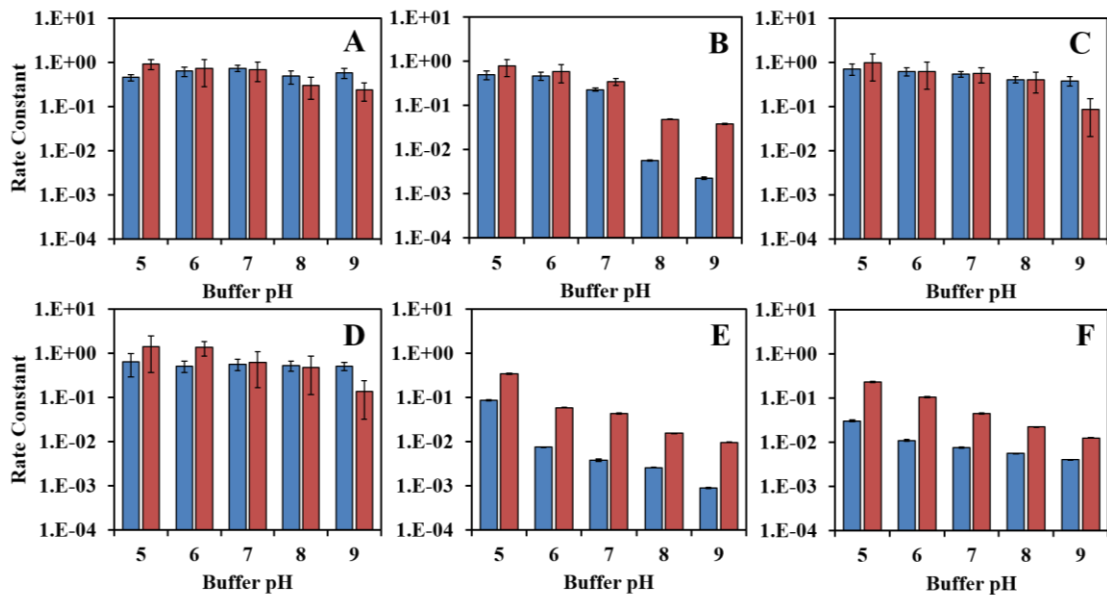


Figure 4.3 F-W model rate constants k_1 (blue) and k_2A_0 (red) fit from absorbance data for mAb A (A), mAb B (B), mAb C (C), mAb D (D), Fc A (E), and polyclonal antibody (F).

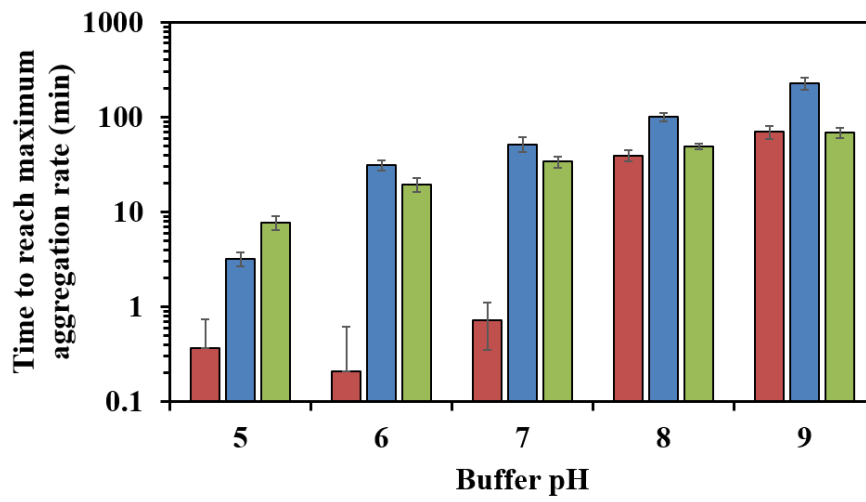


Figure 4.4 Effect of the time to reach maximum aggregation rate on buffer pH for mAb B (red), Fc A (blue), and polyclonal antibody (green).

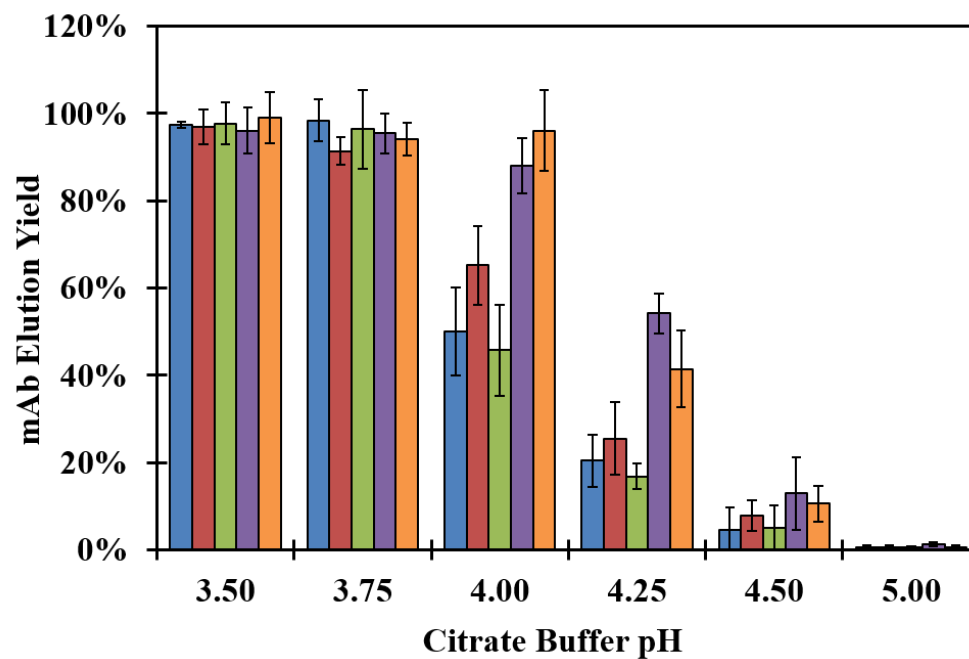


Figure 4.5 Effect of 50 mM sodium citrate buffer pH on mAb elution yield for mAb A (blue), mAb B (red), mAb C (green), mAb D (purple), and Fc A (orange).

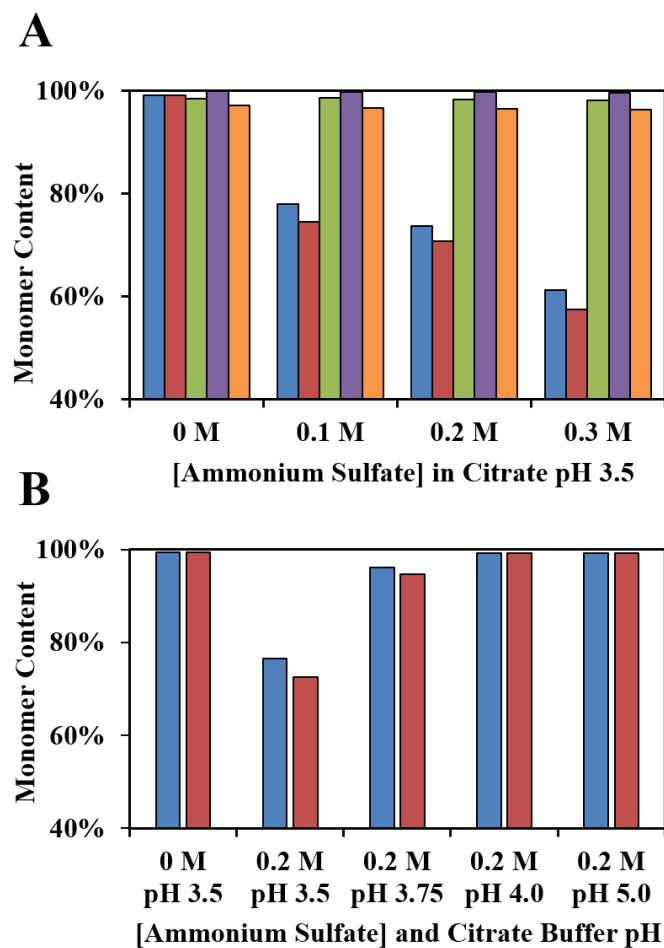


Figure 4.6 mAb elution stability A) Effect of ammonium sulfate concentration on mAb stability in 50 mM sodium citrate pH 3.5 for mAb A (blue), mAb B (red), mAb C (green), mAb D (purple), and Fc A (orange). B) Effect of pH on mAb stability in 50 mM sodium citrate buffers with 0.2 M ammonium sulfate for mAb A (blue) and mAb B (red).

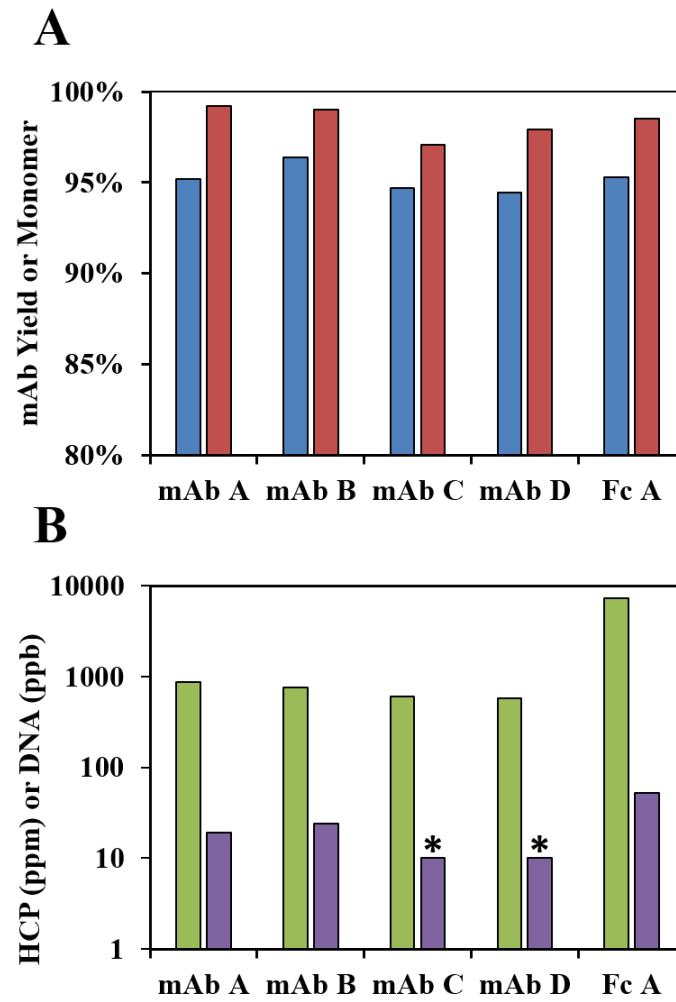


Figure 4.7 Characterization of mAb affinity precipitation from cell culture A) mAb elution yield (blue) or monomer content (red) B) Elution impurity content for HCP (green) or DNA (purple). * indicates concentration less than detectable in assay.

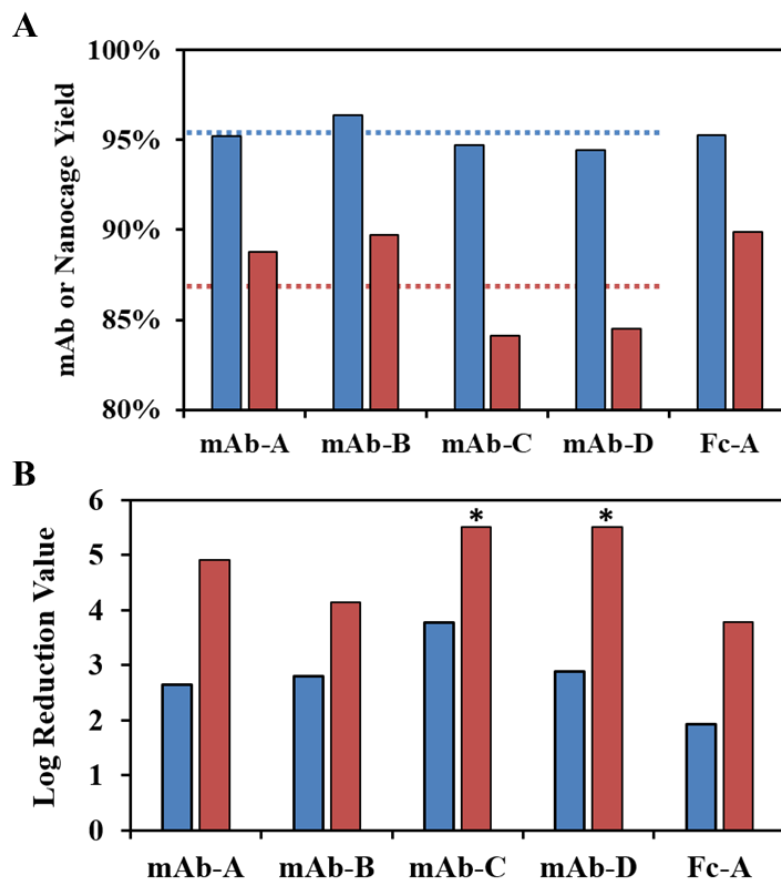


Figure 4.8 Characterization of mAb affinity precipitation A) Average mAb (blue) or nanocage (red) yield for mAbs A-D and Fc-A. Lines indicate average mAb (blue) or nanocage (red) yield for mAbs A-D only. B) Impurity clearance in mAb elution purified from cell culture supernatant for HCP (blue) and DNA (red). * indicates concentration was lower than detectable in assay.

REFERENCES

1. Shukla AA and Thömmes J. Recent advances in large-scale production of monoclonal antibodies and related proteins. *Trends Biotechnol* **2010**, 28(5):253-261.
2. Hober S, Nord K, Linhult M. Protein A chromatography for antibody purification. *J Chromatogr B* **2007**, 848:40-47.
3. Low D, O'Leary R, Pujar NS. Future of antibody purification. *J Chromatogr B* **2007**, 848(1):48-63.
4. Thömmes J, Etzel M. Alternatives to chromatographic separations. *Biotechnol Prog* **2007**, 23(1):42-45.
5. Hillbrig F, Freitag R. Protein Purification by affinity precipitation. *J Chromatogr B* **2003**, 848(1):40-47.
6. Gagnon P. Technology trends in antibody purification. *J Chromatogr A* **2012**, 1221:57-70.
7. Madan B, Chaudhary G, Cramer SM, Chen W. ELP-z and ELP-zz capturing scaffolds for the purification of immunoglobulins by affinity precipitation. *J Biotechnol* **2013**, 163(1):10-16.
8. Sheth RD, Madan B, Chen W, Cramer SM. High throughput screening for the development of a monoclonal antibody affinity precipitation step using ELP-Z stimuli responsive biopolymers. *Biotechnol Bioeng* **2013**, 110:2664-2676.
9. Sheth RD, Jin M, Bhut BV, Liu J, Lee J, Siegfried R, Li Z, Chen W, Cramer SM. Affinity precipitation of monoclonal antibody from industrial harvest feedstock using ELP-Z stimuli responsive biopolymers. *Biotechnol Bioeng* **2014**, 111:1595-1603.
10. Swartz AR, Sun Q, Chen W. Ligand-induced crosslinking of Z-ELP-functionalized E2 protein nanoparticles for enhanced affinity precipitation of antibodies. *Biomacromolecules* **2017**, 18(5):1654-1659.

11. Swartz AR, Xuankuo X, Traylor S, Li ZJ, Chen W. One-step affinity capture and precipitation for improved purification of an industrial monoclonal antibody using Z-ELP functionalized nanocages. *Biotechnology and Bioengineering* **2018**, 115(2):423-432.
12. Fahrner RL, Knudsen HL, Basey CD, Galan W, Feuerhelm D, Vanderlaan M, Blank GS. Industrial purification of pharmaceutical antibodies: development, operation, and validation of chromatography processes. *Biotechnology and Genetic Engineering Reviews* **2001**, 18(1):301-327.
13. Meyer DE, Chilkoti A. Purification of recombinant proteins by fusion with thermally-responsive polypeptides. *Nat Biotechnol* **1999**, 17(11): 1112-1115.
14. Morris AM, Wazky MA, Agar JN, Finke RG. Fitting neurological protein aggregation kinetic data via a 2-step, Minimal/Ockham's Razor Model: The Finke-Watzky mechanism of nucleation followed by autocatalytic surface growth. *Biochem* **2008**, 47:2413-2427.
15. Bentea L, Wazky MA, Finke RG. Nucleation and Growth Curves Across Nature Fit by the Finke-Watzky Model of Slow Continuous Nucleation and Autocatalytic Growth: Explicit Formulas for the Lag and Growth Times Plus Other Key Insights. *J Phys Chem C* **2017**, 121:5302-5312.
16. Jendeberg L, Persson B, Andersson R, Karlsson R, Uhlen M, Nilsson B. Kinetic analysis of the interaction between protein a domain variants and human Fc using plasmon resonance detection. *J Mol Recognit* **1995**, 8(4):270-278.
17. Flygare S, Griffin T, Larsson PO, Mosbach K. Affinity precipitation of dehydrogenases. *Anal Biochem* **1983**, 133:409-416.
18. Watzky MA, Morris AM, Ross ED, Finke RG. Fitting yeast and mammalian prion aggregation kinetic data with the Finke-Watzky two-step model of nucleation and autocatalytic growth. *Biochemistry* **2008**, 47:10790-10800.
19. Szenczi A, Kardos J, Medgyesi G, Zavodszky P. The effect of solvent environment on the conformation and stability of human polyclonal IgG in solution. *Biologicals* **2006**, 36:5-14.
20. Tsukamoto M, Watanabe H, Ooishi A, Honda S. Engineered protein A ligands, derived from a histidine-scanning library, facilitate the affinity purification of IgG under mild acidic conditions. *J Biol Eng* **2014**, 8:15.
21. Uversky VN, Li J, Fink AL. Evidence for a partially folded intermedia in α -synuclein fibril formation. *J Biol Chem* **2001**, 276:10737-10744.

22. Morris AM, Finke RG. α -Synuclein aggregation variable temperature and variable pH kinetic data: A re-analysis using the Finke–Watzky 2-step model of nucleation and autocatalytic growth. *Biophys Chem* **2009**, 140:9-15.
23. Arosio P, Jaquet B, Wu H, Morbidelli A. On the role of salt type and concentration on the stability behavior of a monoclonal antibody solution. *Biophys Chem* **2012**, 168:19-27.
24. Shukla AA, Hubbard B, Tressel T, Guhan S, Low D. Downstream processing of monoclonal antibodies – Application of platform approaches. *J Chrom B* **2007**, 848(1):28-39.
25. Shukla AA and Hinckley P. Host cell protein clearance during protein a chromatography: Development of an improved column wash step. *Biot Prog* **2008**, 24(5):1115-1121.

Chapter 5

SPYTAG/SPYCATCHER FUNCTIONALIZATION OF E2 NANOCAGES WITH Z-ELP AFFINITY DOMAINS FOR TUNABLE ANTIBODY BINDING AND PRECIPITATION PROPERTIES

Abstract

Z-domain-elastin-like polypeptide (Z-ELP₄₀) affinity ligands functionalized to a self-assembled E2 nanocage by Sortase A (SrtA) ligation have been demonstrated in Chapters 2-4 to be an ideal scaffold for monoclonal antibody (mAb) affinity precipitation. However, low Z-ELP-E2 ligation efficiency and nanocage regeneration yields have limited the potential of this technology. Chapter 5 describes an improved conjugation platform using SpyTag/SpyCatcher isopeptide bond formation between SpyTag-E2 and Z-ELP-SpyCatcher fusion proteins of two different ELP chain-lengths. Using this system, E2 ligation efficiencies exceeding 90% were observed for both 40- and 80-repeat Z-ELP-SpyCatcher fusions. This enabled the simple production of nanocages at any target Z-ELP density for tunable aggregation and mAb binding properties. For the elution an industrial mAb cell culture harvest, Z-ELP₈₀-Spy-E2 nanocages were capable of selective precipitation with 0.1 M ammonium sulfate at 23°C and improved the nanocage regeneration recovery to >90%. The functionality of the SpyTag-E2 scaffold may be extended to the affinity precipitation of other non-mAb target proteins using customizable affinity domain-ELP-SpyCatcher fusions.

5.1 Introduction

Affinity precipitation is a bioseparation method that involves the capture and precipitation of a target protein in bulk solution¹, and has been proposed as a more cost-effective and scalable alternative to conventional Protein A affinity chromatography for the purification of therapeutic monoclonal antibodies (mAbs)²⁻³. The two main strategies for affinity precipitation utilize either multivalent affinity ligand crosslinking (primary effect) or stimuli-responsive affinity ligands (secondary effect) to trigger the formation of large aggregates for precipitation⁴. Primary effect affinity ligands such as multivalent haptens have been used to crosslink with dimeric antibodies into oligomeric aggregates⁵⁻⁶, but this strategy is limited by low precipitation yields, slow dissolution kinetics, and the requirement of an additional separation step after elution to remove the dissociated affinity ligands⁷. mAb purification using stimuli-responsive affinity ligands has also been implemented using either pH⁸ or temperature⁹ responsive synthetic polymers and biopolymers such as elastin-like polypeptides (ELP)¹⁰⁻¹¹. However, utility of the technique is hindered by the harsh environmental stimuli such as low pH, high temperature, and/or high salt concentration necessary to induce phase transition of the affinity ligand, resulting in an increase mAb aggregation¹²⁻¹³ or an increase in the co-precipitation of other cell culture impurities¹⁴.

Our group has developed a new protein-based affinity scaffold that combines the benefits of both primary and secondary effect affinity precipitation. As described in Chapters 2-4, we functionalized the surface of a self-assembled 60-mer E2 nanocage with an affinity ligand consisting of a Protein A derived Z-domain-40-repeat ELP (Z-ELP₄₀) fusion and demonstrated binding-induced multivalent crosslinking as the initial capture mechanism of mAbs from cell culture, followed by a selective precipitation of regenerated nanocages after mAb elution for easy separation¹⁵. The 25-nm E2 nanocage

from *Bacillus stearothermophilus* was selected as an ideal scaffold due to its high structural stability ($T_m > 80^\circ\text{C}$) and the ability to genetically modify the exterior N-terminus for protein conjugation¹⁶. Because large genetic fusions have been shown to disrupt proper E2 self-assembly, we modified a truncated E2 subunit with a small N-terminal triglycine tag to allow for post-translational, site-specific conjugation of Z-ELP₄₀ using *Staphylococcus aureus* Sortase A (SrtA) ligation¹⁷⁻¹⁸. Using partially functionalized Z-ELP-E2 nanocages, an affinity precipitation process capable of high yield and efficient impurity clearance equivalent to Protein A chromatography was developed for the purification of industrial mAbs from cell culture harvests¹⁹⁻²⁰.

In Chapter 5, we sought to maximize the Z-ELP ligation density on the E2 nanocage with a longer chain-length 80-repeat ELP and investigate the effects of Z-ELP valency on mAb-nanocage crosslinking and ELP phase transition properties. While SrtA ligation offers the benefits of using small ligation tags (N-terminal GGG and C-terminal LPXTG) and is highly biocompatible²¹, the reaction is reversible,²² resulting in a maximum Z-ELP-E2 density of about 50% (30 conjugated Z-ELP per 60 subunit E2 nanocage) even with a molar reactant ratio of 5:1 Z-ELP:E2. To achieve 100% ligation, an alternative method was evaluated using the SpyTag/SpyCatcher system derived from *Streptococcus pyogenes* fibronectin-binding protein FbaB, which forms an irreversible isopeptide bond between a small, 13 amino acid peptide (SpyTag) and its 15 kDa protein partner (SpyCatcher)²³. We report the high expression and stable assembly of an N-terminally modified SpyTag-E2, and the tunable functionalization of both Z-ELP₄₀-SpyCatcher and Z-ELP₈₀-SpyCatcher fusions to SpyTag-E2 with close to 100% ligation density. We found that greater than 50% Z-ELP conjugation was sufficient for effective crosslinking with mAbs independent of ELP chain length,

however, only fully decorated Z-ELP80 nanocages could be selectively recovered by precipitation at room temperature with minimal salt after mAb elution. We believe that the SpyTag-E2 nanocage system can be extended as a versatile scaffold for the functionalization of any target-SpyCatcher fusion proteins for a wide range applications.

5.2 Materials and Methods

5.2.1 Materials

Escherichia coli strain BLR(DE3) containing pET24(a) vectors encoding for Z-ELP[KV₈F-40]-LPETG, ELP[KV₈F-40]-LPETG, ELP[KV₈F-80]-LPETG, and GGG-ELP-[KV₈F-80], *E. coli* strain BL21(DE3) containing a pET11(a) vector encoding for GGG-E2(158), and another BL21(DE3) strain containing a pMR5 vector encoding for sortase A were constructed and described previously^{15,18}. pDEST14-SpyCatcher was a gift from Mark Howarth (Addgene plasmid # 35044)²³. E2 nanocage plasmids pE2-152, pE2-158, pE2-167, pE2-172, and pE2-179 in pET11(a) vectors were received as a gift from Szu-Wen Wang¹⁶. A purified and clarified cell culture mAb was received as a gift from Bristol-Myers Squibb (BMS) (New York City, NY). Bacto tryptone and yeast extract were purchased from BD Biosciences (Franklin Lakes, NJ). Kanamycin, ampicillin, bovine serum albumen (BSA), and isopropyl- β -D-thiogalactoside (IPTG) were purchased from Fisher Scientific (Pittsburgh, PA). Sodium hydroxide, sodium phosphate, citric acid, tris base, ammonium sulfate, and sodium chloride were purchased from Sigma-Aldrich (St. Louis, MO). 96-well half area UV-transparent plates were purchased from Corning (Corning, NY). 0.8/0.2 μ m Supor Acrodisc syringe filters were purchased from Pall (Port Washington, NY). 100 kDa Sartorius Vivaspin 20 spin columns were purchased from Sartorius (Göttingen, Germany).

5.2.2 Genetic Manipulations and Vector Construction

E. coli strain NEB 5-alpha (NEB #C29871) was used as the host for all genetic manipulations. All ELP constructs were cloned in pET24(a) vectors and all SpyTag-E2 constructs were cloned in pET11(a) vectors. Z-ELP₈₀-LPETG was constructed by PCR of the Z-domain from Z-ELP[KV₈F-40]-LPETG using Primer 1 and Primer 2 and the PCR amplified Z-domain was digested with XbaI and NdeI and ligated into XbaI and NdeI digested ELP[KV₈F-80]-LPETG. A double-repeat streptavidin binding peptide³² DVEAWLDERVPLVET (SP₂, (SP-(GS)₃-SP-(GS)₃) was generated by annealing overlapping Oligos 1-4. The annealed SP₂ was digested with NcoI and NdeI and ligated into NcoI and NdeI digested Z-ELP₄₀-LPETG and Z-ELP₈₀-LPETG vectors to form SP₂-ELP₄₀-LPETG and SP₂-ELP₈₀-LPETG constructs. An (EA₃K)₃ linker was created by annealing Oligos 5-6 and was substituted for the LPETG tag by digesting the Z-ELP₄₀-LPETG and Z-ELP₈₀-LPETG vectors with BamHI and SacII and ligating the BamHI and SacII digested (EA₃K)₃ linker. Z-ELP₄₀-SpyCatcher and Z-ELP₈₀-SpyCatcher were generated by PCR of the pDEST14-SpyCatcher vector using Primer 3-4 and the PCR amplified SpyCatcher was digested with BamHI and XhoI and ligated into BamHI and XhoI digested Z-ELP₄₀-LPETG and Z-ELP₈₀-LPETG vectors to replace the LPETG tag. SpyTag-E2 constructs were generated by annealing SpyTag (AHIVMVDAYKPTK) Oligos 7-8 and digesting with NdeI and NheI. The SpyTag insert was ligated into the NdeI and NheI digested pE2 constructs. See **Table 5.1** for primer/oligo information.

5.2.3 Protein Expression and Purification

All ELP-fusion constructs were expressed in BLR(DE3) *E. coli* grown in Terrific Broth (TB) with 50 µg/mL kanamycin at 37°C and mixed at 250 rpm for 24 h

with leaky expression and were purified by inverse transition cycling (ITC) using 0.5 M ammonium sulfate, as described previously¹⁵. The purified ELP-fusion concentration was estimated by absorbance at 280 nm (UV-1800, Shimadzu) using the theoretical extinction coefficient. Sortase A was expressed in BL21(DE3) *E. coli* grown in Luria-Bertani Medium (LB) with 50 µg/mL kanamycin at 37°C and mixed at 250 rpm until an OD₆₀₀ of 1.0, where the culture was induced with 1 mM IPTG for 4 hs. All E2 constructs (GGG-E2(158) and SpyTag-E2(152-179)) were expressed in BL21(DE3) *E. coli* cells grown in LB with 100 µg /mL ampicillin at 37°C and mixed at 250 rpm until an OD₆₀₀ of 0.5, where the culture was induced with 0.2 mM IPTG at 20°C for 20 h. After protein expression, all cultures were harvested by centrifugation at 4,000g for 15 min at 4°C and resuspended in a TN150 buffer (50 mM Tris, 150 mM sodium chloride, pH 8.0). Cells were lysed using a Fisher Sonicator (Pittsburgh, PA) using 5 s pulse on and 10 s pulse off for 5 min over ice. All E2 constructs were partially purified by incubating at 70°C for 10 min and centrifugation at 15,000g for 15 min to isolate the soluble proteins. The soluble E2 sample was filtered through a 0.8/0.2 µm Supor Acrodisc syringe filter. E2 nanocage assembly was confirmed by dynamic light scattering (DLS) using a Malvern Zetasizer Nano (Malvern, United Kingdom) and a low volume cuvette (ZEN0040, Malvern). Each measurement consisted of 5 runs of 10 s and the correlation function was analyzed by the Protein Analysis algorithm provided by the Malvern software to estimate the hydrodynamic diameter (Z-ave) and polydispersity index. Total protein concentrations of partially purified E2 and soluble SrtA lysate were measured by Bradford protein assay purchased from Bio-Rad (Hercules, CA) using BSA as a standard. Protein expression was confirmed by Coomassie stained, 10% acrylamide SDS-PAGE using a Bio-Rad Mini-PROTEAN

electrophoresis system (Hercules, CA). Protein purity was estimated using densitometry analysis of SDS-PAGE gels using Thermo MyImage software (Waltham, MA).

5.2.4 Sortase A Ligation of ELP-LPETG Fusions to GGG-E2

Sortase A reactions were prepared with 10 μ M GGG substrate, 10 μ M sortase A, and a variable concentration of LPETG substrate (1:1 to 5:1 LPETG:GGG molar ratio) in a reaction buffer (TN150, 6 mM CaCl₂) and mixed for 4 h at 37°C. The ligation product was purified by ITC using 0.5 M ammonium sulfate and resuspended in phosphate buffered saline (PBS, 25 mM sodium phosphate, 150 mM sodium chloride, pH 7.2). The unreacted ELP-LPETG fusion protein was removed by 100 kDa diafiltration into PBS using Sartorius Vivaspin 20 spin columns. The purified ligation products were confirmed by Coomassie stained 10% acrylamide SDS-PAGE and the ELP fusion-E2 ligation density was estimated by densitometry analysis.

5.2.5 Z-ELP-SpyCatcher Conjugation to SpyTag-E2

Purified Z-ELP₄₀-SpyCatcher or Z-ELP₈₀-SpyCatcher was mixed with SpyTag-E2 in PBS for 1-4 h at room temperature followed by one ITC cycle into PBS. The conjugation products were confirmed by Coomassie stained 10% acrylamide SDS-PAGE and the Z-ELP-E2 ligation density was estimated by densitometry analysis. 100% ligation density assumes 60 Z-ELP conjugated per 60-subunit E2 nanocage. Ligation efficiency was calculated by (Z-ELP-E2 ligation density)/([Z-ELP]:[E2] reactant ratio).

5.2.6 Transition Temperature Measurement

Transition temperature (T_t) measurements were made using a Shimadzu UV-1800 spectrophotometer. 100 μ L samples were added in triplicate to an 8-well multicell

microcuvette (Shimadzu) and equilibrated for 10 min at 20°C, and the absorbance at 350 nm was measured every 0.5 degrees from 20-60°C at a ramp rate of 0.5 degree per min with a 30 s equilibration before each measurement. The absorbance curves were analyzed by the provided Tm Analysis Software (Shimadzu) and the T_t , defined as the maximum slope of the transition profile, was evaluated.

5.2.7 Absorbance Measurement

Absorbance measurements were performed using a Synergy plate reader from BioTek (Winooski, VT) run at 23°C. 100 μ L experimental samples and buffer controls were well mixed and added to a half-area 96-well UV transparent plate. For all measurements, the absorbance signal was buffer subtracted and corrected for path length (1 cm). For mAb or nanocage concentration, the absorbance was measured at 280 nm and the theoretical extinction coefficient was used to calculate concentration. For turbidity evaluation, the absorbance was measured at 350 nm.

5.2.8 Z-ELP-E2 Nanocage mAb Binding Capacity

To evaluate the nanocage binding capacity for an industrial mAb, nanocages with varying Z-ELP ligation density were prepared at 25 μ M E2 concentration in microcentrifuge tubes and mixed with excess mAb at room temperature for 2 h in PBS at 23°C. Samples were then adjusted to 0.5 M ammonium sulfate and mixed for 10 min at 23°C, and centrifuged at 15,000 g for 10 min to pellet the precipitated nanocages and bound mAb. The supernatant was removed and the absorbance was measured to evaluate the unbound mAb concentration. The bound mAb concentration was calculated by mass balance. The mAb binding capacity per 60-subunit E2 nanocage was estimated by $[\text{mAb}]_{\text{bound}}/(60 \cdot [\text{E2}])$.

5.2.9 mAb-Nanocage Crosslinking and Precipitation Yield

An solution containing an industrial mAb was prepared in PBS in microcentrifuge tubes with the Z-ELP₄₀-Spy-E2 or Z-ELP₈₀-Spy-E2 nanocages at 1:1, 2:1, 4:1 Z:mAb molar ratios in triplicate. The samples were mixed for 30 min at 23°C and the turbidity was measured using absorbance at 350 nm. The samples were then centrifuged at 15,000 g for 10 min at 23°C to pellet the insoluble components and the supernatant was removed. The pellet was resuspended in 1x volume elution buffer (50 mM sodium citrate, pH 3.5) and mixed for 15 min at 23°C. The samples were adjusted to 0.5 M ammonium sulfate and centrifuged at 15,000 g for 10 min at 23°C to selectively precipitate the dissociated nanocage. The elution supernatant was removed and the absorbance was measured at 280 nm to evaluate mAb precipitation yield by mass balance. The purity of the mAb elution samples were confirmed by SDS-PAGE to ensure no residual nanocage.

5.2.10 Nanocage Regeneration and mAb Affinity Precipitation

~100% ligation Z-ELP₄₀-Spy-E2 or Z-ELP₈₀-Spy-E2 precipitation yield in elution buffer was evaluated using a central composite DOE design (25, 50, 75 μM E2 concentration and 0.05, 0.15, and 0.25 M ammonium sulfate) with three replicates of the centerpoint (50 μM and 0.15 M). After adding ammonium sulfate at 23°C, the samples were centrifuged at 15,000 g for 5 min at 23°C and the supernatant absorbance at 280 nm was measured to evaluate the nanocage concentration and the nanocage precipitation yield was calculated by mass balance. The effect of ammonium sulfate on nanocage regeneration during mAb affinity precipitation was studied. The nanocage was mixed with an industrial mAb cell culture harvest sample at 3:1 Z:mAb molar ratio in cell culture media in triplicate for 5 min at 23°C and centrifuged at 15,000 g for 5 min

at 23°C. The pelleted mAb-nanocage complex was washed with PBS followed by 25 mM sodium citrate pH 5.0. After another centrifugation, the pellet was resuspended in elution buffer and mixed for 15 min. The elution samples were adjusted to either 0.1 or 0.3 M ammonium sulfate for selective nanocage precipitation. The purified mAb was removed in the supernatant and the mAb elution yield was calculated by measuring absorbance at 280 nm. The pelleted nanocage was regenerated in elution buffer and then buffer exchanged back into PBS using ITC. The nanocage recovery was evaluated after one purification cycle by measuring absorbance at 280 nm. See **Table 5.2** for more information.

5.3 Results and Discussion

5.3.1 Evaluation of Sortase A ELP-fusion protein E2 ligation efficiency

The results in Chapter 2-4 demonstrate the successful purification of mAbs using Z-ELP₄₀ functionalized E2 nanocages by binding-induced crosslinking¹⁹. The objective of Chapter 5 was to further improve the efficiency by maximizing the Z-ELP ligation density using a longer chain-length ELP₈₀. We expected that a higher density of the conjugated Z-domain would increase the level of mAb-mediated crosslinking while the longer ELP would decrease the salt concentration required for precipitation²⁴ and improve nanocage regeneration. To compare the SrtA ligation efficiency of Z-ELP₄₀-LPETG and Z-ELP₈₀-LPETG to GGG-E2, reactants were mixed at 1:1 to 5:1 LPETG:GGG molar ratios and the ligation products were purified using ELP inverse transition cycling (ITC)¹⁵. Even with a five-fold molar excess of Z-ELP₄₀-LPETG, only a 50% ligation density was obtained because of the reversible nature of SrtA ligation, while <10% ligation was observed for Z-ELP₈₀-LPETG (**Figure 5.1**). This

unexpectedly low efficiency was only observed only with Z-ELP₈₀-LPETG (Figure 5.2A) as a similar ELP₈₀-LPETG without the Z-domain and an SP₂-ELP₈₀-LPETG fusion containing a similar size peptide to the Z-domain resulted in comparable E2 ligation density as Z-ELP₄₀-LPETG (**Figure 5.2B**). Furthermore, a similar result was obtained using an alternative GGG-ELP substrate instead of GGG-E2 (**Figure 5.3A-B**), indicating that the GGG- substrate did not have a significant impact on ligation efficiency.

All ELP constructs contained a flexible (G₄S)₃ linker between the ELP and LPETG that was added to allow for accessibility of the LPETG tag to the SrtA active site¹⁷. However, ELPs are intrinsically disordered proteins composed of β -turns in a random coil conformation and do not maintain a stable structure²⁵. We suspected the disordered nature of the longer 80-repeat ELP fused to the Z-domain may sterically block access of the LPETG motif, resulting in low ligation. To extend the tag farther away from ELP, the ligation of a new Z-ELP₈₀ fusion containing a rigid (EA₃K)₃ linker²⁶ between ELP and LPETG was evaluated, but no improvement was detected (**Figure 5.4**). Because of the reversibility of SrtA ligation and the limited ligation for Z-ELP₈₀-LPETG²⁷⁻²⁸, we decided to pursue an alternative ligation strategy utilizing the SpyTag-SpyCatcher pair²³.

5.3.2 Expression and conjugation of Spytag-E2 and Z-ELP-SpyCatcher

To overcome the limitations of SrtA ligation, the SpyTag/SpyCatcher conjugation method was selected as an alternative conjugation method because of its irreversible and rapid isopeptide bond formation²⁹. Although we were successful in displaying the GGG- tag to the N-terminus of the E2 monomer, there are very few reports on the display of other N-terminal genetic fusions onto E2³⁰. To identify the best

insertion site, the 13-amino acid SpyTag was attached to different locations on the native N-terminal linker of the E2 monomer and expressed in *E. coli*. Various levels of soluble expression were obtained for all SpyTag-E2 fusion constructs (**Figure 5.5A**). The soluble *E. coli* lysate was heated to 70°C for the partial purification of the E2 nanocages and to check for thermostability (**Figure 5.5B**). All SpyTag-E2 constructs were at least partially soluble after 70°C incubation and dynamic light scattering confirmed assembled nanoparticles of the expected size (**Figure 5.6A**). High soluble expression was obtained for both Z-ELP₄₀-SpyCatcher and Z-ELP₈₀-SpyCatcher (**Figure 5.7A**). SpyTag-E2(158) and SpyTag-E2(173) were selected to test for conjugation with the Z-ELP-SpyCatcher fusions because they exhibited the highest culture productivity and low polydispersity (**Figure 5.6B**). Samples were mixed for 1 h in PBS followed by one ITC cycle to remove any unreacted E2. The reaction resulted in high conjugation of both Z-ELP₄₀- and Z-ELP₈₀-SpyCatcher fusions on either SpyTag-E2(158) and SpyTag-E2(173) (**Figure 5.7B**). SpyTag-E2(158) was selected for future investigation because it contained the same N-terminal extension as the well-characterized GGG-E2(158) used in the SrtA reaction.

To compare the two conjugation methods, SrtA reactants Z-ELP₄₀-LPETG, Z-ELP₈₀-LPETG, and GGG-E2 and SpyTag/SpyCatcher reactants Z-ELP₄₀-SpyCatcher, Z-ELP₈₀-SpyCatcher, and SpyTag-E2 were mixed at a 0.75:1 ELP:E2 molar ratio in target reaction buffers for 4 h followed by one ITC cycle (**Figure 5.8**). In contrast to the low ligation observed for the SrtA method, SpyTag/SpyCatcher conjugation resulted in close to 100% efficiency for both Z-ELP₄₀- and Z-ELP₈₀-SpyCatcher, as no unreacted Z-ELP was detected by SDS-PAGE in the purified products. The simplicity of the 2-component reaction and the high efficiency afforded by SpyTag/SpyCatcher

significantly advance the capabilities of the nanocage affinity precipitation technology and enable access to all 60 E2 subunits for a highly tunable platform.

5.3.3 Effect of ligation density on nanocage aggregation and IgG Binding

To examine the versatility of the SpyTag/SpyCatcher system, a wide range of E2 ligation densities were investigated. Reactions were prepared at 0.25:1, 0.5:1, 0.75:1, and 1:1 Z-ELP-SpyCatcher:SpyTag-E2 molar ratios for the 40- and 80-repeat ELP. For a comparison of conjugation efficiency, SrtA ligation reactions were prepared using 0.5:1, 1:1, 2:1, and 4:1 Z-ELP₄₀-LPETG:GGG-E2 molar ratios (**Figure 5.9A**). The E2 ligation density was proportional to the reactant ratio for the SpyTag/SpyCatcher system, while a significant excess amount of Z-ELP was required to drive the conversion to about 50% for the SrtA ligation (**Figure 5.9B**). The average conjugation efficiency for the SpyTag/SpyCatcher products exceeded 90% (**Figure 5.9C**), indicating any target Z-ELP conjugation density may be achieved by simply mixing at the target Z-ELP:E2 reactant ratio. Because SpyTag/SpyCatcher bond formation eliminates the requirement of a third component for catalysis and the need to remove excess reactants, this system offers a more streamlined and cost-efficient method for the functionalization of E2 nanocages.

The effects of Z-ELP ligation density on nanocage transition temperature (T_t) and IgG binding capacity were investigated. Increasing the ligation density from 50% to 100% resulted in a 5°C lower T_t , and conjugation with the longer 80-repeat ELP further decreased the T_t value by 6-7°C across all samples (**Figure 5.10A**). The fully decorated Z-ELP₈₀-Spy-E2 nanocage at 25 μ M E2 had a T_t value of about 25°C, indicating only a small increase in ionic strength would be required for phase transition

at room temperature. In a mAb affinity precipitation process, this condition is highly desirable for nanocage recovery after mAb elution.

To ensure that the longer ELP and the presence of a SpyCatcher fusion have no impact on IgG binding, the binding capacity per nanocage was evaluated using an industrial mAb in the presence of excess IgG. As expected, a higher Z-ELP ligation density resulted in a higher binding capacity and the ELP chain-length had no influence in mAb binding (**Figure 5.10B**). For the ~100 % ligation samples, the expected molar interaction stoichiometry of 2:1 Z:IgG³¹ was observed with approximately 30 IgG molecules bound per 60 E2 subunits, whereas the low ligation samples ($\leq 25\%$ Z-ELP) bound IgG closer to a 1:1 molar ratio. The high local Z-domain concentration on the high ligation nanocages likely favors 2:1 Z:IgG binding, while at low ligation, the Z-domains may be more sterically restricted for coordinated binding to the same IgG molecule. Collectively, these results demonstrate a new conjugation platform capable of generating E2 nanocages with tunable T_t and high mAb binding capacity without limitations on maximum ligation density and ELP chain-length.

5.3.4 Effect of ligation density on crosslinking and precipitation yield

The results in Chapter 2 demonstrated IgG binding-induced crosslinking with Z-ELP-E2 nanocages through multivalent interactions that form large aggregates sufficient to capture mAbs from cell culture harvests with high yields¹⁹. To test the effect of ligation density on mAb-nanocage crosslinking, the SpyTag/SpyCatcher conjugated Z-ELP₄₀-E2 or Z-ELP₈₀-E2 nanocages were mixed with an industrial mAb at 1:1, 2:1, and 4:1 Z:mAb molar ratios. The sample turbidity (absorbance at 350 nm, PBS, 23°C) was used to monitor the extent of nanocage crosslinking by detecting the formation of large particles that scatter light. At higher ligation densities, both Z-ELP₄₀-

E2 and Z-ELP₈₀-E2 nanocages rapidly turned cloudy upon mixing and a similar trend was observed at all molar ratios tested (**Figure 5.11A-B**).

To examine the effect of Z-ELP ligation density on mAb precipitation yield, samples were centrifuged at 23°C to pellet only the crosslinked, insoluble aggregates. The percentage of captured mAb increased with the ligation density until 50%, beyond which only a slight change in mAb precipitation yield was observed (**Figure 5.11C-D**). This result again confirms that crosslinking is the key mechanism responsible for mAb recovery; only E2 nanocages with a high valency of affinity ligands can nucleate into large mAb-nanocage aggregates that can be efficiently separated from other soluble solution components by centrifugation. Meanwhile, at lower ligation densities, the mAb-nanocage mixtures did not form sufficient crosslinks for phase separation, as evidenced by the lower turbidity and mAb precipitation yields (**Figure 5.12**). It is interesting to note that a slight excess of Z-domain from the expected binding stoichiometry of 2:1 was required to achieve the highest mAb recovery. This may be due to steric limitations in the coordinated intermolecular IgG binding by two adjacent nanocages and the potential for 2:1 intramolecular IgG binding by the same nanocage.

5.3.5 Nanocage selective precipitation and regeneration after mAb Elution

To elute mAbs from the crosslinked aggregate, the sample was resuspended in a pH 3.5 buffer to dissociate the mAb-Z-domain interaction, which resolubilizes both. One drawback using the partially functionalized E2 nanocages generated by SrtA ligation is the requirement of 0.3 M ammonium sulfate for the selective precipitation and separation from the eluted mAbs¹⁹. From an industrial perspective, it is desirable to minimize the salt concentration necessary for nanocage phase transition because exposure to high ionic strength at low pH can result in increased aggregation for some

mAbs^{12,20}. Because the 100% ligation Z-ELP₄₀- and Z-ELP₈₀-Spy-E2 nanocages resulted in 5 to 10°C lower T_i value compared to the 50% ligation nanocages produced by SrtA, we expected improved precipitation yields at lower salt concentrations. The enhanced aggregation properties may also help prevent leaching into the final mAb supernatant and to reduce nanocage regeneration losses. The salt concentration required for greater than 95% nanocage precipitation was evaluated at Z-ELP-Spy-E2 concentrations ranging from 25-75 μM (**Figure 5.13**). Compared to Z-ELP₄₀-Spy-E2, the fully decorated Z-ELP₈₀-Spy-E2 nanocages exhibited higher precipitation yields over the entire salt concentration range. At a nanocage concentration used in a typical mAb purification process (75 μM Z-ELP-E2), 95% precipitation was achieved for Z-ELP₈₀-Spy-E2 with 0.1 M ammonium sulfate, while 0.3 M ammonium sulfate was required to achieve the same yield for Z-ELP₄₀-Spy-E2.

To evaluate the effect of salt concentration on nanocage recovery, an industrial mAb was purified from cell culture harvest using the fully ligated Z-ELP₄₀- and Z-ELP₈₀-Spy-E2 nanocages. After crosslinking at 3:1 Z:mAb molar ratio, the complex was washed and resuspended in elution buffer, followed by the addition of either 0.1 M or 0.3 M ammonium sulfate for nanocage precipitation. The nanocage samples were then regenerated and recycled back into PBS by ITC and nanocage recovery was calculated. The purification cycle recovery of Z-ELP₈₀-Spy-E2 nanocages exceeded 90% using both 0.1 M and 0.3 M ammonium sulfate (**Figure 5.14A**) and high mAb elution yields were obtained (**Figure 5.14B**). This high nanocage recovery was a significant improvement over previous work using SrtA functionalized nanocages²⁰. In contrast, precipitation of Z-ELP₄₀-Spy-E2 nanocages with 0.1 M ammonium sulfate resulted in <50% recovery, again highlighting the benefit of using a longer ELP for

nanocage recovery. The mAb affinity precipitation process (**Table 5.2**) with Z-ELP₈₀-Spy-E2 and 0.1 M ammonium sulfate resulted in efficient selective nanocage precipitation and regeneration, with no detectable leaching in the mAb elution by SDS-PAGE (**Figure 5.14C**). The high ligation density in combination with longer chain-length ELP resulted in improved nanocage regeneration steps that may make the affinity precipitation system a more viable alternative to Protein A chromatography for mAb purification.

5.4 Conclusion

In Chapter 5, we sought to improve the functionalization of E2 protein nanocages for mAb affinity precipitation by increasing the ligation density of longer chain-length Z-ELP affinity domains. We suspected that a fully decorated E2 using a longer Z-ELP backbone would decrease the salt concentration required for nanocage precipitation and increase antibody binding capacity. However, the SrtA ligation of an 80-repeat Z-ELP resulted in less than 10% ligation efficiency. This was attributed to steric interference of the SrtA active site by the disordered nature of the longer ELP in combination with the Z-domain fusion.

To bypass this limitation, the SpyTag/SpyCatcher ligation strategy was evaluated as an alternative conjugation method. SpyTag was fused to the N-terminus of the E2 subunit, and high soluble expression of assembled, thermostable nanoparticles was obtained. Upon addition of Z-ELP₄₀- or Z-ELP₈₀-SpyCatcher fusion proteins, a ligation efficiency of >90% was obtained such that any Z-ELP-E2 density may be achieved by simply mixing at the target Z-ELP:E2 reactant ratio. Compared to the maximum ligation nanocage attainable by SrtA (~50% ligation at 4:1 Z-ELP₄₀:E2 reactant ratio), the ~100% ligation Z-ELP₈₀-Spy-E2 nanocage had a 10°C lower

transition temperature with 2-fold higher IgG binding capacity. A Z-ELP ligation of >50% was sufficient for efficient nucleation into large aggregates, while low ligation density nanocages resulted in lower precipitation yields due to the formation of small oligomers or monomers not large enough for phase transition.

For the purification of an industrial mAb cell culture harvest, the critical salt concentration was evaluated to optimize the selective precipitation of the ~100% ligation Z-ELP₄₀- and Z-ELP₈₀-Spy-E2 nanocages after mAb elution. Greater than 90% nanocage recovery and 95% mAb elution yield were obtained using 0.1 M ammonium sulfate with the Z-ELP₈₀-Spy-E2 nanocage, while a three-fold higher salt concentration was required for similar performance using Z-ELP₄₀-Spy-E2 nanocages. Compared to SrtA mediated ligation, the SpyTag/SpyCatcher ligation reaction enables the generation of nanocages with tunable ligation densities up to ~100% conversion, resulting in lower T_t values, higher mAb binding capacity, and reduced production costs (**Table 5.3**). Because of these benefits, we believe the SpyTag-E2 nanocage may be an ideal scaffold for the efficient, site-specific conjugation of other SpyCatcher fusion proteins. Future work will seek to establish a generalized affinity precipitation platform that can be implemented for the purification of any target protein using customizable affinity ligands.

TABLES

Sample	Primer Name	DNA Sequence (5-3')
Primer 1	Z-domain Forward	TCTAGAAATAATTTTGTTTAACTTTAAGAAGGAGATATACC ATGGGGGTAGACAACAAATTCAACAAAGAAC
Primer 2	Z-domain Reverse	ATATCATATGAAGCTTGCTGCCGC
Primer 3	SpyCatcher Forward	GGATCCGGAGGGGGAAGCGGTGGAGGTGATAGTGCTACCC ATATTAAATTCTC
Primer 4	SpyCatcher Reverse	CTCGAGGGTACCTTATCAGCCATTTACAGTAACCTGAC
Oligo 1	SP2 Top 1	CATGGGATGTGGAAGCGTGGCTGGACGAACGTGTGCCCTG GTGGAGACCGGGAGCGGC
Oligo 2	SP2 Top 2	AGCGGGTCTGGATCTGGCAGCGGGAGCGGCAGCGGGTCTG GATCTGGTACCCA
Oligo 3	SP2 Bottom 1	CCCGGTCTCCACCAGGGGCACACGTTTCGTCCAGCCACGCTT CCACATCC
Oligo 4	SP2 Bottom 2	TATGGGTACCAGATCCAGACCCGCTGCCGCTCCCGCTGCCA GATCCAGACCCGCTGCCGCT
Oligo 5	(EA3K)3 Top	GATCCGAAGCGGCGGGCGAAAGAAGCGGCGGCGAAAGAAG CGGCGGCGAAACCGC
Oligo 6	(EA3K)3 Bottom	GGTTTCGCCGCGCTTCTTTCCGCCGCGCTTCTTTCCGCCG GCTTCG
Oligo 7	SpyTag Top	TATGGCACACATAGTAATGGTAGACGCCTACAAGCCGACG AAGG
Oligo 8	SpyTag Bottom	CTAGCCTTCGTCCGGCTTGTAGGCGTCTACCATTACTATGTGT GCCA

Table 5.1 Primers and oligos used for gene construction.

#	Description	Buffer	pH	Target VCF (x)	Amm Sulf (M)	Step Time (min)
1	Z-ELP ₈₀ -Spy-E2	PBS	7.2	1	0	n/a
2	mAb Harvest	Media	7.2	1	0	n/a
3	Mix 3:1 Z:mAb	Media	7.2	1	0	5
4	Precipitation	Media	7.2	1	0	5
5	Wash 1	PBS	7.2	2	0	5
6	Wash 2	Citrate	5.0	2	0	5
7	Elution	Citrate	3.5	4	0.10	15
8	Regeneration	Citrate	3.5	4	0.10	5
9	Recycle	PBS	7.2	8	0	5

Table 5.2 Affinity precipitation process steps corresponding to the lane number in **Figure 5.14C**.

#	Attribute	Sortase A Ligation	SpyTag/SpyCatcher Conjugation	Impact
1	Z-ELP ₄₀ Ligation Efficiency	Low < 25%; Require excess Z-ELP	High > 90%; Z-ELP:E2 ratio proportional to density	High density: lower T _i , higher [IgG] binding. Production costs
2	Z-ELP ₈₀ Ligation	Very low ligation	Similar to Z-ELP ₄₀	Longer ELP, lower T _i
3	Reversibility	Product also contains LPETG tag	Irreversible under all conditions	Ligation efficiency
4	# Components	3 components including SrtA	Simple 2-component mixture	Production costs
5	Reaction Conditions	4-6 hours at 37°C	1-hour room temperature	Operational efficiency
6	Reaction Cofactor	6 mM CaCl ₂	None required, just mix components	Buffer restrictions

Table 5.3 Comparison of SrtA ligation and SpyTag/SpyCatcher methods for Z-ELP conjugation to E2 nanocages.

FIGURES

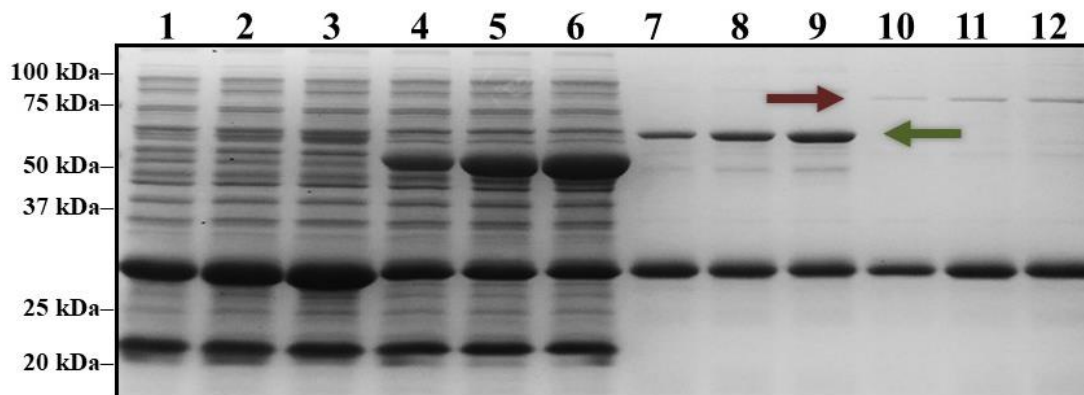


Figure 5.1 SDS-PAGE gel of SrtA ligation comparison of the conjugation of Z-ELP₄₀-LPETG or Z-ELP₈₀-LPETG to GGG-E2. Initial reactants mixed at 1:1, 3:1, and 5:1 Z-ELP₄₀:E2 (Lane 1-3) or Z-ELP₈₀:E2 (Lane 4-6) molar ratios. Final purified ligation products shown with indicated ligation product bands for Z-ELP₄₀-E2 (green arrow, Lane 7-9) and Z-ELP₈₀-E2 (red arrow, Lane 10-12).

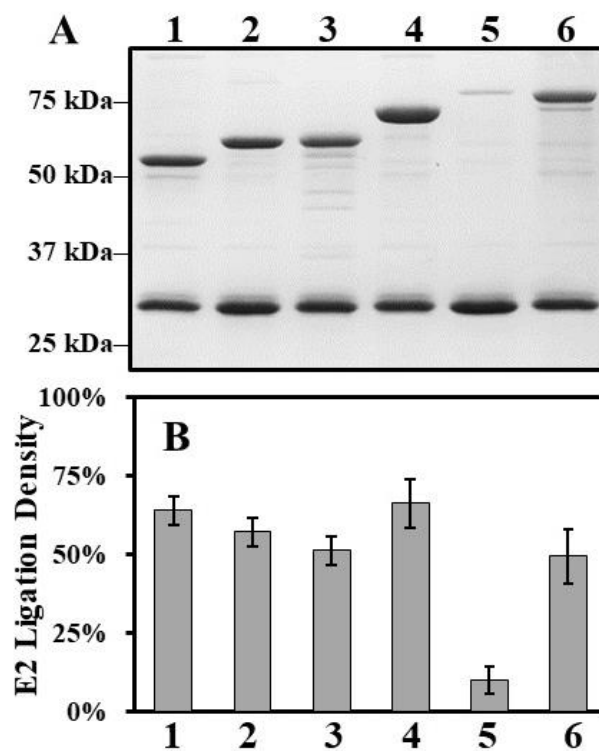


Figure 5.2 Low Z-ELP₈₀-LPETG ligation efficiency to GGG-E2. A) SDS-PAGE gel of SrtA ligation reaction products using various ELP-LPETG substrates mixed at a 3:1 molar ratio with GGG-E2. B) Average ELP-E2 ligation density estimated by densitometry. Lane 1: ELP₄₀-LPETG. Lane 2: Z-ELP₄₀-LPETG. Lane 3: SP₂-ELP₄₀-LPETG. Lane 4: ELP₈₀-LPETG. Lane 5: Z-ELP₈₀-LPETG. Lane 6: SP₂-ELP₈₀-LPETG. Error bars represent 95% confidence interval.

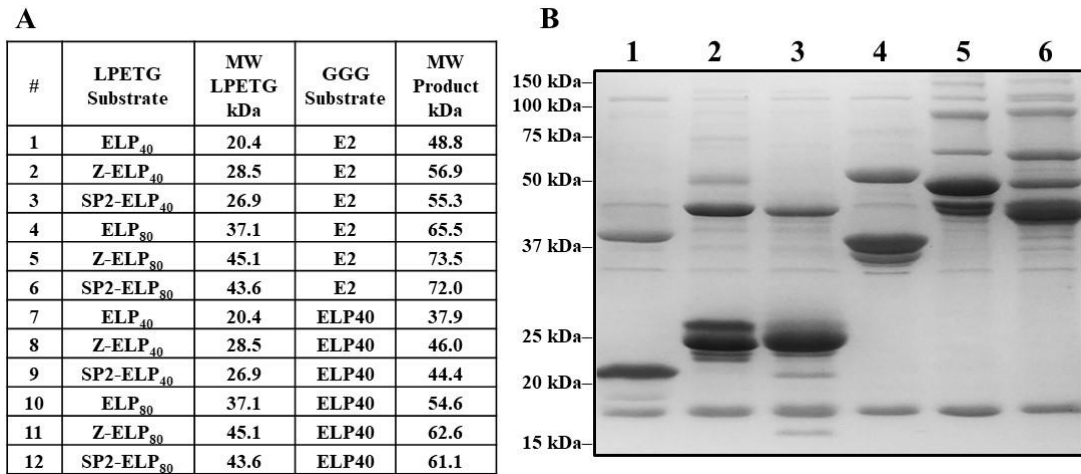


Figure 5.3 Low Z-ELP₈₀-LPETG ligation efficiency to GGG-ELP. A) ELP-LPETG and GGG substrates and molecular weights (MW) used for the evaluation of SrtA ligation reaction. B) SDS-PAGE gel of ligation products using GGG-ELP₄₀ substrate with ELP₄₀-LPETG (Lane 1), Z-ELP₄₀-LPETG (Lane 2), SP₂-ELP₄₀-LPETG (Lane 3), ELP₈₀-LPETG (lane 4), Z-ELP₈₀-LPETG (Lane 5), SP₂-ELP₈₀-LPETG (Lane 6) mixed at a 3:1 LPETG:GGG molar ratio.

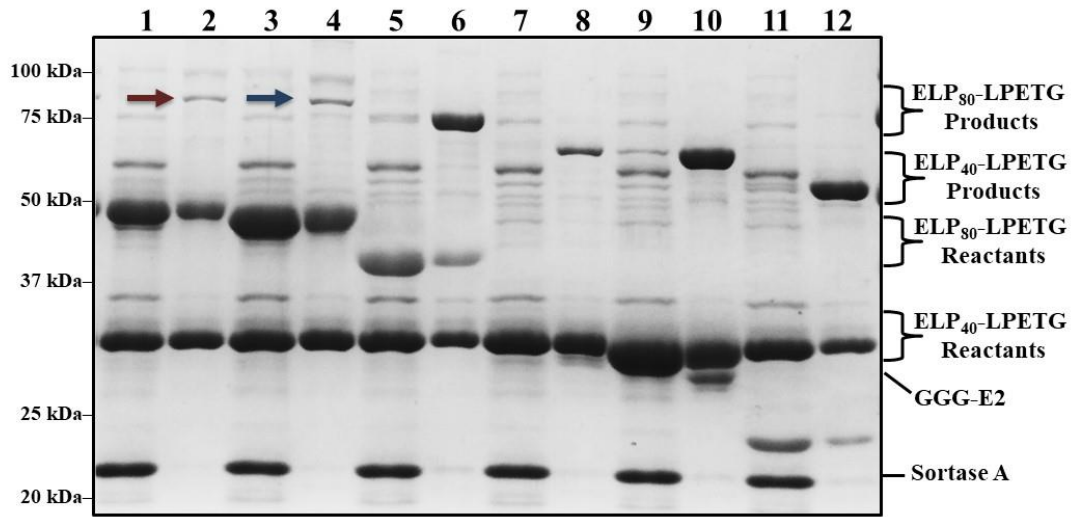


Figure 5.4 SDS-PAGE gel of SrtA ligation comparison with flexible linker (G₄S)₃ and rigid linker (EA₃K)₃ between ELP and LPETG motif for Z-ELP₈₀-(EA₃K)₃-LPETG initial reaction (Lane 1) and purified ligation product (Lane 2, red arrow), Z-ELP₈₀-(G₄S)₃-LPETG initial reaction (Lane 3) and purified ligation product (Lane 4, blue arrow), ELP₈₀-(G₄S)₃-LPETG initial reaction (Lane 5) and purified ligation product (Lane 6), Z-ELP₄₀-(EA₃K)₃-LPETG initial reaction (Lane 7) and purified ligation product (Lane 8), Z-ELP₄₀-(G₄S)₃-LPETG initial reaction (Lane 9) and purified ligation product (Lane 10), and ELP₄₀-(G₄S)₃-LPETG initial reaction (Lane 11) and purified ligation product (Lane 12).

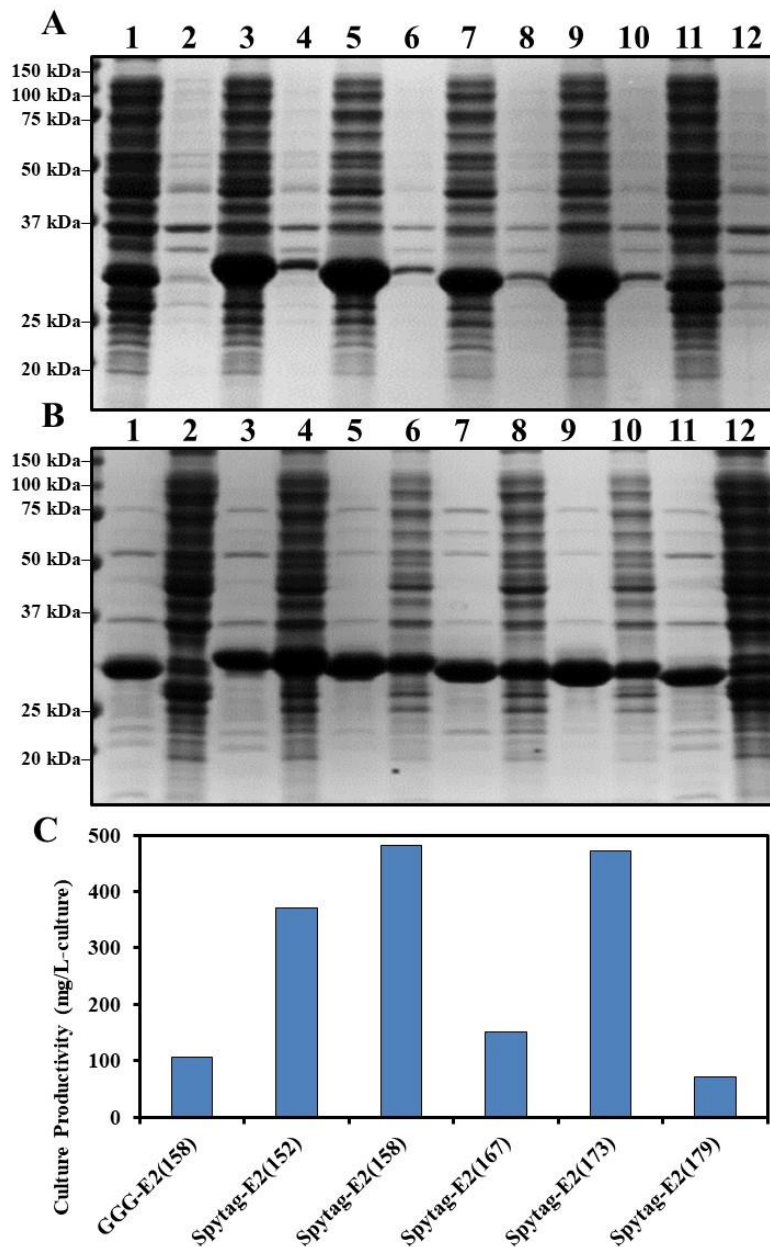


Figure 5.5 SpyTag-E2 nanocage expression and partial purification. A) SDS-PAGE gel for soluble and insoluble expression for GGG-E2(158) (Lane 1-2), SpyTag-E2(152) (Lane 3-4), SpyTag-E2(158) (Lane 5-6), SpyTag-E2(167) (Lane 7-8), SpyTag-E2(179) (Lane 9-10), SpyTag-E2(179) (Lane 11-12). B) Coomassie stained 10% acrylamide SDS-PAGE gel for soluble and insoluble fractions after heating to 70°C for GGG-E2(158) (Lane 1-2), SpyTag-E2(152) (Lane 3-4), SpyTag-E2(158) (Lane 5-6), SpyTag-E2(167) (Lane 7-8), SpyTag-E2(179) (Lane 9-10), SpyTag-E2(179) (Lane 11-12). C) Soluble, thermostable E2 culture productivity.

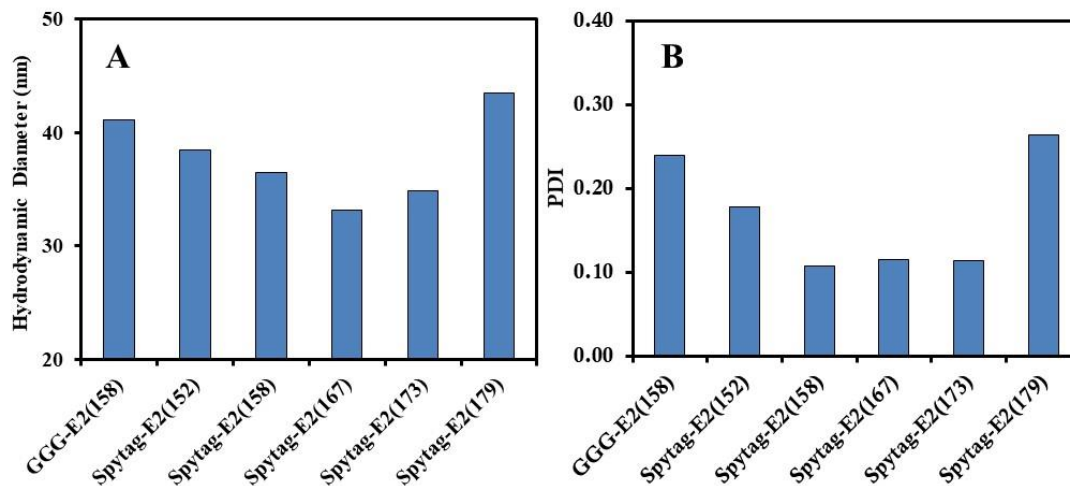


Figure 5.6 Confirmation of E2 assembly by DLS. A) Hydrodynamic diameter measured by dynamic light scattering for E2 constructs. B) Polydispersity index (PDI) measured by dynamic light scattering for E2 constructs.

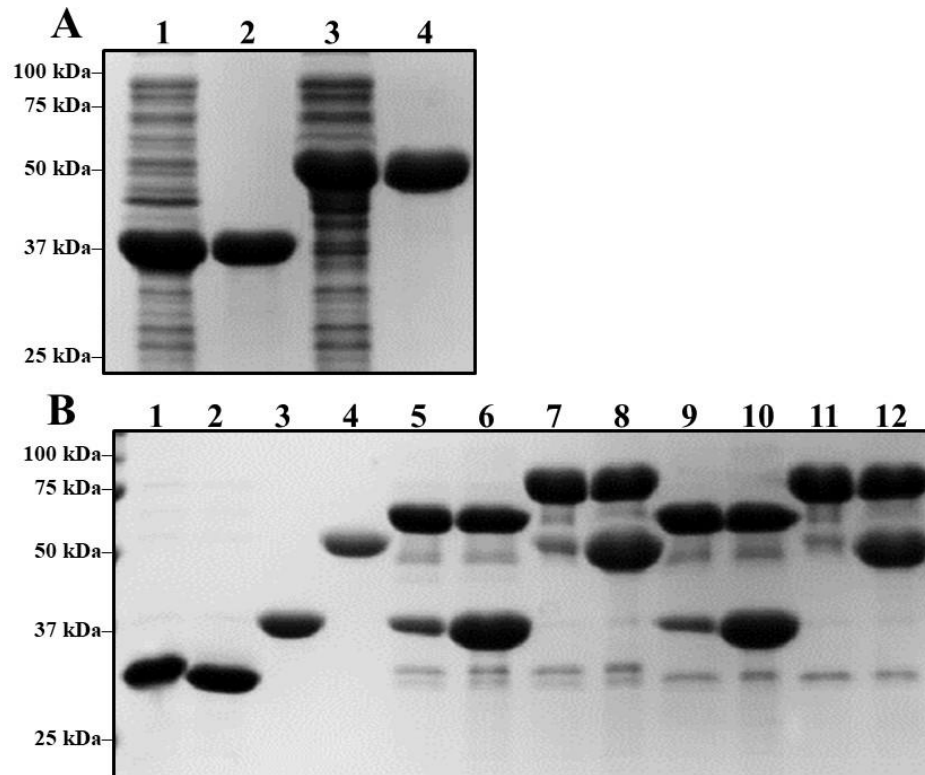


Figure 5.7 Z-ELP-SpyCatcher expression and SpyTag/SpyCatcher reaction. A) SDS-PAGE gel for Z-ELP₄₀-SpyCatcher soluble expression (Lane 1) and purified by ITC (Lane 2) and Z-ELP₈₀-SpyCatcher soluble expression (Lane 3) and purified by ITC (Lane 4). B) SDS-PAGE gel for comparison of SpyTag-E2(158) (Lane 1) and SpyTag-E2(173) (Lane 2) conjugation with Z-ELP₄₀-SpyCatcher (Lane 3) and Z-ELP₈₀-SpyCatcher (Lane 4). Conjugation products after 1 h reaction in PBS for mixture of 2:1 and 5:1 molar reactant ratio SpyCatcher:SpyTag for Z-ELP₄₀-SpyCatcher and SpyTag-E2(158) (Lane 5-6), Z-ELP₈₀-SpyCatcher and SpyTag-E2(158) (Lane 7-8), Z-ELP₄₀-SpyCatcher and SpyTag-E2(173) (Lane 9-10), Z-ELP₈₀-SpyCatcher and SpyTag-E2(173) (Lane 11-12).

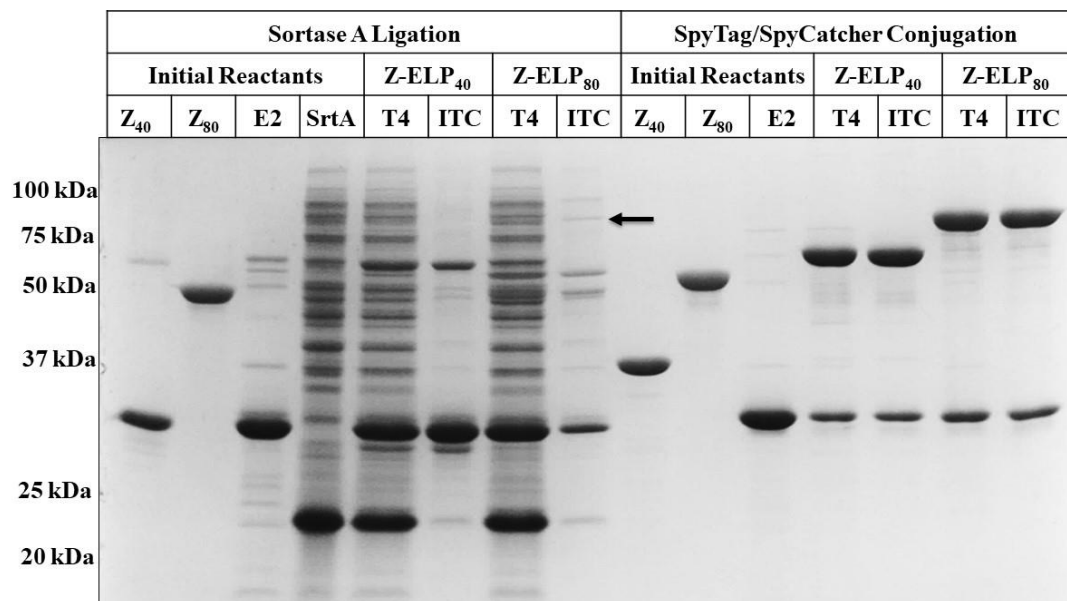


Figure 5.8 SDS-PAGE gel for comparison of SrtA and SpyCatcher-SpyTag conjugation methods with Z-ELP₄₀-LPETG and Z-ELP₈₀-LPETG (black arrow) conjugation to GGG-E2(158) in TN150 and Z-ELP₄₀-SpyCatcher and Z-ELP₈₀-SpyCatcher conjugation to SpyTag-E2(158) in PBS. Reactants mixed at a 0.75:1 Z-ELP:E2 molar ratio and incubated for 4 hours in a reaction buffer (T4) followed by purification by ITC.

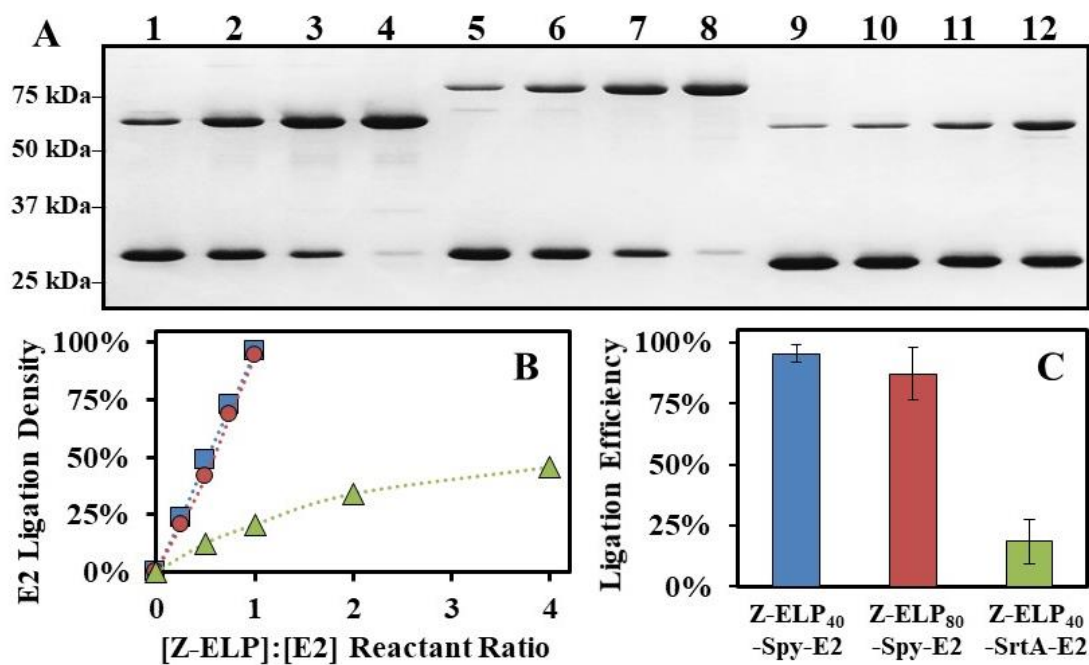


Figure 5.9 Ligation efficiency comparison. A) SDS-PAGE gel of the conjugation of Z-ELP₄₀-SpyCatcher (Lane 1-4) or Z-ELP₈₀-SpyCatcher (Lane 5-8) onto SpyTag-E2 and the SrtA reaction of Z-ELP₄₀-LPETG (Lane 9-12) onto GGG-E2 mixed at various Z-ELP:E2 molar reactant ratios. B) ELP-E2 ligation density estimated by densitometry plotted against the molar Z-ELP:E2 reactant ratio for Z-ELP₄₀-Spy-E2, Z-ELP₈₀-Spy-E2, and Z-ELP₄₀-SrtA-E2. C) Comparison of average ligation efficiencies of the conjugation reaction. Error bars represent 95% confidence intervals.

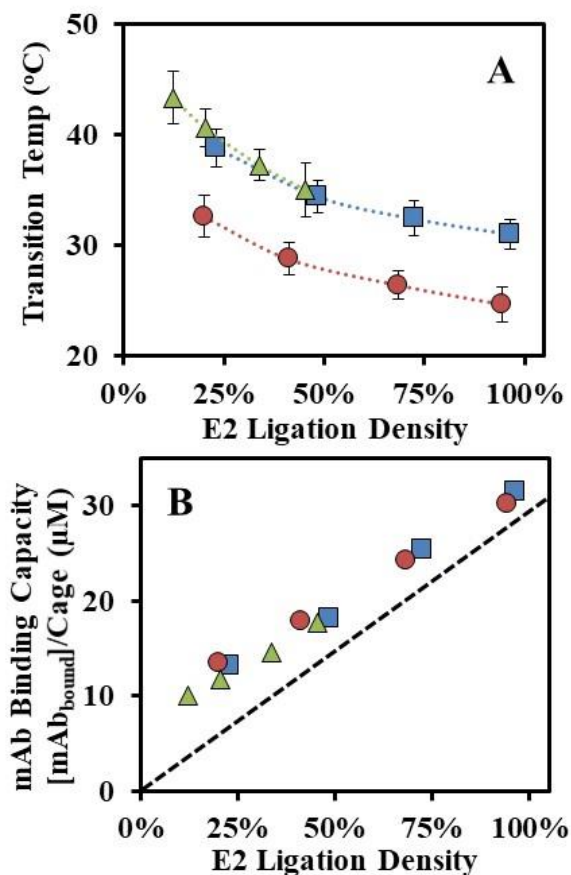


Figure 5.10 T_t and mAb Binding. A) Comparison of average transition temperature of Z-ELP₄₀-Spy-E2 (blue squares), Z-ELP₈₀-Spy-E2 (red circles), and Z-ELP₄₀-SrtA-E2 (green triangles) in PBS with various E2 ligation densities. B) Comparison of molar mAb binding capacity estimated per 60-subunit E2 nanocage in the presence of excess mAb mixed for 2 hr in PBS at 23°C. 100% ligation density assumes 60 μM conjugated Z-ELP per 1 μM 60-subunit E2 nanocage. Line represents expected 2:1 Z:IgG interaction stoichiometry.

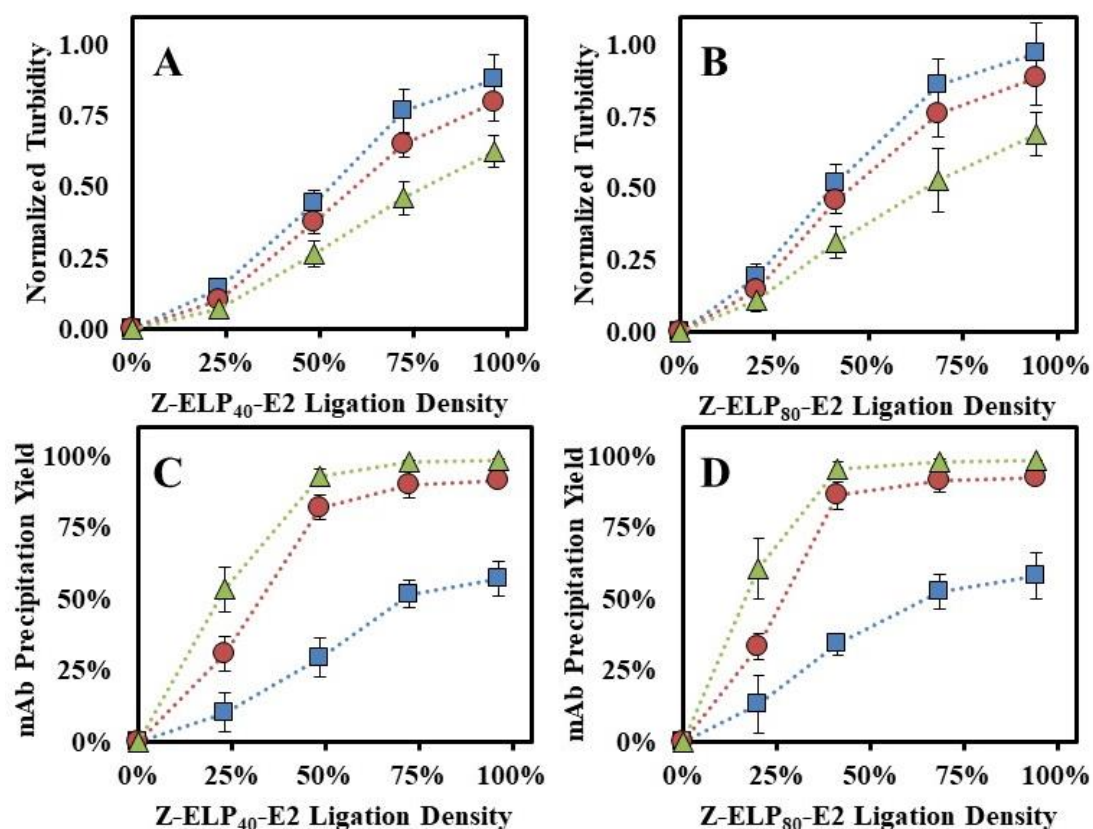


Figure 5.11 mAb-Nanocage crosslinking and precipitation. Normalized turbidity measured by absorbance at 350 nm upon mixing Z-ELP₄₀-Spy-E2 (A) or Z-ELP₈₀-Spy-E2 (B) with mAb at 1:1 (blue square), 2:1 (red circle), or 4:1 (green triangles) Z:mAb reactant ratios in PBS at 23°C. mAb precipitation yield estimated by mAb recovery after elution for Z-ELP₄₀-Spy-E2 (C) or Z-ELP₈₀-Spy-E2 (D) mixed with mAb at 1:1 (blue square), 2:1 (red circle), or 4:1 (green triangles) Z:mAb reactant ratios.

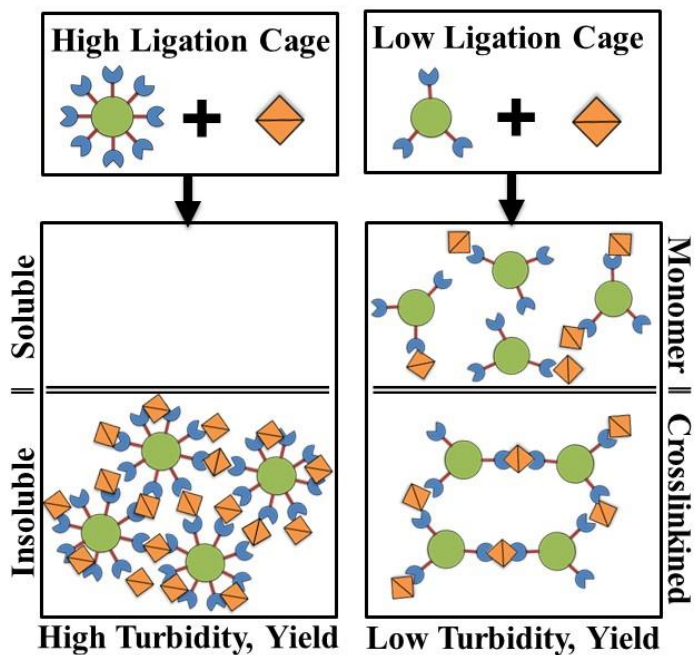


Figure 5.12 Mechanism for mAb-crosslinking with high and low Z-ELP-E2 ligation density. High conjugation of Z-ELP resulted in efficient multi-valent crosslinking with the dimeric mAb and formed large, insoluble aggregates capable of capturing > 90% of mAb in solution. Low Z-ELP conjugation nanocages reduced crosslinking efficiency due to lower valency and resulted in a yield loss due to the formation of smaller, soluble oligomers or monomers.

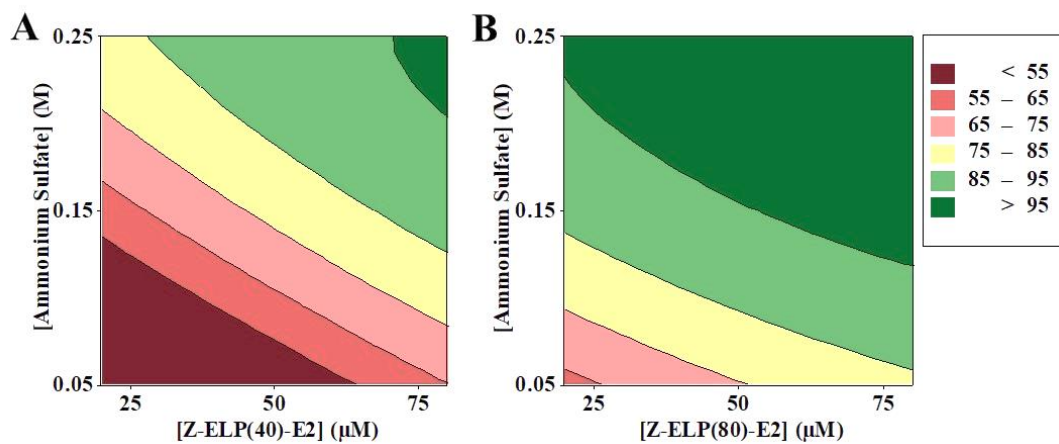


Figure 5.13 Optimization of ammonium sulfate concentration in 50 mM sodium citrate pH 3.5 buffer for selective nanocage precipitation after mAb elution for ~100% ligation density Z-ELP₄₀-Spy-E2 (A) or Z-ELP₈₀-Spy-E2 (B).

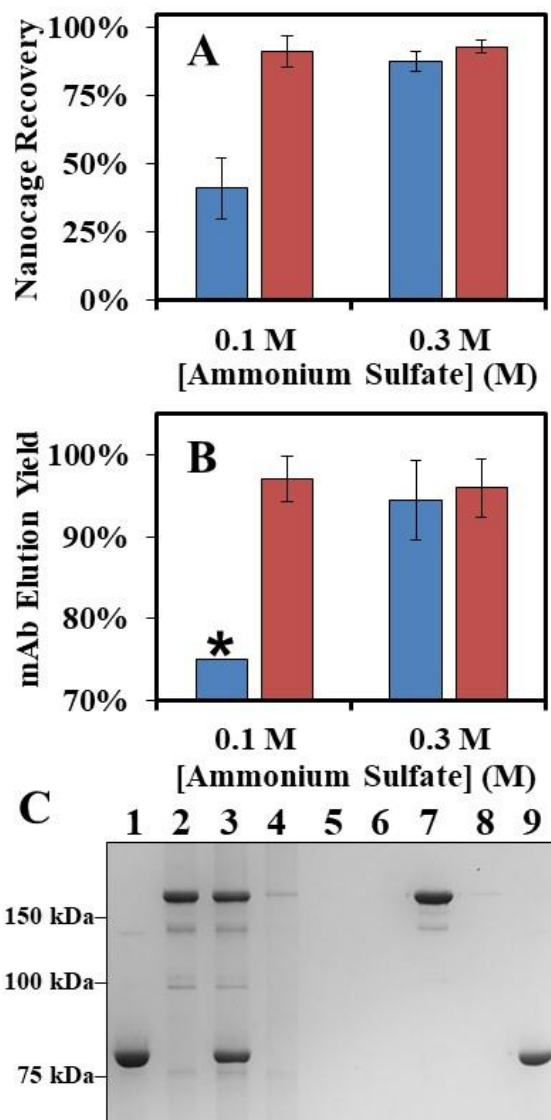


Figure 5.14 mAb affinity precipitation from cell culture harvest using ~100% ligation density Z-ELP₄₀-Spy-E2 (blue bars) or Z-ELP₈₀-Spy-E2 (red bars) nanocages. A) Nanocage recovery after mAb elution and regeneration with 0.1 or 0.3 M ammonium sulfate used for precipitation. B) mAb elution yield with 0.1 or 0.3 M ammonium sulfate used for precipitation. * indicates leaching of nanocage in the elution due to incomplete precipitation. C) SDS-PAGE of mAb purification from cell culture harvest using Z-ELP₈₀-Spy-E2 and 0.1 M ammonium sulfate for precipitation. Lane 1: Purified nanocage stock. Lane 2: mAb cell culture. Lane 3: 3:1 Z:mAb molar ratio mixture Lane 4: Precipitation supernatant. Lane 5-6: Wash buffer supernatant. Lane 7: Elution supernatant. Lane 8: Regeneration supernatant. Lane 9: Recycled nanocage. Refer to Table 5.2 for more information.

REFERENCES

1. Gupta MN, Kaul R, Guoqiang D, Dissing U, Mattiasson B. Affinity Precipitation of Proteins. *Journal of Molecular Recognition* **1996**, 9:356-359.
2. Thömmes J, Etzel M. Alternatives to chromatographic separations. *Biotechnology Progress* **2007**, 23(1):42-45
3. Hammerschmidt N, Tscheliessnig A, Sommer R, Helk B, Jungbauer A. Economics of recombinant antibody production processes at various scales: Industry-standard compared to continuous precipitation. *Biotechnology Journal* **2017**, 9:766-775.
4. Hillbrig F, Freitag R. Protein purification by affinity precipitation. *Journal of Chromatography B* **2003**, 790(1):79-90.
5. Handlogten MW, Stefanick JF, Deak PE, Bilgicer B. Affinity-based precipitation via a bivalent peptidic hapten for the purification of monoclonal antibodies. *Analyst* **2014**, 139:4247-4255.
6. Bilgicer B, Thomas SW, Shaw BF, Kaufman GK, Krishnamurthy VM, Estroff LA, Yang J, Whitesides GM. A non-chromatographic method for the purification of a bivalently active monoclonal IgG antibody from biological fluids. *Journal of American Chemical Society* **2009**, 131(26):9361-9367.
7. Pearson JC, Clonis YD, Lowe CR. Preparative affinity precipitation of L-lactate dehydrogenase. *Journal of Biotechnology* **1989**, 11(2):267-274.
8. Taipa MA, Kaul RH, Mattiasson B, Cabral JMS. Recovery of a monoclonal antibody from hybridoma culture supernatant by affinity precipitation with Eudragit S-100. *Bioseparation* **2000**, 9(5):291-298.
9. Anastase-Ravion S, Ding Z, Pelle A, Hoffman AS, Letourneur D. New antibody purification procedure using a thermally responsive poly(N-isopropylacrylamide)-dextran derivative conjugate. *Journal of Chromatography B* **2001**, 761(2):247-254.
10. Madan B, Chaudhary G, Cramer SM, Chen W. ELP-z and ELP-zz capturing scaffolds for the purification of immunoglobulins by affinity precipitation. *Journal of Biotechnology* **2013**, 163(1):10-16.

11. Sheth RD, Jin M, Bhut BV, Li A, Chen W, Cramer SM. Affinity precipitation of a monoclonal antibody from an industrial harvest feedstock using an ELP-Z stimuli responsive biopolymer. *Biotechnology and Bioengineering* **2014**, 111(8):1595-1603.
12. Sheth RD, Madan B, Chen W, Cramer SM. High-throughput screening for the development of a monoclonal antibody affinity precipitation step using ELP-Z stimuli responsive biopolymers. *Biotechnology and Bioengineering* **2013**, 110(10):2664-2676.
13. Arioso R, Jaquet B, Wu M, Morbidelli M. On the role of salt type and concentration on the stability behavior of a monoclonal antibody solution. *Biophysical Chemistry* **2012**, 168:19-27.
14. Gagnon P. Technology trends in antibody purification, *Journal of Chromatography A* **2012**, 1221:57-70.
15. Swartz AR, Sun Q, Chen W. Ligand-induced cross-linking of Z-elastin-like polypeptide-functionalized E2 protein nanoparticles for enhanced affinity precipitation of antibodies. *Biomacromolecules* **2017**, 18:1654-1659.
16. Dalmau M, Lim S, Chen HC, Ruiz C, Wang S-W. Thermostability and molecular encapsulation within an engineered caged protein scaffold. *Biotechnology and Bioengineering* **2008**, 101(4):654-664.
17. Chen Q, Sun Q, Molino NM, Wang S-W, Boder ET, Chen W. Sortase A-mediated multi-functionalization of protein nanoparticles. *Chemical Communications* **2015**, 51:12107-12110.
18. Sun Q, Blackstock D, Chen W. Post-translational modification of bionanoparticles as a modular platform for biosensor assembly. *ACS Nano* **2015**, 9(8):8554-8561.
19. Swartz AR, Xu X, Traylor SJ, Li ZJ, Chen W. One-step affinity capture and precipitation for improved purification of an industrial monoclonal antibody using Z-ELP functionalized nanocages. *Biotechnology and Bioengineering* **2018**, 115(2):423-432.
20. Swartz AR, Xu X, Traylor SJ, Li ZJ, Chen W. High-efficiency affinity precipitation of multiple industrial mAbs and Fc-fusion proteins from cell culture harvests using Z-ELP-E2 nanocages. *Biotechnology and Bioengineering*, **2018**, 1-9 (in press).
21. Levary DA, Parthasarathy R, Boder ET, Ackerman ME. Protein-protein fusion catalyzed by Sortase A. *PLOS One* **2011**, 6(4):e18342.

22. Clancy KW, Melvin JA, McCafferty DG. Sortase Transpeptidases: Insights into Mechanism, Substrate Specificity and Inhibition. *Biopolymers* **2010**, 94(4):385-396.
23. Zakeri B, Fierer JO, Celik E, Chittock EC, Schwarz-Linek U, Moy VT, Howarth M. Peptide tag forming a rapid covalent bond to a protein, through engineering a bacterial adhesin. *PNAS* **2012**, 109(12):690-697.
24. Meyer DE, Chilkoti A. Quantification of the effects of chain length and concentration on the thermal behavior of elastin-like polypeptides. *Biomacromolecules* **2004**, 5(3):846-851.
25. Reichheld SE, Muiznieks LD, Keeley FW, Sharpe S. Direct observation of structure and dynamics during phase separation of an elastomeric protein. *PNAS* **2017**, 114(22):e4408-e4415.
26. Chen X, Zaro JL, Shen WC. Fusion protein linkers: property, design and functionality. *Adv Drug Deliv Rev* **2013**, 65(10):1357-1369.
27. Liu F, Luo EY, Flora DB, Mezo AR. Irreversible sortase A-mediated ligation driven by diketopiperazine formation. *J Org Chem* **2014**, 72(2):487-492.
28. Guimaraes CP, Witte MW, Theile CS, Bozkurt G, Kundrat L, Blom AEM, Ploegh HL. Site-specific C-terminal internal loop labeling of proteins using sortase-mediated reactions. *Nat Protoc* **2013**, 8(9):1778-1799.
29. Reddington SC, Howarth M. Secrets of a covalent interaction for biomaterials and biotechnology: SpyTag and SpyCatcher. *Current Opinion in Chemical Biology* **2015**, 29:94-99.
30. Domingo GJ, Orru S, Perham RN. Multiple display of peptides and proteins on a macromolecular scaffold derived from a multienzyme complex. *J Mol Biol* **2001**, 305(2):259-267.
31. Jendeberg L, Persson B, Andersson R, Karlsson R, Uhlen M, Nilsson B. Kinetic analysis of the interaction between protein a domain variants and human Fc using plasmon resonance detection. *J Mol Recognit* **1995**, 8(4):270-278.
32. Lamla T, Erdmann VA. The Nano-tag, a streptavidin-binding peptide for the purification and detection of recombinant proteins. *Protein Expr Purif* **2004**, 33(1):39-47.

Chapter 6

RAPID DETECTION AND QUANTIFICATION OF MONOCLONAL ANTIBODY CONCENTRATION IN CELL CULTURE HARVESTS THROUGH ANTIBODY-NANOPARTICLE CROSSLINKING TURBIDITY

Abstract

Existing assays for the quantification of monoclonal antibody cell culture titer typically require expensive equipment or reagents or are limited by low-throughput or tedious protocols. In Chapter 6, we developed a quick and cost-effective alternative assay utilizing mAb-nanoparticle crosslinking with Z-domain-ELP-E2 nanoparticles functionalized by SpyTag/SpyCatcher conjugation. Results from Chapters 2-5 demonstrated a rapid increase in solution turbidity after mAb-nanoparticle binding through crosslinking into large aggregates. After mixing mAb samples with a fixed nanoparticle concentration for 10 min, we found that the turbidity, measured by absorbance at 600 nm, exhibited a high signal to background ratio and was proportional to mAb concentration. A simple logarithmic regression was found to fit ($R^2 = 0.99$) the turbidity data for mAb concentrations between 100-1000 $\mu\text{g/mL}$. The optimized assay protocol was validated using two industrial mAb cell culture harvests and a bridging study with Octet biolayer interferometry confirmed accurate and reproducible results. A simple mixing and turbidity-based measurement can be adapted to high-throughput methods and the mAb samples can be purified after analysis using affinity precipitation. We expect that analyte detection using multivalent nanoparticle crosslinking turbidity can be extended to other target molecules using our modular system.

6.1 Introduction

To capitalize on the rapidly increasing demand¹ for therapeutic monoclonal antibodies¹ (mAbs), process manufacturing platforms have been established to reduce the time required during clinical development². High-throughput, streamlined approaches³ have enabled the advancement from gene discovery to investigational new drug approval in less than one year⁴. In this early stage of development, mAb secreting CHO cell lines are screened in bioreactors and optimized for high productivity and quality⁵. Cell line clone selection involves the generation of numerous samples for analytical characterization of key attributes such as mAb titer, glycosylation, charge variants, aggregation, and sequence heterogeneity⁶. mAb titer is quantified by the specific detection of mAbs in cell culture media with contaminating host cell proteins. Common techniques for the evaluation of antibody titer include HPLC-based analytical protein A chromatography⁷, enzyme-linked immunosorbent assay (ELISA)⁸, biolayer interferometry (BLI) using ForteBio's Octet instrument⁹, or agglutination-based assays¹⁰. However, these methods typically require expensive equipment or reagents or have limitations in throughput, sensitivity, or ease of use. In Chapter 6, we sought to develop a simple, high-throughput mAb quantification assay that can be performed on the benchtop without specialized liquid handling equipment.

A turbidity-based assay may be one potential alternative. Solution turbidity is caused by the formation of large particles that decrease the transmittance of light due to scattering and can be easily measured using a spectrophotometer¹¹. Because of the low-cost procedure, turbidity has been used to study protein interactions and aggregation behavior¹²⁻¹³. In Chapter 4, we used turbidity to characterize antibody-nanoparticle crosslinking in the development of a mAb affinity precipitation process using Z-domain-elastin-like polypeptide functionalized E2 (Z-ELP-E2) nanoparticles¹⁴.

Staphylococcal Sortase A¹⁵ was used to ligate Z-ELP affinity ligands to a self-assembled, 60-subunit E2 nanocage derived from *Bacillus stearothermophilus*¹⁶⁻¹⁷. Upon antibody-Z-domain binding, the nanoparticles crosslinked through multivalent interactions into large, insoluble aggregates that captured > 95% of the initial mAb in solution¹⁸. However, the utility of this system was restricted by poor Z-ELP conjugation efficiency due to the reversible nature of SrtA ligation¹⁹.

In Chapter 5, we described a new method of E2 nanoparticle functionalization using SpyTag/SpyCatcher isopeptide bond formation²⁰ that enabled the economical production of Z-ELP-E2 nanoparticles with close to 100% conjugation efficiency and improved antibody binding and aggregation properties²¹. Using these 60-valent affinity scaffolds, we speculated that the sample turbidity arising from mAb-nanoparticle crosslinking may be proportional to the mAb concentration. This relationship between crosslinking agent concentration and aggregate size or solution turbidity has been well studied for polymeric nanoparticle systems²²⁻²³, but these systems lack uniformity in nanoparticle modifications that may affect consistent analytical measurements. Here, we report a convenient and rapid turbidity-based assay for quantification of industrial mAb cell culture samples using a spectroscopic measurement of absorbance at 600 nm based on mAb-induced E2 nanoparticle crosslinking. After analysis, the mAb sample can also be purified by resuspension in a low pH elution buffer to dissociate the mAb-nanoparticle complex for other quality control measurements. All steps can be adapted to a high-throughput format using this cost-effective and rapid assay procedure (**Figure 6.1**).

6.2 Materials and Methods

6.2.1 Materials

An *Escherichia coli* strain BLR(DE3) containing a pET24(a) vector encoding for Z-ELP[KV₈F-80]-SpyCatcher and an *E. coli* strain BL21(DE3) containing a pET11(a) vector encoding for SpyTag-E2(158) were constructed and described previously²¹. Two purified and clarified cell culture mAbs (mAb A and mAb B) were received as a gift from Bristol-Myers Squibb (BMS) (New York City, NY) and mAb cell culture titer and host cell protein (HCP) content were determined previously¹⁸. Bacto tryptone and yeast extract were purchased from BD Biosciences (Franklin Lakes, NJ). Kanamycin, ampicillin, isopropyl- β -D-thiogalactoside (IPTG), Cellgro DMEM + 4.5 g/L glucose + L-glutamine + 25 mM HEPES media, and 96-well 200uL conical PCR plates were purchased from Fisher Scientific (Pittsburgh, PA). Sodium hydroxide, sodium phosphate, citric acid, ammonium sulfate, sodium chloride, and glycine were purchased from Sigma-Aldrich (St. Louis, MO). 96-well half area UV-transparent plates and 96-well solid black microplates were purchased from Corning (Corning, NY). Octet Dip and Read ProA biosensors were purchased from Pall ForteBio (Menlo Park, CA).

6.2.2 Protein Expression Purification and Conjugation

Z-ELP₈₀-SpyCatcher was expressed in BLR(DE3) *E. coli* grown in Terrific Broth (TB) with 50 μ g/mL kanamycin at 37°C and mixed at 250 rpm for 24 h with leaky expression, and SpyTag-E2 was expressed in BL21(DE3) *E. coli* grown in Luria-Bertani Medium (LB) with 100 μ g/mL ampicillin at 37°C and mixed at 250 rpm until induction at an OD₆₀₀ of 0.5 with 0.2 mM IPTG at 20°C for 20 h. Cells were harvested and sonicated, and Z-ELP₈₀-SpyCatcher was purified by inverse transition cycling (ITC)²⁴ with 0.5 M ammonium sulfate, and SpyTag-E2 was partially purified by incubating at

70°C for 10 min, as described previously²¹. 50 μ M purified Z-ELP₈₀-SpyCatcher was mixed with 50 μ M SpyTag-E2 in phosphate buffered saline (PBS, 25 mM sodium phosphate, 150 mM sodium chloride, pH 7.2) for 1 h at 20°C followed by one ITC cycle into PBS, concentrating to 500 μ M Z-ELP-E2 (20x stock solution). 100% Z-ELP₈₀-Spy-E2 ligation density was confirmed by 10% acrylamide SDS-PAGE.

6.2.3 Turbidity Measurement and Analysis

All turbidity measurements were performed using a Synergy plate reader from BioTek (Winooski, VT) and run at 23°C. mAb samples were prepared with 25 μ M nanocage at 23°C in 96-well 200 μ L conical PCR plates and mixed on a shake plate. Before measurement of absorbance, samples were well mixed using a multi-channel pipette by pipetting up and down. Then, 100 μ L was added to a half-area 96-well UV transparent plate and absorbance was measured at 600 nm. The absorbance value was buffer subtracted and corrected for path length to 1 cm. Standard samples were prepared with purified mAb diluted in cell culture media and validation samples were prepared with mAb cell culture harvests diluted in media. For ease of analysis, standard samples in the linear range were fit to the equation $Abs_{600} = m \cdot \ln[mAb] + b$ using the LINEST function in Microsoft Excel and the regression coefficients ($m = \text{slope}$, $b = \text{intercept}$) were used to estimate [mAb] of the cell culture harvests.

6.2.4 mAb-Nanoparticle Crosslinking Turbidity

For crosslinking kinetics, purified mAbs were prepared at 100, 250, 500, and 750 μ g/mL in cell culture media at pH 7.2 and mixed with 25 μ M nanocage for 2 min before measuring turbidity for indicated time. For mAb B, analysis of crosslinking kinetics was repeated with samples prepared in media titrated to pH 5.0 using 1 M citric

acid (**Figure 6.9A**). For crosslinking turbidity validation, mAb standards were prepared from 50 – 1000 $\mu\text{g}/\text{mL}$ using purified mAb and validation samples were prepared from cell culture harvest at 100, 200, 300, and 500 $\mu\text{g}/\text{mL}$ and mixed with 25 μM nanocage for 10 min. Six replicate experiments were run for each mAb, and logarithmic regression was performed using standard samples from 100-750 $\mu\text{g}/\text{mL}$. The validation samples were evaluated by the model and the mean and prediction error were calculated. All error bars represent 95% confidence intervals.

6.2.5 Octet Bridging Study

Octet experiments were performed on an Octet RED96e system. 8 protein A biosensors were pre-soaked in media for 10 min prior to measurement. 200 μL samples were prepared in a black 96-well plate with mAb standards diluted in media from 5 – 750 $\mu\text{g}/\mu\text{L}$ and validation cell culture samples diluted in media at 100, 200, 300, and 500 $\mu\text{g}/\mu\text{L}$ according to the layout shown in **Figure 6.11**. mAb binding was measured every 0.2 s for 60 s, and the sensors were regenerated (glycine, pH 1.5) and neutralized (media) 3x between each set of 8 samples. The full data set was then repeated twice more. The binding data were analyzed by the Octet data analysis software and the initial binding rate of the standard samples was fit to a 4-parameter dose response model³⁰. The validation samples were evaluated using the fitted regression coefficients.

6.2.6 mAb Purification after Turbidity Measurement

The mAb sample can be purified after turbidity measurement using simple washing and elution steps, as described previously¹⁸. Briefly, the insoluble mAb-nanocage complex was centrifuged and the pellet was washed with PBS and/or 25 mM sodium citrate, pH 5.0. The pellet was resuspended in elution buffer (50 mM sodium

citrate, pH 3.5) and the purified mAbs were collected in the supernatant after a selective nanoparticle precipitation using 0.25 M ammonium sulfate. The nanoparticles may be regenerated and recycled back into PBS by ITC.

6.3 Results and Discussion

Result from Chapters 2-5 demonstrated rapid, spontaneous crosslinking into large aggregates after mixing Z-ELP functionalized E2 nanoparticles with industrial mAb samples¹⁷. This property was advantageous for mAb purification because it enabled the capture and precipitation of > 95% mAb in cell culture harvests at a 3:1 Z-domain:mAb molar binding ratio without the need for an external stimulus. The goal of the current work was to correlate the observed increase in solution turbidity to mAb concentration as a simple, cost effective assay for cell culture mAb titer (**Figure 6.1**). The assay protocol was investigated using two model industrial mAbs with different properties including IgG subclass, isoelectric point, and cell culture titer and host cell protein (HCP) content (**Table 6.1**).

6.3.1 Optimization of turbidity measurement

Sample turbidity is commonly analyzed by absorbance at wavelengths ranging from 350-700 nm using a spectrophotometer. Because we want to detect light scattering from large mAb-Z-ELP-E2 nanoparticle aggregates, the measurement wavelength should have minimum interference from other solution components²⁵. The background from mAb A cell culture samples was determined by measuring the absorbance spectrum for mAb-nanoparticle mixtures (5 μ M mAb A + 25 μ M Z-ELP-E2) and the individual components in culture media and PBS (**Figure 6.2A**). A high background was observed for cell culture samples from 350-450 nm, likely due to large host cell

debris or absorbing chemicals in the media. The spectra for mAb-nanoparticle mixtures in media and PBS converged at wavelengths ≥ 500 nm, indicating minimal matrix interference. In this regime, the signal to background ratio was approximately 50:1 and 600 nm was selected as the optimal detection wavelength (**Figure 6.2B**). For media containing pH indicator dyes such as phenol red²⁶, a higher wavelength (700 nm) may be used with a small loss of sensitivity.

To investigate the effect of mAb A concentration on crosslinking turbidity, samples were prepared at various concentrations and mixed with 25 μM Z-ELP-E2 in PBS at 23°C, and the absorbance was measured at 600 nm. For all measurements, E2 nanoparticles containing 60 Z-ELP per E2 were used to achieve uniform mAb binding and highest sensitivity. A logarithmic dependence of mAb concentration on absorbance was observed with a sigmoidal response on a semi-log plot (**Figure 6.2C**). At mAb concentrations ≥ 10 μM , very high visible solution turbidity was observed and the aggregated particles began to settle out of solution after mixing, as evidenced by a decrease in absorbance signal and increased variability. mAb concentrations between 0.5 – 10.0 μM exhibited a strong dependence of mAb concentration on solution turbidity. Because of the high valency of the Z-ELP-E2 affinity scaffold²¹, we suspected that the nanoparticles captured $> 95\%$ mAb in solution and that extent of crosslinking and aggregate size was proportional to mAb concentration in this range. The limit of detection was approximately 100 nM (~ 0.02 g/L), as minimal mAb-nanoparticle crosslinks were formed to induce a significant increase in turbidity.

6.3.2 mAb-Nanoparticle crosslinking kinetics

The mAb-nanoparticle aggregation kinetics were investigated within the linear concentration range (100 – 750 $\mu\text{g/mL}$) to ensure fast and reproducible results. Previous

work indicated mAbs with a basic isoelectric point aggregate immediately upon mixing at neutral pH, while mAbs with a more acidic isoelectric point required titration to pH 5.0 for similar fast kinetics¹⁸. In cell culture media at pH 7.2, the mAb A (net positive, pI = 8.3) crosslinking turbidity value reached a steady state within approximately 5 min of mixing (**Figure 6.3A**). A logarithmic regression was used to fit the absorbance data to mAb concentration at various mixing times. Analysis of the fitted regression coefficients indicated minimal difference between 5 -15 min (**Figure 6.4A**). In contrast, mAb B (pI = 6.8) exhibited slower kinetics in media at neutral pH (**Figure 6.3B**), similar to previous results¹⁸. However, a simple titration of mAb B cell culture media to pH 5.0 using 1 M citric acid resulted in fast kinetics (**Figure 6.3C**), with consistent regression coefficients after 10 min mixing (**Figure 6.4B**). A similar analysis was performed for nanoparticle crosslinking with a human polyclonal IgG at pH 5.0, and a good fit was obtained after mixing for 10 min (**Figure 6.9B**). These results indicate that any mAb cell culture samples diluted into the linear range (~100 – 1000 $\mu\text{g/mL}$) may be quickly quantified by nanoparticle crosslinking turbidity with minimal required optimization.

6.3.3 Quantification and validation of mAb-nanoparticle crosslinking turbidity

The mAb-nanoparticle crosslinking turbidity assay was validated using standard curves prepared from purified mAbs to calculate the mAb titer of cell culture harvests. The concentrations of mAb A and B cell culture samples were previously determined by an analytical protein A assay performed by BMS. These samples were diluted to 100, 200, 300, and 500 $\mu\text{g/mL}$ in media, pH 7.2, for mAb A or in media titrated to pH 5.0 for mAb B. The standards were prepared at 50-1000 $\mu\text{g/mL}$ in the target media and all samples were mixed with 25 μM fully decorated Z-ELP₈₀-E2 nanocages for 10 min before measurement of absorbance at 600 nm. Six replicate data sets were evaluated and

logarithmic regression was performed using the mAb standards within the linear range (100-750 $\mu\text{g/mL}$) to determine the concentration of the mAb culture samples (**Figure 6.5 A-B**). A good fit ($R^2 \sim 0.99$) was obtained for both data sets with similar regression coefficients.

The validation cell culture samples were analyzed by the regression model and the predicted concentrations were close to the expected values (**Figure 6.6A**). Higher variability was observed at higher mAb concentration, but the coefficient of variation (CV) was less than 10% for all samples. The prediction error ranged from -10 to +25%, and on average, the predicted values resulted in a slight overestimation of mAb titer for both mAb A and B (**Figure 6.6B**). This may be due to the co-precipitation of host cell protein or media components that also increase the turbidity during the initial mAb-nanoparticle crosslinking. Since the mAb B culture contained significantly less HCP than mAb A and exhibited a higher overall positive prediction error, the main sources of variability are likely due to inefficient mixing and dilution/pipetting errors.

To further validate the accuracy of these results, a bridging study was performed, comparing the crosslinking turbidity assay with an industrial Octet RED96e mAb quantification assay based on protein A purchased from Pall ForteBio. The Octet assay was carried out following standard protocols. Purified mAb standard curves were used to determine mAb A and B cell culture samples prepared at 100, 200, 300, 500 $\mu\text{g/mL}$ using a 4-parameter dose-response model to fit the initial binding rates (**Figure 6.7A-C**). The calculated cell culture mAb concentrations measured by Octet were compared to the turbidity assay and excellent agreement was obtained ($R^2 > 0.99$) for both mAbs. The Octet assay exhibited very low variability at $[\text{mAb}] < 250 \mu\text{g/mL}$, but the variability was similar to the turbidity assay at higher concentrations. These results confirm that

mAb-nanoparticle crosslinking can be used to provide the same accurate determination of mAb titers as the Octet assay without the use of expensive sensors or reagents. In addition, mAbs samples may be collected after measurement and purified in a high-throughput format using established affinity precipitation protocols for other quality control measurements¹⁴. As an example, a 1 mg/mL mAb cell culture sample was captured by 25 μ M Z-ELP-E2, and after the turbidity measurement, the mAb-nanocage complex was pelleted, washed, and resuspended with high mAb elution yield and purity (**Figure 6.10**). There was no detectable leaching of the nanoparticle into the mAb elution supernatant by SDS-PAGE analysis. These purified samples can be submitted directly or buffer exchanged for additional analytical characterization. This may be especially beneficial for assays that require purified protein such as glycosylation analysis²⁷. The Z-ELP-E2 nanoparticles can also be regenerated for future testing.

6.4 Conclusion

With a surplus of mAb candidates currently in clinical development, a high-throughput, cost-effective assay for mAb titer is beneficial to accommodate the numerous samples produced from early upstream process optimization. Existing assays require expensive, specialized equipment and may be limited by throughput or sensitivity. In Chapter 6, we developed a new cost-effective method for measuring mAb cell culture titers through concentration-dependent E2 nanoparticle crosslinking turbidity. The nanoparticles were generated by fully functionalizing E2 nanocages with 60 Z-domain-ELP affinity ligands using SpyTag/SpyCatcher conjugation. Other than the two *E. coli* fermentations required for the recombinant expression of Z-ELP and E2²⁸, there are minimal capital or material costs associated with the production of the nanoparticles. ITC is used for purification from *E. coli* lysate²⁹, and equimolar mixing

of the two components is all that is required for conjugation. More importantly, the Z-ELP-E2 nanoparticles can be regenerated for subsequent assays, as demonstrated previously²¹.

After mixing the Z-ELP-E2 nanoparticles with a mAb sample, the rapid increase in turbidity was analyzed using a spectroscopic measurement of absorbance at 600 nm. This enabled the specific detection of Z-domain-mAb binding and crosslinking into large aggregated particles with a 50-fold signal enhancement over the background cell culture media. For mAbs with a more acidic isoelectric point less than 7.0, the cultures may be titrated to pH 5.0 to ensure fast kinetics and an approximate steady-state measurement¹⁸. A logarithmic dependence of mAb concentration and crosslinking turbidity was observed in the range of 100-1000 $\mu\text{g/mL}$. Logarithmic regression was performed using purified mAb standards in the linear range to evaluate the mAb culture titer.

Using two model industrial mAbs, the aggregation kinetics were studied to identify the necessary mixing time for stable turbidity measurements. In cell culture media at pH 7.2, mAb A quickly increased in turbidity and reached equilibrium after 5 min mixing, but mAb B crosslinking was much slower and required titration to pH 5.0 for similar fast kinetics. The optimized turbidity assay was validated using mAb cell culture sample with known concentrations and compared to an Octet assay based on Protein A. Excellent agreement was obtained between the two methods. After the turbidity measurement, highly pure mAb samples are obtained using a simple washing and elution steps for additional quality control measurements.

The reported mAb-nanoparticle crosslinking turbidity assay may be particularly useful for antibody secreting cell line development and clone selection. A simple 10-

min mixing step and absorbance measurement can quantify the mAb titers, sufficient for rapid screening purposes. Future work will investigate the detection of other target analytes through nanoparticle crosslinking turbidity by conjugating interchangeable affinity domain-ELP-SpyCatcher fusion proteins to the SpyTag-E2 scaffold.

TABLES

#	Molecule Name	IgG Subclass	MW (kDa)	pI	Culture Titer (mg/mL)	Culture HCP (mg/mL)
1	mAb A	IgG1	150	8.3	1.8	6.5
2	mAb B	IgG4	155	6.8	3.1	1.5

Table 6.1 Properties of mAbs used in this study. MW = molecular weight, pI = isoelectric point, HCP = host cell protein.

FIGURES

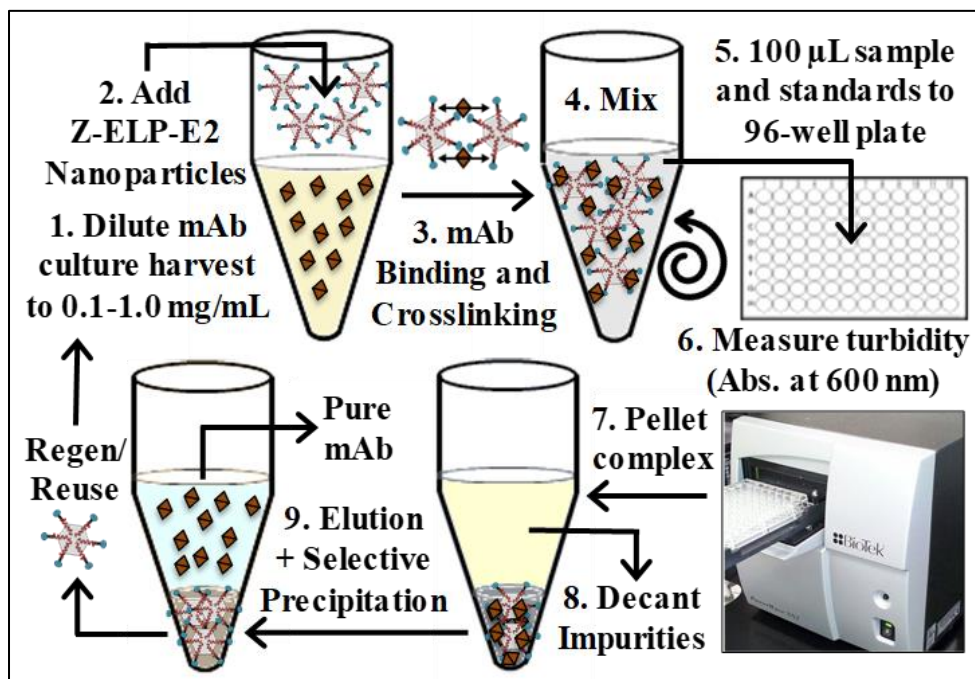


Figure 6.1 Procedure for measuring mAb-nanocage crosslinking turbidity and optional mAb purification.

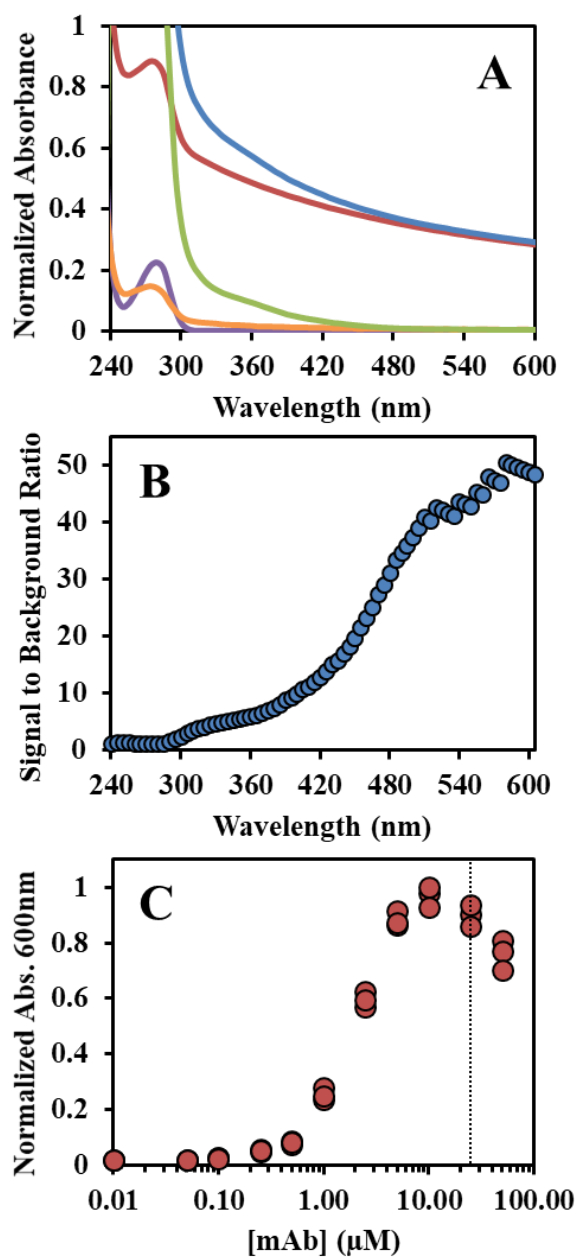


Figure 6.2 Optimization of turbidity measurement. A) Absorbance spectrum for mAb A cell culture-nanoparticle mix in media (blue), mAb A pure-nanoparticle mix in PBS (red), mAb A cell culture in media (green), mAb A pure (purple), and nanoparticle pure (orange). B) Ratio of absorbance for mAb A cell culture-nanoparticle mix to mAb A cell culture only. C) Normalized absorbance at 600 nm for pure [mAb A] from 0.01 – 50 μM (red circle) mixed with 25 μM nanoparticle (black line) in triplicate.

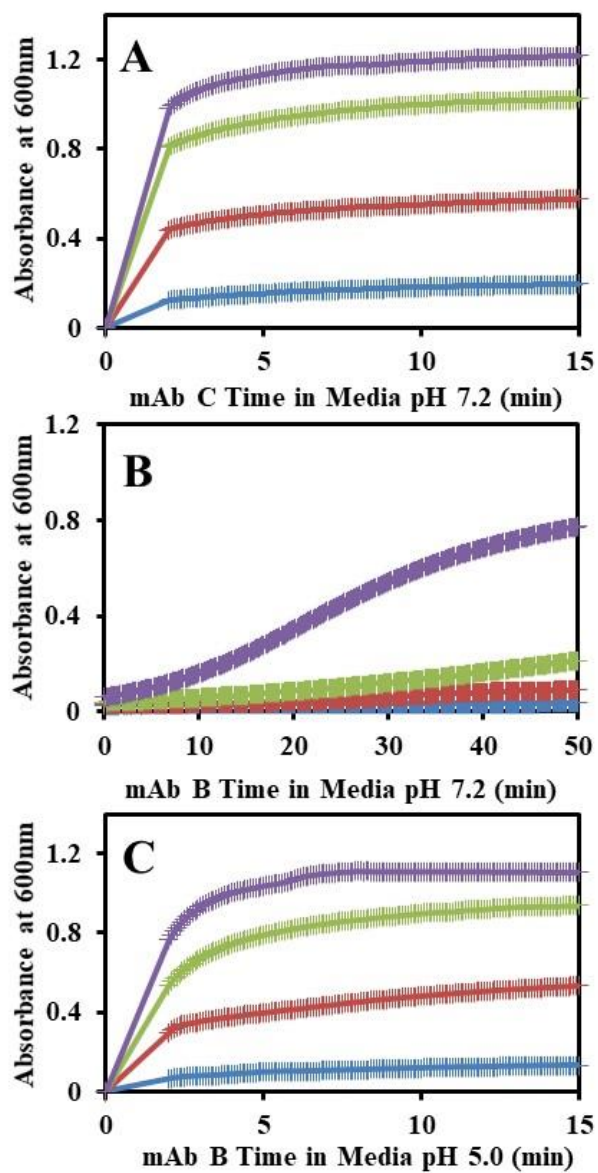


Figure 6.3 mAb-nanoparticle aggregation kinetics for 750 (purple), 500 (green), 250 (red), or 100 (blue) $\mu\text{g/mL}$ mAb mixed with 25 μM nanocage for mAb A in media pH 7.2 (A), mAb B in media pH 7.2 (B), or mAb B in media titrated to pH 5.0 (C).

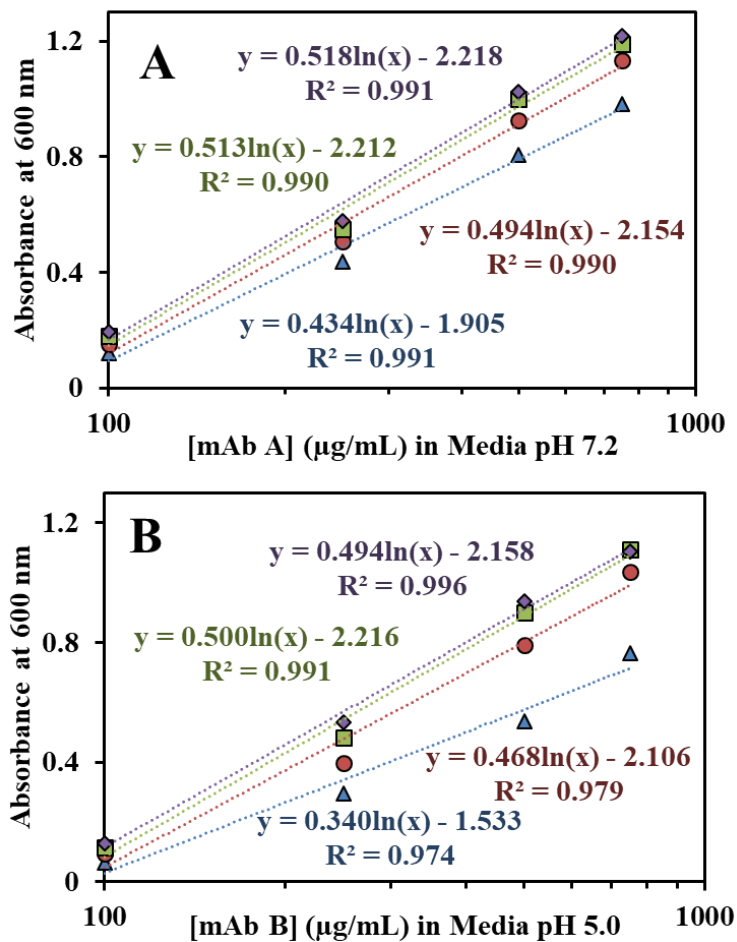


Figure 6.4 Dependence of mixing time on logarithmic regression fit. Absorbance at 600 nm values from mAb-nanocage crosslinking taken from aggregation curves shown in Figure 3 at 2 min (blue), 5 min (red), 10 min (green), and 15 min (purple) for mAb A in media pH 7.2 (A) or mAb B in media titrated to pH 5.0 (B).

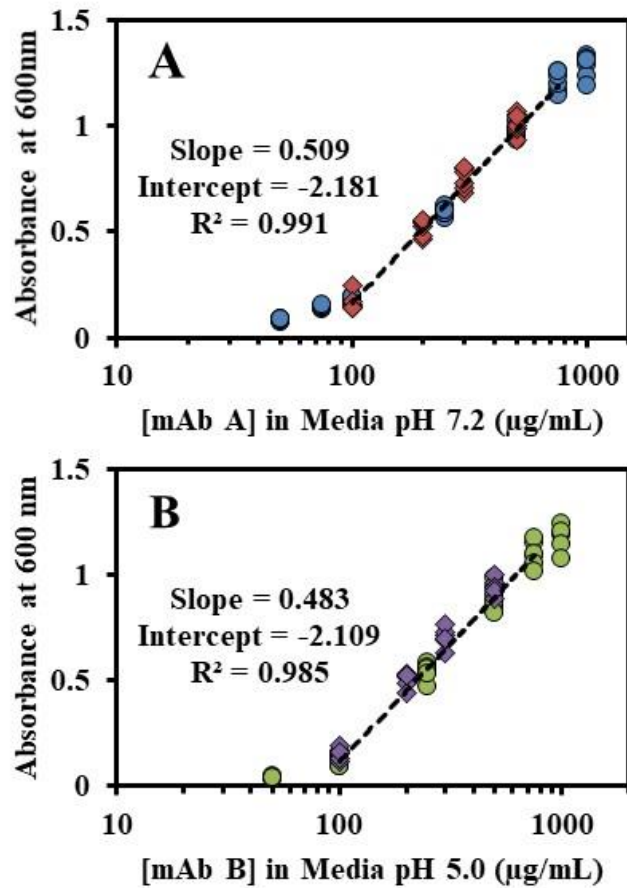


Figure 6.5 Crosslinking turbidity assay validation. A) mAb A standards (blue circle) prepared with purified mAb and validation mAb cell culture (red diamond). B) mAb B standards (green circle) prepared with purified mAb and validation mAb cell culture (purple diamond). All samples run with 6 replicates. Logarithmic regression performed for 100-750 $\mu\text{g/uL}$ standards.

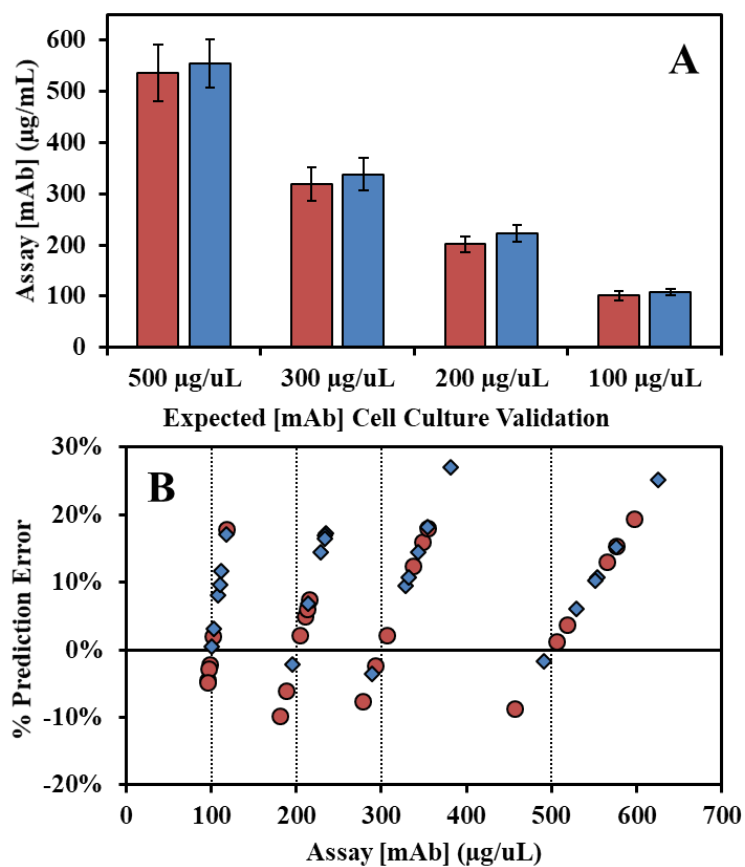


Figure 6.6 Nanoparticle crosslinking turbidity assay variability and prediction error. A) Fitted validation data for mAb A (red) or mAb B (blue). Error bars represent 95% confidence intervals. B) Prediction error for fitted validation data for mAb A (red circle) or mAb B (blue diamond).

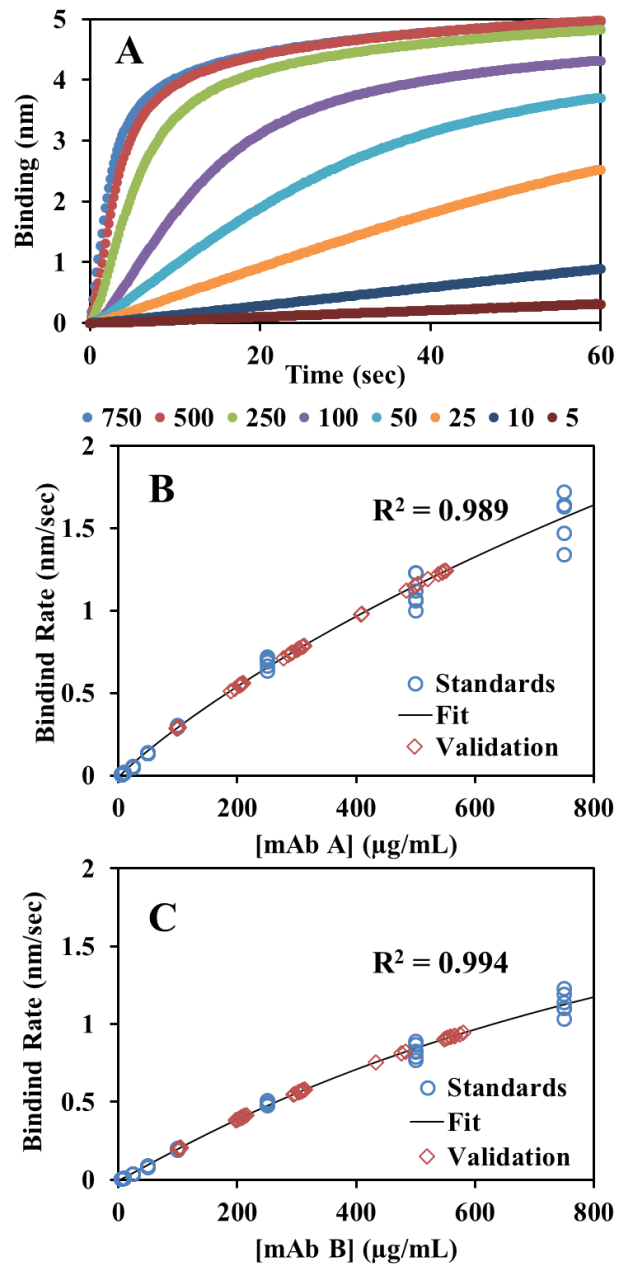


Figure 6.7 mAb titer measurement using ForteBio Octet instrument. A) Binding curves for one set mAb A standards. B) mAb A fitted standard curve using purified mAb (blue circle) and validation samples using mAb cell culture (red diamonds). C) mAb B standard and validation samples.

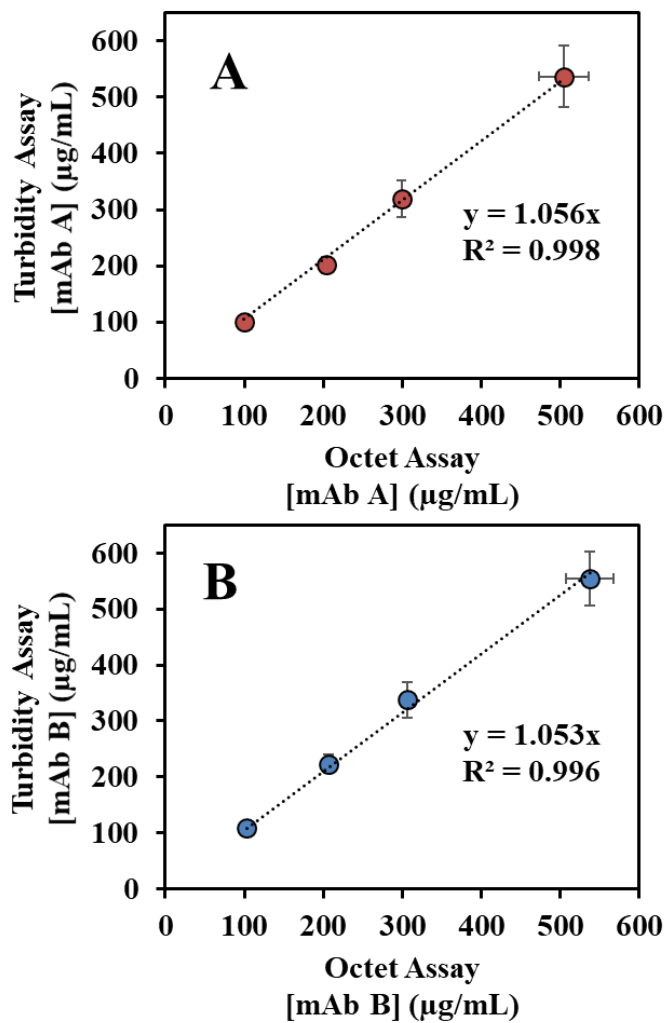


Figure 6.8 Comparison of turbidity assay and Octet assay for validation samples of mAb cell culture harvests for mAb A (A) and mAb B (B). Error bars represent 95% confidence intervals.

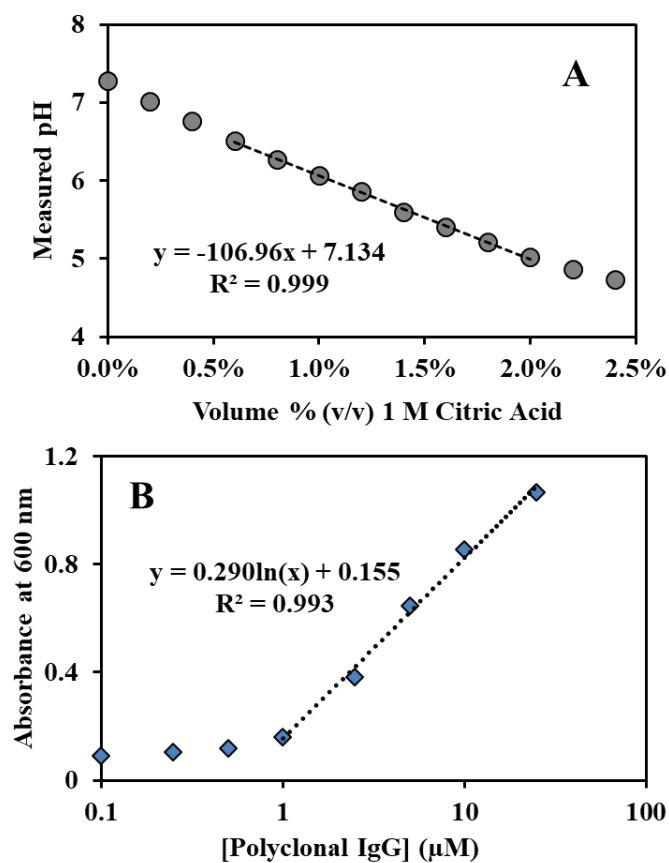


Figure 6.9 mAb cell culture titration and nanoparticle crosslinking with a human polyclonal IgG A) mAb B cell culture titration curve with 1 M citric acid used for the titration of mAb B cell culture to pH 5.0. B) Absorbance at 600 nm for the crosslinking of a purified polyclonal human IgG in sodium citrate pH 5.0 at various concentrations with 25 μM nanoparticles. Logarithmic fit (black line) shown for indicated concentration range.

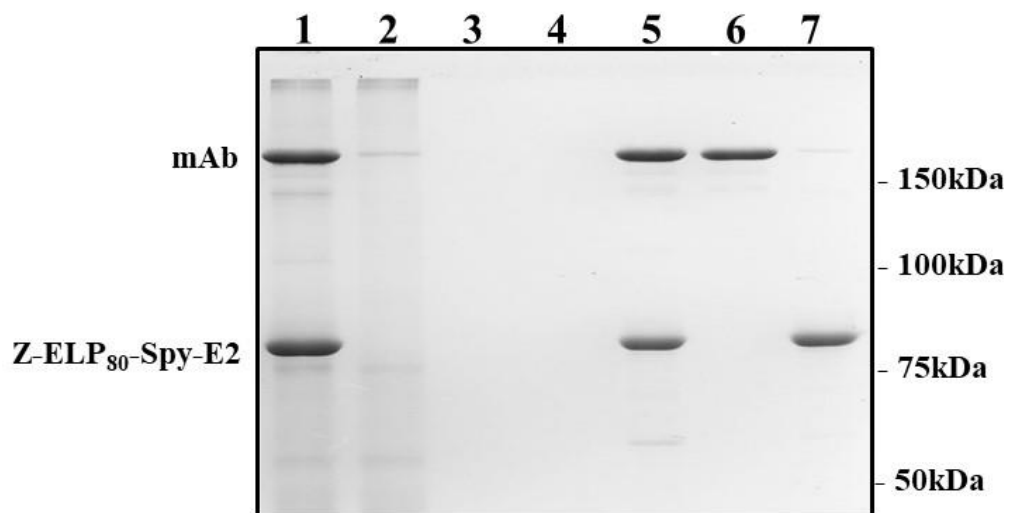


Figure 6.10 SDS-PAGE of mAb purification after turbidity measurement with 8% acrylamide Coomassie stained non-reducing SDS-PAGE analysis. Lane 1. mAb-nanoparticle mixture for 25 μ M nanoparticle mixed with 1 mg/mL mAb in cell culture. Lane 2: Precipitation supernatant. Lane 3-4: Wash 1-2. Lane 5: Elution resuspension. Lane 6: Elution supernatant. Lane 7: Elution pellet.

	1	2	3	4	5	6	7	8	9	10	11	12
A	AS1	AV1	AV4	AS8	BS1	BV1	BV4	BS8			Reg	Neut
B	AS2	AV2	AV3	AS7	BS2	BV2	BV3	BS7			Reg	Neut
A	AS3	AV3	AV2	AS6	BS3	BV3	BV2	BS6			Reg	Neut
D	AS4	AV4	AV1	AS5	BS4	BV4	BV1	BS5			Reg	Neut
E	AS5	AV4	AV1	AS4	BS5	BV4	BV1	BS4			Reg	Neut
F	AS6	AV3	AV2	AS3	BS6	BV3	BV2	BS3			Reg	Neut
G	AS7	AV2	AV3	AS2	BS7	BV2	BV3	BS2			Reg	Neut
H	AS8	AV1	AV4	AS1	BS8	BV1	BV4	BS1			Reg	Neut

Figure 6.11 Plate layout for ForteBio Octet experiment for mAb A and mAb B. S = standard sample. V = validation sample. Reg = regeneration buffer. Neut = Media.

REFERENCES

1. Ecker SD, Jones D, Levine H. The therapeutic monoclonal antibody market. *mAbs* **2015**, 7(1):9-14.
2. Kelley B. Industrialization of mAb production technology: The bioprocessing industry at a crossroads. *mAbs* **2009**, 1(5):443-452.
3. Bhambure R, Kumar K, Rathore AS. High-throughput process development for biopharmaceutical drug substances. *Trends Biotechnol* **2011**, 29:127-135.
4. Shukla AA, Wolfe LS, Mostafa SS, Norman C. Evolving trends in mAb production processes. *Bioeng Transl Med* **2017**, 2(1):58-69.
5. Zhu J. Mammalian cell protein expression for biopharmaceutical production. *Biotechnol Adv* **2011**, 30:1158-1170.
6. Li F, Vijayasankaran N, Shen A, Kiss R, Amanullah A. Cell culture processes for monoclonal antibody production. *Pharm Sci Encycl* **2010**, 2:466-479.
7. Loew C, Knoblich C, Fichtl J, Alt N, Diepold K, Bulau P, Goldbach R, Adler M, Mahler HC, Grauschopf U. Analytical protein a chromatography as a quantitative tool for the screening of methionine oxidation in monoclonal antibodies. *J Pharm Sci* **2012**, 101(11):4248-4257.
8. Barrette RW, Urbonas J, Silbart LK. Quantifying Specific Antibody Concentrations by Enzyme-Linked Immunosorbent Assay Using Slope Correction. *Clin Vaccine Immunol* **2006**, 13(7):802-805.
9. Yu Y, Mitchell S, Lynaugh H, Brown M, Nobrega RP, Zhi X, Sun T, Caffry I, Cao Y, Yang R, Burnina I, Xu Y, Estep. Understanding ForteBio's Sensors for High-Throughput Kinetic and Epitope Screening for Purified Antibodies and Yeast Culture Supernatant. *J Biomol Screen* **2016**, 21(1):88-95.
10. Costabile M. Determining the Reactivity and Titre of Serum using a Haemagglutination Assay. *J Vis Exp* **2010**, 35:1752.

11. Soos M, Lattuada M, Sefcik J. Interpretation of Light Scattering and Turbidity Measurements in Aggregated Systems: Effect of Intra-Cluster Multiple-Light Scattering. *J Phys Chem B* **2009**, 113(45):14962-14970.
12. Zhao R, So M, Maat H, Ray NJ, Arisaka F, Goto Y, Carver JA, Hall D. Measurement of amyloid formation by turbidity assay—seeing through the cloud. *Biophys Rev* **2016**, 8(4):445-471.
13. Toro TB, Nguyen TP, Watt TJ. An improved 96-well turbidity assay for T4 lysozyme activity. *MethodsX* **2015**, 2:256-262.
14. Swartz AR, Xu X, Traylor SJ, Li ZJ, Chen W. One-step affinity capture and precipitation for improved purification of an industrial monoclonal antibody using Z-ELP functionalized nanocages. *Biotechnology and Bioengineering* **2018**, 115(2):423-432.
15. Levary DA, Parthasarathy R, Boder ET, Ackerman ME. Protein-protein fusion catalyzed by Sortase A. *PLOS One* **2011**, 6(4):e18342.
16. Chen Q, Sun Q, Molino NM, Wang S-W, Boder ET, Chen W. Sortase A-mediated multi-functionalization of protein nanoparticles. *Chemical Communications* **2015**, 51:12107-12110.
17. Swartz AR, Sun Q, Chen W. Ligand-induced cross-linking of Z-elastin-like polypeptide-functionalized E2 protein nanoparticles for enhanced affinity precipitation of antibodies. *Biomacromolecules* **2017**, 18:1654-1659.
18. Swartz AR, Xu X, Traylor SJ, Li ZJ, Chen W. High-efficiency affinity precipitation of multiple industrial mAbs and Fc-fusion proteins from cell culture harvests using Z-ELP-E2 nanocages. *Biotechnology and Bioengineering*, **2018**, 1-9. (in press)
19. Wu Z, Guo Z. Sortase-Mediated Transpeptidation for Site-Specific Modification of Peptides, Glycopeptides, and Proteins. *J Carbohydr Chem* **2013**, 31(1):48-66.
20. Zakeri B, Fierer JO, Celik E, Chittock EC, Schwarz-Linek U, Moy VT, Howarth M. Peptide tag forming a rapid covalent bond to a protein, through engineering a bacterial adhesin. *PNAS* **2012**, 109(12):690-697.
21. Swartz AR, Chen W. SpyTag/Spycatcher functionalization of E2 nanocages with stimuli-responsive Z-ELP affinity domains for tunable monoclonal antibody binding and precipitation properties. *Bioconjugate Chemistry* **2018**, (in review).

22. Patil AS, Gadad AP, Hiremath RD, Dandagi PM. Exploration of the Effect of Chitosan and Crosslinking Agent Concentration on the Properties of Dual Responsive Chitosan-g-Poly (N-Isopropylacrylamide) Co-polymeric Particles. *Journal of Polymers and the Environment* **2018**, 26(2):596-606.
23. Sreekumar S, Goycoolea FM, Moershbacher BM, Rivera-Rodriguez GR. Parameters influencing the size of chitosan-TPP nano- and microparticles. *Scientific Reports* **2018**, 8:4695-4705.
24. Hassouneh W, Christensen T, Chilkoti A. Elastin-like Polypeptides as a Purification Tag for Recombinant Proteins. *Curr Protoc Protein Sci* **2010**, Chapter 6: Unit 6.11.
25. Regnima GO, Koffi T, Bagui O, Kouacou A, Kristensson E, Zoueu J, Berrocal E. Quantitative measurements of turbid liquids via structured laser illumination planar imaging where absorption spectrophotometry fails. *Applied Optics* **2017**, 56(13):3929-3938.
26. Kostelnik A, Cegan A, Pohanka M. Color Change of Phenol Red by Integrated Smart Phone. *Sensors* **2016**, 16:1212.
27. Zhang L, Luo S, Zhang B. Glycan analysis of therapeutic glycoproteins. *mAbs* **2016**, 8(2):205-215.
28. Rosano GL, Ceccarelli EA. Recombinant protein expression in Escherichia coli: advances and challenges. *Front Microbiol* **2015**, 5:172.
29. Trabbic-Carlson K, Liu L, Kim B, Chilkoti A. Expression and purification of recombinant proteins from Escherichia coli: Comparison of an elastin-like polypeptide fusion with an oligohistidine fusion. *Protein Science* **2004**, 13:3274-3284.
30. Gadagkar SR, Call GB. Computational tools for fitting the Hill equation to dose-response curves. *Journal of Pharmacological and Toxicological Methods* **2015**, 71:68-76.

Chapter 7

CONCLUSIONS AND FUTURE WORK: PLATFORMED ANTIGEN DETECTION AND PURIFICATION THROUGH NANOBODY FUNCTIONALIZED NANOPARTICLE CROSSLINKING

7.1 Motivation for new affinity precipitation ligand design

Non-chromatographic monoclonal antibody (mAb) purification technologies have been developed as a potential solution to downstream platform process bottlenecks¹. Affinity precipitation using protein A ligands conjugated to stimuli-responsive molecules has been proposed as scalable alternative². A Z-domain-elastin-like polypeptide (Z-ELP) ligand was evaluated for mAb affinity precipitation³, but the high salt concentration and/or temperature required for ELP precipitation and other operational constraints have limited its widespread application⁴⁻⁵. To overcome the shortcomings of existing affinity ligands, a new scaffold was designed to minimize the salt necessary for phase transition at ambient temperature. By functionalizing Z-ELP to a protein derived nanoparticle, we hypothesized that the increased multivalency and dimension would simultaneously result in antibody-binding induced crosslinking and lower ELP aggregation transition temperatures.

7.2 IgG-binding induced crosslinking with Z-ELP-E2 nanoparticles

To investigate the effect of scaffolding affinity ligands, Sortase A ligation was used to conjugate Z-ELP to a self-assembled 25-nm, 60-mer E2 nanocage. Because of

the enlarged dimension, ligated Z-ELP resulted in more than a 10°C lower transition temperature than equal concentrations of free Z-ELP in solution. Using a human polyclonal IgG, specific binding to the Z-ELP-E2 nanoparticles increased the aggregate size to > 1 μ M and significantly less salt concentration was required for precipitation compared to free ELP. Furthermore, the precipitated antibody-nanoparticle complex remained insoluble in PBS (pH 7.2) even after mixing at 4°C for 3 days, indicating the potential for washing with neutral pH buffers. We concluded this “locked-in” insoluble phase was due to a crosslinked network formed through multivalent antibody binding. After centrifugation, the aggregated pellet was capable of resolubilization by dissociating the IgG-Z-domain interaction in an elution buffer with pH < 4.

7.3 Development of a platform for industrial mAb purification

A one-step affinity capture and precipitation procedure was developed with a purified industrial mAb using high-throughput optimization experiments and was applied to the purification of mAb cell culture harvests. Most notably, the nanoparticles crosslinked into large aggregates immediately upon mixing with mAbs in cell culture media at 23°C without the addition of salt, and a 3:1 Z-mAb molar ratio was sufficient to capture > 95% mAb in solution. Furthermore, the “locked-in,” insoluble mAb-Z-ELP-E2 particles allowed for washing with the same series of wash buffers used in protein A chromatography (pH \geq 5) without resolubilizing the aggregated complex. This enabled efficient impurity clearance, and when compared to protein A chromatography eluates, nanoparticle-based affinity precipitation demonstrated a similar HCP reduction and an order of magnitude higher DNA (<10 ppb) reduction from cell culture harvests.

The optimized affinity precipitation procedure was challenged using four industrial mAbs and one Fc-fusion protein. For all molecules, a 3:1 Z:mAb binding ratio

crosslinked and precipitated > 95% mAb in solution, but there was a strong dependence of solution pH on aggregation kinetics for mAbs with an isoelectric point less than 7. A simplified two-step kinetic rate model of crosslinking nucleation and growth was applied to analyze aggregation behavior in solution pH 5-9. Slow kinetics ($t_{\max} > 30$ min) were observed at a solution pH near or greater than the protein pI, but a simple titration of cell culture media to pH 5 permitted fast aggregation ($t_{\max} < 10$ min) with high yields (> 90%). For mAbs A-D, purification from cell culture harvests resulted in high mAb yield (95%) and monomer (> 97%) with an impurity clearance of 99.9% for HCP and > 99.99% for DNA. This work established an affinity precipitation platform that may be applied to any target mAb with minimal optimization of binding and elution conditions.

7.4 Improved nanoparticle functionalization with SpyTag/SpyCatcher

After mAb elution, the nanoparticles were regenerated for use in subsequent purification cycles, but recovery yields of < 90% were observed. We suspected that increasing the E2 ligation density of longer chain-length Z-ELP affinity domains may improve the regeneration yield by reducing the transition temperature. However, the Sortase A ligation efficiency of an 80-repeat Z-ELP₈₀ to E2 was less than 10% due to steric limitations and/or reaction reversibility. To increase ligation efficiency, a new method was evaluated by conjugating Z-ELP-SpyCatcher to SpyTag-E2 through isopeptide bond formation. Z-ELP₄₀- or Z-ELP₈₀-SpyCatcher fusion proteins were conjugated with greater than 90% efficiency after mixing for one hour. Close to 100% ligation was obtained for equimolar reactant mixtures, indicating the functionalization of all 60 SpyTag-E2 binding sites. The 100% ligation Z-ELP₈₀-Spy-E2 nanoparticles had a 10°C lower transition temperature and 2-fold higher mAb binding capacity than

the previous nanoparticles generated by Sortase A ligation. In addition, nanocage recoveries of > 90% were obtained using just 0.1 M ammonium sulfate for selective nanoparticle precipitation after mAb elution.

7.5 Quantification of mAb-nanoparticle crosslinking turbidity

The 100% ligation Z-ELP₈₀-E2 nanoparticles produced by the SpyTag/SpyCatcher reaction ensure a 60-valent, site-specific conjugation of Z-ELP and exhibited improved antibody binding and aggregation properties compared to nanoparticles produced by Sortase A. We supposed that this uniform and multivalent surface display of affinity ligands may be ideal for consistent and sensitive mAb detection through mAb-nanoparticle crosslinking turbidity. Using an absorbance measurement at 600 nm, a logarithmic dependence was observed for mAb concentrations between 100-1000 µg/mL and a good fit was obtained ($R^2 = 0.99$) using logarithmic regression. The aggregation kinetics reached steady state after about 10 min mixing in cell culture media pH 7.2 for a mAb with a pI > 8 or in cell culture media titrated to pH 5.0 for a mAb with a pI < 7. Two mAb cell culture harvests were used to validate the assay and a bridging study with Octet RED96e biolayer interferometry confirmed accurate and reproducible results. We envision that a simple, 10 min mixing step followed by an absorbance measurement may be a more practical and cost-efficient alternative to the existing mAb titer assays limited by expensive equipment or tedious, low-throughput protocols.

7.6 Generalized protein purification and detection with nanobodies

The proposed mechanism for mAb-nanoparticle crosslinking involves the multivalent binding of two Z-domain from different nanoparticles to the same dimeric

antibody⁶ (**Figure 7.1A**). Primary effect affinity precipitation ligands typically require multivalent binding to multimeric proteins for network formation and will not crosslink with monomeric proteins⁷. To generalize the nanoparticle crosslinking strategy using monomeric proteins, we hypothesized that two or more conjugated affinity ligands with orthogonal binding motifs may crosslink upon binding of both ligands to the same protein in tandem (**Figure 7.1B**).

Affinity chromatography captures target proteins from a complex mixture using immobilized affinity ligands that enable highly specific binding and elution⁸. For non-tagged, non-mAb proteins, commercially available affinity chromatography media may not be available for the target⁹. However, combinatorial screening of peptide or protein libraries can identify selective binders, and customized affinity ligands can be chemically conjugated to the chromatographic support¹⁰. A parallel strategy can be easily implemented using the modular ELP-SpyCatcher:SpyTag-E2 platform to functionalize interchangeable affinity domains. An affinity peptide or protein may be genetically fused to the ELP-SpyCatcher construct, recombinantly expressed in *E. coli*, and conveniently purified using ELP ITC. Because of the high efficiency of SpyTag/SpyCatcher conjugation, we would expect a highly tunable ligation of multiple affinity domains on the E2 nanocage.

One group of proteins called nanobodies are ideally suited for integration into our affinity domain-ELP-SpyCatcher:SpyTag-E2 system. Nanobodies are small (15 kDa), single-domain variable heavy chain antibody fragments derived from a Camelid immune system that bind with high specificity to target antigens¹¹. They can also be screened for high affinity binding to a target protein through several different strategies including llama immunization¹² or *E. coli* surface display¹³. Seven high-binding

nanobodies (GBP1-7) raised against green fluorescent protein (GFP) have been well characterized¹⁴. Through a functional screening assay, it was determined that GBP2 and GBP7 were the most compatible pair for orthogonal binding to GFP¹⁵. As a model system, the GBP2+7 nanobody pair was evaluated for crosslinking with GFP to demonstrate proof of concept purification and concentration-dependent turbidity (**Figure 7.1B**).

7.7 GFP-nanoparticle crosslinking with orthogonal nanobody-ELP-E2

GBP2-ELP₈₀-SpyCatcher and GBP7-ELP₈₀-SpyCatcher were expressed, purified, and mixed at equimolar ratios with SpyTag-E2 for conjugation, and high efficiency (> 90%) was obtained (**Figure 7.2A**). To test for crosslinking, GBP2-E2 and GBP7-E2 (GBP2+7) nanoparticles, GBP2 only, or GBP7 only were mixed at a 3:1 GBP:GFP molar ratio with GFP soluble *E. coli* lysate in PBS, pH 7.2. A significant increase in turbidity occurred within minutes of mixing the GBP2+7 nanoparticles at 23°C, a slight increase in turbidity was observed for GBP7, and no increase in turbidity was observed for GBP2 (**Figure 7.2B**). The minor increase in turbidity for GBP7 was likely due to a secondary binding site on GFP, but with much weaker affinity than the main binding site.

To investigate crosslinking extent and to verify binding, the samples were centrifuged to pellet the insoluble components without or with addition of salt, and the supernatant GFP fluorescence was analyzed to quantify precipitation yield. Similar to mAb-nanoparticle crosslinking, the GBP2+7 mixture exhibited high GFP precipitation yield (> 95%) through crosslinking without added salt, while the GBP2 or GBP7 nanobodies did not form sufficient crosslinks to fully phase transition (**Figure 7.2C-D**, blue bars). However, it was verified that GBP2 and GBP7 were each capable of binding

to and capturing > 85% GFP in solution after salt addition (**Figure 7.2C-D**, red bars). To confirm the GFP fluorescence data, the supernatant and pellets of the mixtures without added salt were analyzed by SDS-PAGE, where the pellet was resuspended in an elution buffer (100 mM sodium citrate, pH 3.0) (**Figure 7.3A**). A large, GFP-enriched pellet was clearly visualized for the mixture of GBP2+7, a small pellet was observed for GBP7, and nothing visibly pelleted for GBP2 (**Figure 7.3B**). After washing and resuspending the GBP2+7 pellet in elution buffer and selectively precipitating the nanoparticles with 0.25 M ammonium sulfate, GFP was eluted with ~85% yield (**Figure 7.3C**, lane 6). SDS-PAGE analysis reveals residual GFP in the regenerated nanoparticle sample as well as some leaching of nanoparticle in the elution supernatant, indicating an incomplete dissociation of the nanobody-GFP interaction. This result is not unexpected as a pH between 2.0-2.5 is commonly used for nanobody-target dissociation¹⁶. However, the E2 nanocage becomes increasingly unstable below pH 3.0, so an elution pH < 3.0 is not ideal⁶. Further optimization of the elution buffer and dissociation kinetics is necessary to increase the GFP yield and minimize nanoparticle leaching.

The effect of GFP concentration on GFP2+7 crosslinking turbidity was studied for 5.0 μM of both GFP2 and GFP7 nanoparticles mixed with 0.1-5.0 μM GFP in soluble lysate. Analysis of the absorbance spectrum confirmed minimal background from GFP lysate at an absorbance of 600 nm (**Figure 7.4A**). The crosslinking turbidity was measured 10 min after mixing at 23°C and a logarithmic relationship was obtained, similar to mAb-nanoparticle crosslinking turbidity. Logarithmic regression from 0.1-5.0 μM GFP indicated good fit ($R^2 = 0.96$) in this range. After the turbidity measurement, samples were centrifuged to pellet crosslinked GFP-nanoparticles and

determine the sensitivity of crosslinking at low GFP concentrations. Above a 2:1 GBP:GFP molar ratio, > 95% yield was obtained even at 50:1 ratio with just 100 nM GFP (**Figure 7.4C-D**). We suspected the high nanoparticle valency and binding affinity enabled enough crosslinks for sensitive detection.

7.8 Future research opportunities

These results indicate the benefits of a modular platform for the purification or detection of either monomeric or multimeric proteins using nanobody-functionalized nanoparticles. Future work will seek to expand this platform using other model systems and establish a generalized method of protein purification and analytical quantification. Further optimization must be done to increase elution yield and reduce nanoparticle leaching, but an elution step is not needed for a turbidity-based assay. Antigen-Nanobody-ELP-Spy-E2 nanoparticle crosslinking has many exciting new research opportunities and potential applications including the quantification of non-mAb cell culture titer, diagnostic testing¹⁷, molecular probing¹⁸, or detection of pathogens such as viruses¹⁹, microbes²⁰, or other toxins²¹. The interchangeability of nanobody-ELP-SpyCatcher affinity ligands combined with the tunable, efficient conjugation to SpyTag-E2 make this platform conveniently adaptable for new applications.

FIGURES

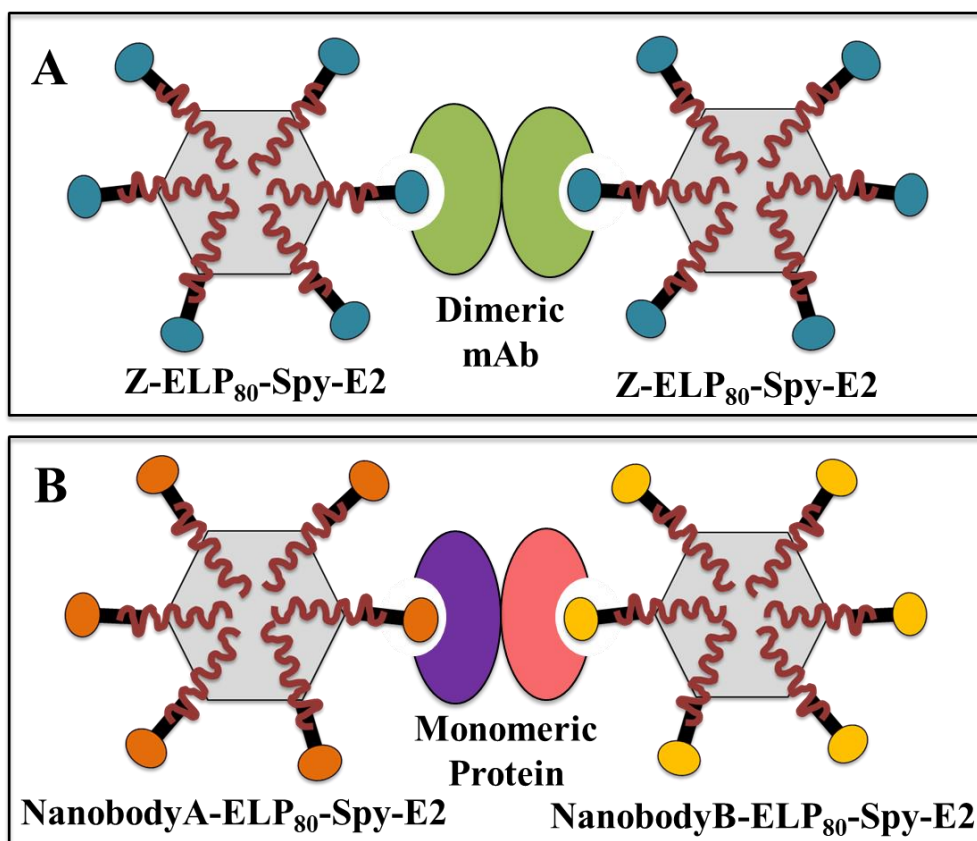


Figure 7.1 Mechanism for target protein-nanoparticle crosslinking with **multimeric** and **monomeric** proteins. A) Multimeric protein (dimeric mAb) crosslinking with single affinity domain conjugated nanoparticles. B) Monomeric protein crosslinking with multiple affinity domain (nanobody-ELP) conjugated nanoparticles through orthogonal binding motifs.

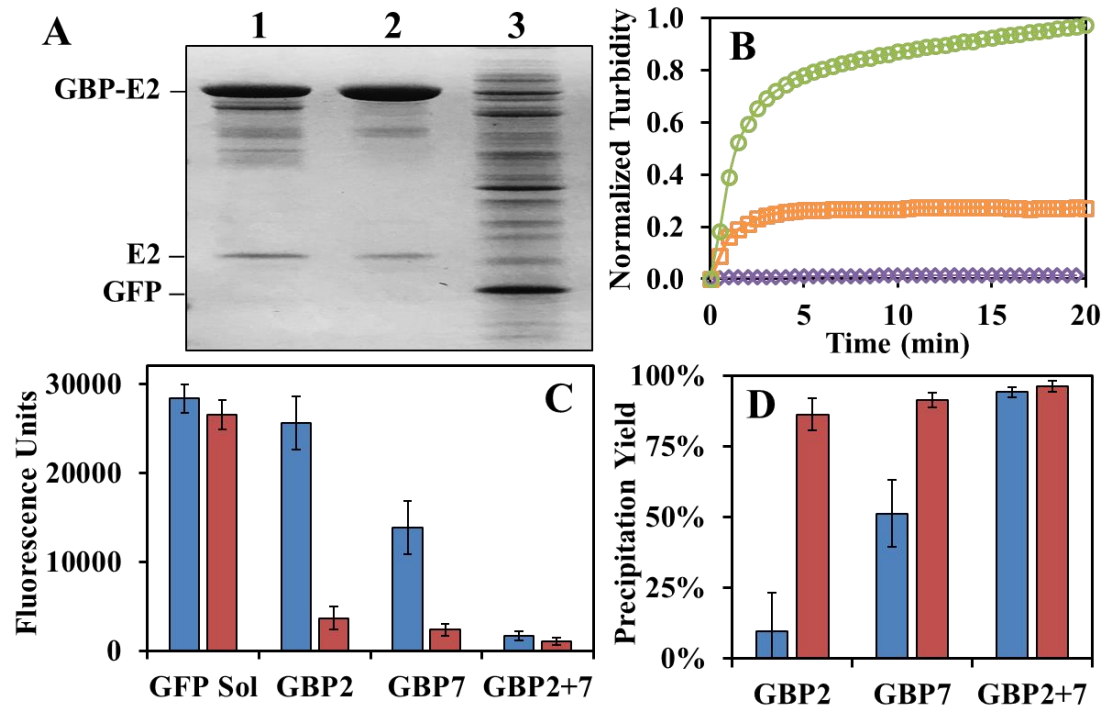


Figure 7.2 Orthogonal Anti-GFP nanobody (GBP2, GBP7) binding and crosslinking with GFP. A) SDS-PAGE of GBP2/7-ELP₈₀-SpyCatcher conjugation to SpyTag-E2 mixed at equimolar ratios. Lane 1: GBP2-ELP₈₀-Spy-E2 product. Lane 2: GBP7-ELP₈₀-Spy-E2 product. Lane 3: GFP in soluble *E. coli* lysate. B) 15 μ M GBP-ELP₈₀-Spy-E2 crosslinking kinetics with 5 μ M GFP in soluble lysate (PBS, pH 7.2) at 23°C for GBP2-ELP₈₀-Spy-E2 only (purple diamond), GBP7-ELP₈₀-Spy-E2 only (orange square), or, or mix of GBP2+7-ELP₈₀-Spy-E2 (green circle). C) Supernatant GFP fluorescence after mixing targets at 23°C for 10 min and pelleting insoluble aggregates without (blue) or with addition of 0.3 M ammonium sulfate (red). D) GFP precipitation yield after mixing targets without (blue) and with addition of salt (red).

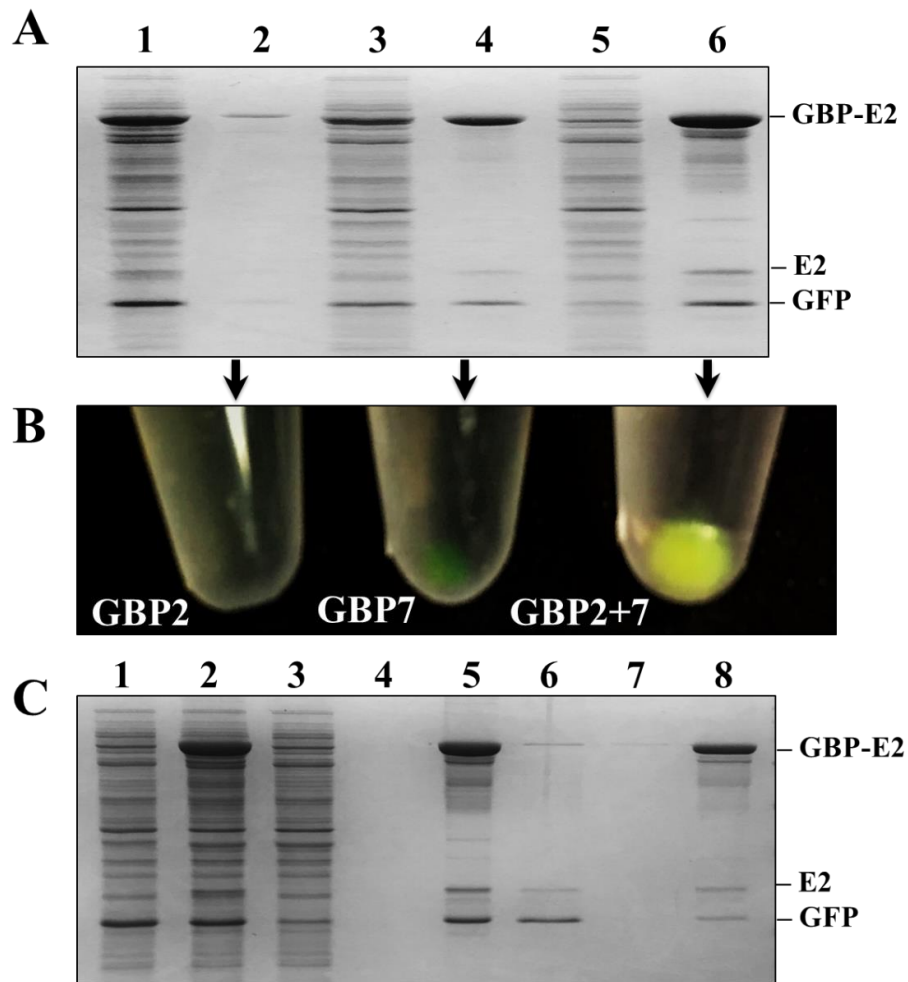


Figure 7.3 GFP capture in soluble *E. coli* lysate through crosslinking with **GBP2+7-ELP₈₀-Spy-E2 nanoparticles without added salt**. A) SDS-PAGE after centrifugation of GFP and GBP2/7-ELP₈₀-Spy-E2 mixtures for GBP2-ELP₈₀-Spy-E2 only supernatant (lane 1) and resuspended pellet (lane 2), GBP7-ELP₈₀-Spy-E2 only supernatant (lane 3) and resuspended pellet (lane 4), or GBP2+7-ELP₈₀-Spy-E2 mixture supernatant (lane 5) and resuspended pellet (lane 6). Pellets were resuspended in 100 mM sodium citrate pH 3.0 buffer. B) Picture of pellets for indicated samples. C) SDS-PAGE for purification of GFP soluble lysate (lane 1) by mixing GBP2+7-ELP₈₀-Spy-E2 (lane 2), centrifuging to remove impurities in the supernatant (lane 3), washing pellet in PBS (lane 4), resuspending pellet in 100 mM sodium citrate pH 3.0 (lane 5), eluting GFP in supernatant after selective nanocage precipitation (lane 6), regenerating nanocage (lane 7) and recycling back into PBS (lane 8).

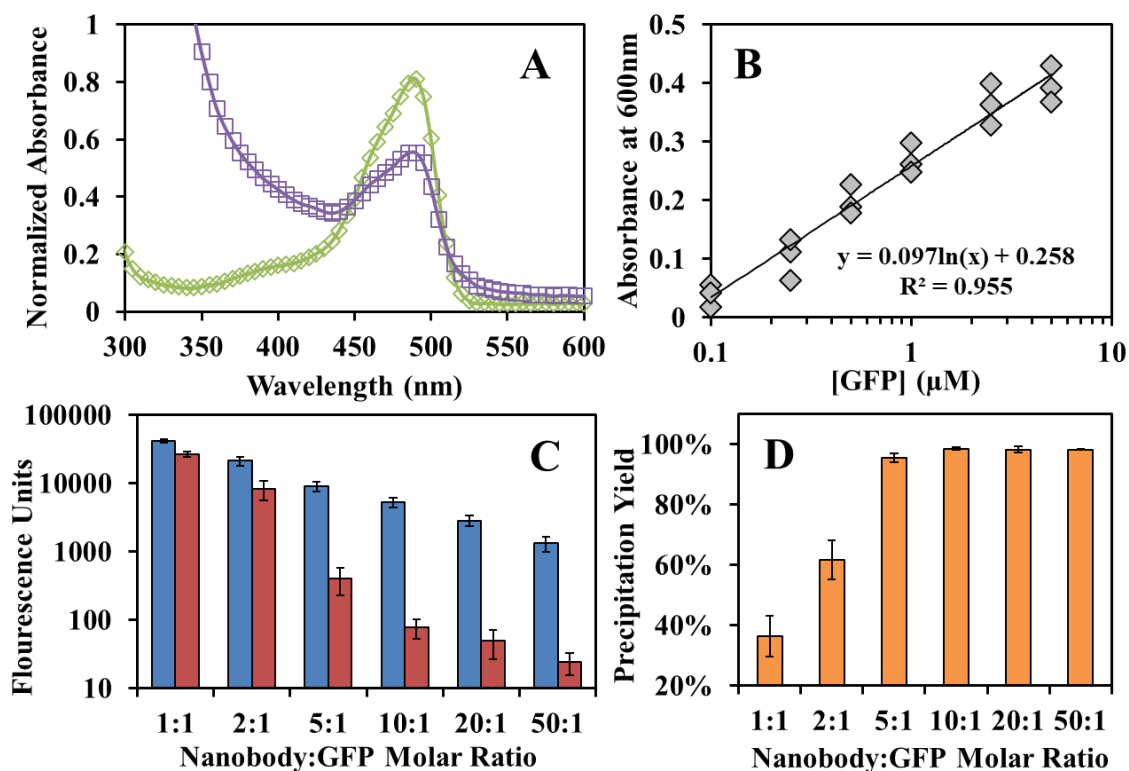


Figure 7.4 Concentration dependent detection of GFP-nanoparticle crosslinking turbidity and crosslinking sensitivity at low GFP concentrations. A) Absorbance spectrum for GFP soluble lysate (purple square) and pure GFP (green diamond). B) Detection of turbidity by absorbance at 600 nm for mixtures of 5 μM GBP2-ELP₈₀-Spy-E2 and 5 μM GBP7-ELP₈₀-Spy-E2 mixed with 5.0-0.1 μM GFP in lysate for 10 min at 23°C fit to a logarithmic regression. C) Initial GFP fluorescence (blue) and supernatant GFP fluorescence (red) after mixing target GFP concentration with 5 μM GBP2+7 at 23°C for 15 min and pelleting insoluble aggregates. D) GFP precipitation yield after mixing targets.

REFERENCES

1. P. Gronemeyer, R. Ditz and J. Strube. Trends in upstream and downstream process development for antibody manufacturing. *Bioengineering* **2014**, 1:188-212.
2. M. W. Handlogten, J. F. Stefanick, P. E. Deak and B. Bilgicer. Affinity-based precipitation via a bivalent peptidic hapten for the purification of monoclonal antibodies. *Analyst* **2014**, 139:4247-4255.
3. B. Madan, G. Chaudhary, S.M. Cramer and W. Chen. ELP-z and ELP-zz capturing scaffolds for the purification of immunoglobulins by affinity precipitation. *J Biotechnol* **2013**, 163(1):10-16.
4. R. D. Sheth, B. Madan, W. Chen and S. M. Cramer. High-throughput screening for the development of a monoclonal antibody affinity precipitation step using ELP-Z stimuli responsive biopolymers. *Biotechnology and Bioengineering* **2013**, 110(10):2664-2676.
5. P. Gagnon. Technology trends in antibody purification. *Journal of Chromatography A* **2012**, 1221:57-70.
6. A. R. SwartzA, X. Xu, S. J. Traylor, Z. J. Li and W. Chen. One-step affinity capture and precipitation for improved purification of an industrial monoclonal antibody using Z-ELP functionalized nanocages. *Biotechnology and Bioengineering* **2018**, 115(2):423-432.
7. F. Hillbrig and R. Freitag. Protein purification by affinity precipitation. *Journal of Chromatography B* **2003**, 790(1):79-90.
8. M. Urh, D. Simpson and K. Zhao. Affinity chromatography: general methods. *Methods Enzymol* **2009**, 463:417-438.
9. M. Saraswat, L. Musante, A. Ravida, B. Shortt, B. Byrne and H. Holthofer. Preparative purification of recombinant proteins: Current status and future trends. *Biomed Res Int.* **2013**, 312709.
10. O. A. Camperi, M. M. Marani, M. C. Martinez-Ceron, F. Albercio and O. Cascone. Protein purification by affinity chromatography with peptide ligands selected from the screening of combinatorial libraries. *Trends in Chromatography* **2010**, 6:11-22.

11. S. Steeland, R. E. Vandenbrouche and C. Libert. Nanobodies as therapeutics: big opportunities for small antibodies. *Drug Discov Today* **2016**, 21(7):1076-1113.
12. P. C. Firidy, Y. Li, S. Keegan, M. K. Thompson, I. Nudelman, J. F. Scheid, M. Oeffinger, M. C. Nussenzweig, D. Fenya and B. T. Chait. A robust pipeline for rapid production of versatile nanobody repertoires. *Nat Methods* **2014**, 11(12):1253-1260.
13. V. Salema and L. A. Fernandez. Escherichia coli surface display for the selection of nanobodies. *Microb Biotechnol* **2017**, 10(6):1468-1484.
14. A. Kirchhofer, J. Helma, K. Schmidthals, C. Frauer, S. Cui, A. Karcher, M. Pellis, S. Muyldermans, C. S. Casas-Delucchi, M. C. Cardoso, H. Leonhardt, K. P. Hopfner and U. Rothbauer. Modulation of protein properties in living cells using nanobodies. *Nat Struct Mol Bio* **2010**, 17(1):133-138.
15. J. C. Y. Tang, T. Szikra, Y. Kozorovskiy, M. Tiexiera, B. L. Sabatini, B. Roska and C. L. Cepko. A nanobody-based system using fluorescent proteins as scaffolds for cell-specific gene manipulation. *Cell* **2013**, 154(4):928-939..
16. T. N. Baral, R. MacKenzie and A. M. Ghahroudi. Single-domain antibodies and their utility. *Curr Protoc Immunol* **2013**, 103:1-57.
17. L. Huang, S. Muyldermans and D. Saerens. Nanobodies: proficient tools in diagnostics. *Expert Rev Mol Diagn* **2010**, 10(6):777-785.
18. E. Platonova, C. M. Winterflood, A. Junemann and H. Ewers. Single-molecule microscopy of molecules tagged with GFP or RFP derivatives in mammalian cells using nanobody binders. *Methods* **2015**, 88:89-97.
19. L. J. Sherwood, L. E. Osborn, R. Carrion, J. L. Parreson and A. Hayhurst. Rapid assembly of sensitive antigen-capture assays for Marburg virus, using in vitro selection of llama single-domain antibodies, at biosafety level 4. *J Infect Dis* **2007**, 196(2):213-219.
20. N. Deckers, D. Saerens, K. Kanobana, K. Conrath, B. Victor, U. Wernery, J. Vercruyse, S. Muyldermans and P. Dorny. Nanobodies, a promising tool for species-specific diagnosis of *Taenia solium* cysticercosis. *Int J Parasitol* **2009**, 39(5):625-633.

21. J. Wesolowski, V. Alzogaray, J. Reyelt, M. Unger, K. Juarez, M. Urrutia, A. Cauerhff, W. Denquah, B. Rissiek, F. Scheuplein, N. Schwarz, S. Adriouch, O. Boyer, M. Seman, A. Licea, D. V. Serreze, F. A. Goldbaum, F. Haag and F. Koch-Nolte. Single domain antibodies: promising experimental and therapeutic tools in infection and immunity. *Medical Microbiology and Immunology* **2009**, 198(3):157-174.

Appendix A

LIST OF ABBREVIATIONS

- AP: affinity precipitation
- BLI: biolayer interferometry
- BMS: Bristol-Myers Squibb
- BSA: bovine serum albumin
- CHO: Chinese hamster ovary
- CV: coefficient of variation
- DLS: dynamic light scattering
- ELISA: enzyme-linked immunosorbent assay
- ELP: elastin-like polypeptide
- ELP₄₀: 40-repeat ELP
- ELP₈₀: 80-repeat ELP
- Fab: antigen binding antibody domain
- Fc: constant antibody domain
- F-W: Finke-Watzky
- GBP: GFP binding protein nanobody
- GFP: green fluorescent protein
- HCP: host cell protein
- HMW: high molecular weight
- HPLC: high-performance liquid chromatography
- IgG: immunoglobulin G

IPTG: isopropyl- β -D-thiogalactoside
ITC: inverse transition cycling
 k_1 : nucleation rate constant
 k_2 : growth rate constant
kDa: kilodalton
LB: Luria-Bertani medium
LMW: low molecular weight
LRV: log reduction value
mAb: monoclonal antibody
MW: molecular weight
OD: optical density
PA: protein A
PBS: phosphate buffered saline
PCR: polymerase chain reaction
PDI: polydispersity index
pI: isoelectric point
PLSR: partial least squares regression
PS-80: polysorbate-80
qPCR: quantitative polymerase chain reaction
 R^2 : coefficient of determination
SDS-PAGE: sodium dodecyl sulfate polyacrylamide gel electrophoresis
SEC: size-exclusion chromatography
SP₂: streptavidin binding peptide
Spy: SpyTag/SpyCatcher conjugation

SrtA: Sortase A

TB: terrific broth medium

TEM: transmission electron microscopy

T_m : midpoint unfolding temperature

t_{max} : time at maximum aggregation rate

TN150: tris buffered saline

T_t : transition temperature

UPLC: ultra-performance liquid chromatography

UV: ultraviolet

VCF: volume concentration factor

Z-ave: cumulants mean size

Appendix B

REPRINT PERMISSIONS

Chapter 2 is reproduced with permission from American Chemical Society. Source:

Swartz AR, Sun Q, Chen W. Ligand-induced crosslinking of Z-ELP-functionalized E2 protein nanoparticles for enhanced affinity precipitation of antibodies. *Biomacromolecules* **2017**, 18(5):1654-1659.



RightsLink®

Home

Create Account

Help



Title:

Ligand-Induced Cross-Linking of Z-Elastin-like Polypeptide-Functionalized E2 Protein Nanoparticles for Enhanced Affinity Precipitation of Antibodies

Author:

Andrew R. Swartz, Qing Sun, Wilfred Chen

Publication: Biomacromolecules

Publisher: American Chemical Society

Date: May 1, 2017

Copyright © 2017, American Chemical Society

LOGIN

If you're a copyright.com user, you can login to RightsLink using your copyright.com credentials. Already a RightsLink user or want to [learn more?](#)

PERMISSION/LICENSE IS GRANTED FOR YOUR ORDER AT NO CHARGE

This type of permission/license, instead of the standard Terms & Conditions, is sent to you because no fee is being charged for your order. Please note the following:

- Permission is granted for your request in both print and electronic formats, and translations.
- If figures and/or tables were requested, they may be adapted or used in part.
- Please print this page for your records and send a copy of it to your publisher/graduate school.
- Appropriate credit for the requested material should be given as follows: "Reprinted (adapted) with permission from (COMPLETE REFERENCE CITATION). Copyright (YEAR) American Chemical Society." Insert appropriate information in place of the capitalized words.
- One-time permission is granted only for the use specified in your request. No additional uses are granted (such as derivative works or other editions). For any other uses, please submit a new request.

Chapter 3 is reproduced with permission from John Wiley and Sons. Source:

Swartz AR, Xu X, Traylor S, Li ZJ, Chen W. One-step affinity capture and precipitation for improved purification of an industrial monoclonal antibody using Z-ELP functionalized nanocages. *Biotechnol Bioeng* **2018**, 115(2):423-432.



The screenshot shows the RightsLink interface. At the top left is the Copyright Clearance Center logo. To its right is the RightsLink logo. Further right are navigation buttons for Home, Account Info, and Help, along with a chat bubble icon. Below the logos is a grid of information. On the left is a thumbnail of a journal cover titled 'BIOTECHNOLOGY & BIOENGINEERING'. To the right of the thumbnail are the following details: Title: One-step affinity capture and precipitation for improved purification of an industrial monoclonal antibody using Z-ELP functionalized nanocages; Author: Andrew R. Swartz, Xuankuo Xu, Steven J. Traylor, et al; Publication: Biotechnology & Bioengineering; Publisher: John Wiley and Sons; Date: Oct 30, 2017; Copyright © 2017, John Wiley and Sons. To the right of this information is a user login box showing 'Logged in as: Andrew Swartz' and a 'LOGOUT' button.

Order Completed

Thank you for your order.

This Agreement between Andrew Swartz ("You") and John Wiley and Sons ("John Wiley and Sons") consists of your license details and the terms and conditions provided by John Wiley and Sons and Copyright Clearance Center.

Your confirmation email will contain your order number for future reference.

[printable details](#)

License Number	4366490777405
License date	Jun 12, 2018
Licensed Content Publisher	John Wiley and Sons
Licensed Content Publication	Biotechnology & Bioengineering
Licensed Content Title	One-step affinity capture and precipitation for improved purification of an industrial monoclonal antibody using Z-ELP functionalized nanocages
Licensed Content Author	Andrew R. Swartz, Xuankuo Xu, Steven J. Traylor, et al
Licensed Content Date	Oct 30, 2017
Licensed Content Volume	115
Licensed Content Issue	2
Licensed Content Pages	10
Type of use	Dissertation/Thesis
Requestor type	Author of this Wiley article
Format	Print and electronic
Portion	Full article

Chapter 4 is reproduced with permission from John Wiley and Sons. Source:

Swartz AR, Xu X, Traylor S, Li ZJ, Chen W. High-efficiency affinity precipitation of multiple industrial mAbs and Fc-fusion proteins from cell culture harvests using Z-ELP-E2 nanocages. *Biotechnol Bioeng* **2018**, 1-9. (in press)